

REF  
669.95  
1995

SHA Study of Structural Changes and Effect of Alloy  
Addition of Ceramic Materials by X-ray and  
Neutron Diffraction Technique

A. K. M. Shaestagir Chowdhury

A thesis submitted to the Department of Metallurgical Engineering of  
Bangladesh University of Engineering and Technology, Dhaka, in partial  
fulfilment of the requirements for the degree of Master of Science in  
Engineering (Metallurgical).



August, 1995



BANGLADESH UNIVERSITY OF ENGINEERING AND TECHNOLOGY  
DHAKA, BANGLADESH.

STUDY OF STRUCTURAL CHANGES AND EFFECT OF  
ALLOY ADDITION OF CERAMIC MATERIALS BY X-RAY  
AND NEUTRON DIFFRACTION TECHNIQUE.

## DECLARATION

This is to certify that this research work has been carried out by the author under the supervision of Dr. A. K. M. Bazlur Rashid, Assistant Professor, Department of Metallurgical Engineering, BUET, Dhaka, and it has not been submitted elsewhere for the award or degree of any kind.

Countersigned by



Supervisor



Signature of the Author

The undersigned examiners appointed by the Committee of Advanced Studies and Research (CASR) hereby recommend to the Department of Metallurgical Engineering of Bangladesh University of Engineering and Technology, Dhaka, the acceptance of the thesis entitled "Study of Structural Changes and Effect of Alloy Addition of Ceramic Materials by X-Ray and Neutron Diffraction Technique" submitted by A. K. M. Shaestagir Chowdhury, Lecturer, Department of Metallurgical Engineering, BUET, Dhaka, in partial fulfillment of the requirements for the Degree of Master of Science in Engineering (Metallurgical).

1. Rashid 15/8/95

Dr. A. K. M. Bazlur Rashid  
Assistant Professor  
Department of Metallurgical Engg.  
BUET, Dhaka.

Chairman  
(Supervisor)

2. Ahmed 15-8-95

Dr. Farid Uddin Ahmed  
Principal Scientific Officer  
Institute of Nuclear Science and Technology  
Atomic Energy Research Establishment  
Savar, Dhaka

Co-Supervisor

3. Mohafizul Haque 15/8/95

Professor Dr. Mohafizul Haque  
Head,  
Department of Metallurgical Engg.  
BUET, Dhaka.

Member  
(Ex-officio)

4. E. Haque 15.8.95

Professor Dr. Ehsanul Haque  
Department of Metallurgical Engg.  
BUET, Dhaka.

Member

5. M. Ibrahim

Professor Dr. M. Ibrahim  
House No. 31, Road No. 4.  
Dhanmondi R/A, Dhaka-1205.

Member  
(External)

## Abstract

Investigation on the structural changes of ceramic insulator materials, with a view to improve their quality, were undertaken. For this purpose a number of clays were mixed with up to 4 per cent potash feldspar (to reduce the firing temperature) and then fired. Alkaline earth oxides, i.e., zirconium silicate, zinc oxide, titanium oxide, manganese oxide etc. from 2 to 4 per cent were also used as fluxing materials. Effects of alkaline earth oxides on the strength, texture, and some thermal properties were investigated. The influence of these alkaline earth oxides on the reaction during firing was studied by DTA. The phases were identified by x-ray diffraction and the texture was analyzed by neutron scattering technique. It was found in the present investigation that the addition of alkaline earth oxides lowered down the firing temperature, promoted the growth of mullite and tridymite phases, and eliminated the textural defects of the ceramic insulator body. Zirconium silicate and zinc oxide were appeared to have the best influence on increasing the strength and decreasing the coefficient of thermal expansion of the material. Although a combination of zirconium silicate and titanium dioxide addition lowered down the density of the material in an encouraging level, the strength values of these materials, however, could not match this achievement. Rather a disappointing finding relating to the addition of a combination of oxides is probably due to the presence of a higher percentage of titanium dioxide in the body composition. Clearly, more work is required to clarify this observation.

## ACKNOWLEDGEMENTS

The author expresses his profound indebtedness and heartfelt gratitude to his thesis supervisor Dr. A. K. M. Bazlur Rashid, Assistant Professor, Department of Metallurgical Engineering, Bangladesh University of Engineering and Technology (BUET), Dhaka for his valuable suggestions, constant guidance, encouragement and kind help in carrying out the project work as well as in writing this thesis.

The author is also deeply indebted and much obliged to Dr. Farid Uddin Ahmed, Principal Scientific Officer, Institute of Nuclear Science & Technology, Atomic Energy Research Establishment, Savar, Dhaka, for his kind co-supervision and encouragement in carrying out the project work as well as in writing this thesis.

The author is grateful to professor Md. Mohafizul Haque, Head, Department of Metallurgical Engineering, BUET, Dhaka for his kind inspiration in every step of work.

The author is grateful to Md. A. E. M. Eshaq, Managing Director of Bangladesh Insulator and Sanitary ware Factory Limited (BISF), Mirpur, Dhaka for giving him permission to use the industrial facility in every area of the industry. The author is also thankful to Md. Talebur Rahman, Additional Chief Manager (Production) and Md. Gias Uddin Ahmed, Deputy Chief Manager of BISF for their kind help and dynamic support in this regard.

Thanks are also due to Dr. Nurul Islam Molla, Director of Institute of Nuclear Science & Technology, Atomic Energy Research Establishment, Savar, Dhaka for giving him permission to use the nuclear reactor, and Dr. Akhter Uddin Ahmed, Principal Research Officer, Housing & Building Research Institute, Mirpur, Dhaka for his kind support in using the DTA, TGA instruments in this regard.

Thanks are also due to the officers and staff of the Department of Metallurgical Engineering, BUET and of BISF for their help in various stages of the study.

Finally, the author wishes to record his gratitude to his parents and well wishers for their continued inspiration throughout the period of this research work.

The Author  
Department of Metallurgical Engineering  
BUET, Dhaka.

*To My Parents*

## CONTENTS



Certificate  
Abstract  
Acknowledgments

	Page No.
<b>1 INTRODUCTION</b>	<b>1</b>
<b>2 THEORETICAL BACKGROUND</b>	
2.1 Electrical Insulators	3
2.2 Porcelain	5
2.3 Electrical Porcelain	6
2.4 Chemical Composition of Ceramic Insulating Materials	6
2.5 Mechanism of Formation of Porcelain	8
2.6 Ceramic Phase Equilibrium Diagram	11
2.6.1 One component system - The $\text{SiO}_2$ system	11
2.6.2 Two component system - The $\text{Al}_2\text{O}_3$ - $\text{SiO}_2$ system	13
2.6.3 Three component systems	13
2.7 Heat Treatment of Clays	14
2.7.1 Phase changes which occur on heating Kaolin clays	14
2.7.1.1 Heat treatment in the range 600-800°C	14
2.7.1.2 Heat treatment in the range 800-1400°C	18
2.7.1.3 The exothermic reaction at 900-1050°C	19
2.7.2 Mullite formation and effect of alloy additions	20
2.7.3 Firing of Porcelain	22
2.7.3.1 Firing of Clays, Feldspar and Quartz	22
2.7.3.2 Constitution of fired porcelain body and effect of heat treatment	23
2.7.4 The Modifications of silica during heating	26
2.7.5 Quartz conversion and effect of alloy addition	28
2.8 Phase Analysis by X-ray Diffraction	29
2.9 Texture Analysis by Neutron Diffraction Technique	30
2.9.1 Introduction	31
2.9.2 Processing and Properties	32
2.9.3 Neutron Diffraction for Texture Analysis	32
2.10 Thermal Analysis of Ceramic Insulator	34
2.10.1 Introduction	34
2.10.2 Thermogravimetric Analysis	34



2.10.2.1	Basic Principles	34
2.10.2.2	Applications to clays and allied materials	35
2.10.3	Differential thermal analysis	36
2.10.3.1	Basic principles	36
2.10.3.2	Applications to clays and minerals	38
2.10.4	Thermal expansion analysis	39
2.10.4.1	Application of Dilatometer	39
2.11	Scope of the present work	41
<b>3</b>	<b>EXPERIMENTAL</b>	<b>42</b>
3.1	Introduction	42
3.2	Sample Preparation	42
3.2.1	Raw material selection	42
3.2.2	Chemical analysis	43
3.2.3	Crushing	43
3.2.4	Ball milling or pot milling	43
3.2.5	Magnetic particle separation	43
3.2.6	Reservoir	44
3.2.7	Filter press or Cating in plaster of paris mould	44
3.2.8	Pug Milling	44
3.2.9	Drying	44
3.2.10	Firing	45
3.3	Additives and Composition	45
3.4	Physical Properties Measurements	45
3.4.1	Bending strength measurement	45
3.4.2	Density measurement	46
3.5	Optical Metallography	46
3.6	Phase Analysis by X-ray Diffraction	47
3.7	Texture analysis	48
3.8	Thermal Analysis	48
3.8.1	Differential thermal analysis	48
3.8.2	Thermogravimetric analysis	48
3.8.3	Dilatometer	49
<b>4</b>	<b>RESULTS AND DISCUSSION</b>	<b>50</b>
4.1	Bending Strength	50
4.2	Density Measurement	51
4.3	Texture analysis	51
4.4	Thermo-Gravimetric Analysis	52

4.5	Differential Thermal analysis	52
4.6	Coefficient of Thermal Expansion	53
4.7	Optical Metallography	53
4.8	Phase Analysis by X-ray Diffraction	55
<b>5</b>	<b>CONCLUSIONS</b>	<b>56</b>
<b>6</b>	<b>SUGGESTIONS FOR FUTURE WORK</b>	<b>57</b>
<b>7</b>	<b>BIBLIOGRAPHY</b>	<b>58</b>

Tables

Figures



## 1 INTRODUCTION

Ceramic insulators are widely used in the electrical power-transmission system. They possess a number of valuable properties - high mechanical and electric strength, good chemical resistance etc. As these are clay products, their properties are related to the structural modification of clays when they are fired. The mechanical strength, chemical resistance etc. of the insulating material increase as the amount of mullite phase in its structure is increased. The properties of these type of material are determined to a considerable extent by the mullite content, the amount and properties of the feldspar glass, and also the volume of sealed pores. As the quartz and the residue left from other impurities dissolve in the glass, the insulator skeleton becomes weaker and there is more deformation. Depending on the fineness of the grinding of the quartz, the composition of the mixture, the temperature and the period of the firing, from 15 to 40 per cent of the total amount of quartz added to the mixture enters the vitreous phase. The mullite crystals formed in the insulator improve the structural toughness of the product during firing. Mullite produced by heating up to 1400°C for 1 hour appears under the microscope pseudomorphic with kaolinite.

The formation of mullite is catalyzed by the presence of only 1 per cent ZnO, LiO<sub>2</sub>, MgO, Fe<sub>2</sub>O<sub>3</sub>, MnO, Ce<sub>2</sub>O<sub>3</sub> and MeO<sub>3</sub>; B<sub>2</sub>O<sub>3</sub> and CaO are less effective, Na<sub>2</sub>O, K<sub>2</sub>O, TiO<sub>2</sub> and SnO<sub>2</sub> least of all. Their catalytic action varies with temperature; Li<sub>2</sub>O and MgO are active at both high and low, ZnO only at high temperatures. Catalysts containing 4-5 components are the most effective, e.g. mixture of 2 MnO-1 MgCl<sub>2</sub>-2 TiO<sub>2</sub>-4 CaF<sub>2</sub>.

Owing to the high proportion of silica in fired clay its presence in the free, crystalline state  $[3(\text{Al}_2\text{O}_3 \cdot 2\text{SiO}_2) = 3 \text{Al}_2\text{O}_3 \cdot \text{SiO}_2 + 4\text{SiO}_2]$  must always be expected beside mullite. The silica can be demonstrated by X-ray methods. The dilatometer, furthermore, occasionally discloses a well developed cristobalite phase at its conversion temperature of about 230°C, more rarely the tridymite phase at 117°C.

The formation of mullite from clay is not quantitative, because part of the theoretically possible amount dissolves in the glass formed from the fluxes. The presence of mullite in ceramic materials is nearly always regarded favorable, because it improves the properties of the product owing to its great hardness and low coefficient of expansion. The main production of mullite takes place between 1000° and 1200°C, i.e. after production of a glassy melt, and it increases further between 1200° and 1500°C. The mullite content found was 7-9 per cent less than the amount calculated from the chemical composition of the raw materials; the rest had probably entered the glassy phase.

Thus quality of the fired products depends on the rate of firing, rate of sintering, growth of crystalline structure etc. According to the reaction kinetics, the rate of solid state reactions and growth of crystalline structure can be increased by addition of some catalytic oxides to the clay - feldspar mixture. The fluxing effect of these alkaline earth oxide lowers down the formation temperature of the crystalline phases and thus gives enough time to grow. These alkaline earth oxides act as the preferred sites to nucleate the crystalline phases, thus increases the toughness and strength of the resulting body.

Bangladesh Insulator and Sanitary ware Factory (BISF) is one of the leading organizations in producing the ceramic insulating materials in Bangladesh. A research work was carried out using the BISF body materials to study structural and thermal expansion characteristics of the materials produced for research and attempts were taken to improve the quality of these materials. A number of clays were mixed with feldspar and then the processed material was fired. Feldspar was used as fluxing material to reduce the firing temperature. Alkaline earth oxides, i.e., zirconium silicate, zinc oxide, titanium oxide, manganese oxide etc. were added from 2 to 4 per cent as fluxing materials for the ceramic insulator. Thus the material with no alkaline earth and with alkaline earth oxides were fired and their comparative study was carried out in respect to strength, texture, and some thermal properties. The tools used to study these properties include the bending strength to measure strength properties, the x-ray diffraction technique to make crystalline identification, neutron diffraction technique to do texture analysis, and DTA, TGA, dilatometry to perform thermal analysis.

## 2 THEORETICAL BACKGROUND

### 2.1 Electrical Insulators

Electrical insulators are required to isolate all electrical circuits. Ceramics are used where high strength, elevated temperature, heat dissipation, or long-term hermeticity (sealed from pressure to the atmosphere) are required. The most demanding application for high-resistivity ceramics is insulators for high-voltage power lines. Most people are aware that ceramics are used for these insulators, but do not realize how demanding the application really is. First, the insulators must be very strong because they support the weight of the power lines and should endure during a heavy wind or any other catastrophic calamities. Then the material should be considered how long these insulators are designed to last. They must be highly reliable. Second, the insulator must be resistant to weather damage and to absorption of water. Internal adsorption can result in arcing at the high voltages involved.

Ceramic materials that are good electrical insulators are referred to as dielectric materials. Although these materials do not conduct electric current when an electric field is applied, they are not inert to the electric field. The field causes a slight shift in the balance of charge within the material to form an electric dipole, thus the term "dielectric" applies. Electrons can move when a material has electron energy levels that overlap or are not filled. Ions can move when point defects are present in the crystal ions in large structural channels. Most ceramics do not have mobile electrons or ions and do not permit passage of an electrical current when placed in an electric field. These non conductive ceramics are called electrical insulators. The high value of electrical resistivity for these materials results from the way that the electrons are tied up during atomic bonding. In each case, valence electrons are either shared (covalently) or transferred (ionically) such that each atom achieves a full outer shell of electrons. This leaves no overlap of electron energy bands and no low-energy mechanisms for electron conduction (Fig. 2.1).

The specifications for insulators cover surface and breakdown resistance, dielectric strength, dielectric constant and dielectric loss. Surface resistance depends mainly on the dirt and absorption layer on the glaze surface and is, therefore, not a material constant of the insulator body. All the same, the nature and the condition of the surface is of importance. Surface resistance falls rapidly in moist air: at 40 per cent relative humidity it may be 2000000 M $\Omega$ , at 60 per cent 65000, at 80 per cent 2000 and at 100 per cent only 100.

Flash-over tension is defined as the potential gradient (KV/cm) at which, on slowly raising the voltage, a flash-over occurs in the air outside the solid or liquid insulator. As moisture has a strong but variable influence on the flash-over tension, it is measured on air-dry insulators.

The electrical breakdown, or puncture, resistance is one of the most important properties of an electric insulator. It gives the potential gradient (KV/mm) at which a spark discharge will take place through the material, i.e. at which the insulator will fail. Expressed in another manner, electrical strength is the voltage at which puncture of a plate of the material of 1 mm thick occurs. On raising the temperature it decreases slightly up to 150°C. Because of the unavoidable irregularities in the body breakdown resistance is not directly proportional to thickness, but diminishes with increasing thickness. Slabs of porcelain 3 mm thick subjected to 1 KV/sec voltage increase have an electrical breakdown resistance of 30-40 KV/mm.

Insulation resistance, on the other hand, is a true material constant of the porcelain, determined according to Ohm's law (ohmic resistance). Conductivity, the reciprocal of resistivity, becomes appreciable only above about 300°C.

The dielectric constant indicates how much denser the electric force field is in the insulating medium than in dry air. It is affected by temperature and the frequency of the applied electric field or the frequency of other electromagnetic fields impinging on the material. For porcelain, the dielectric constant lies between 5.7 to 8.0.

Dielectric losses only occur with alternating current. They represent the work done in reversing the electric fields in the body (dielectric hysteresis) and must be kept low. The losses reappear as heat, but have nothing to do with heat losses due to the passage of current (resistance heat losses). In America they are measured by the power factor,  $\cos\theta$ ,  $\theta$  being the phase angle. The power loss,  $N$ , can be expressed by  $N = V^2 \cdot 2\pi \cdot f \cdot C \cdot \tan\theta$ , where  $V$ =voltage,  $f$ =frequency,  $C$ =capacity, and  $\theta$ =loss angle.  $C$  can be expressed by the dielectric constant,  $\epsilon$ , and a shape constant,  $K$ , which depends on the form of the insulator, so that  $N = V^2 \cdot 2\pi \cdot f \cdot K \cdot \epsilon \cdot \tan\theta$ . Since all other magnitudes depend on type of current and construction of the insulator, we are left with  $\epsilon$  and  $\tan\theta$  as material constants. They must be kept low in order to reduce losses of a.c. insulation (especially for high frequency). Energy loss can be large even with a low loss angle at high radio frequencies and high voltages.

Electrical conductivity and dielectric loss depend on the migration of ions in the glassy phase, the movement of loosely bound ions on crystal surfaces and that of ions in the

crystal lattice. The in the crystal lattice must be mobile or there must be holes in the lattice. After a certain activation energy has been reached, conductivity rises exceptionally with temperature. The lowest dielectric loss occurs in homogeneous glasses free from striae and in bodies with uniformly distributed small crystals.  $\tan\theta$  diminishes with rising frequency; at constant frequency and with rising temperature both  $\tan\theta$  and  $\epsilon$  generally fall, and likewise their product, the loss factor. The extent of the fall depends on the shape of the article.

## 2.2 Porcelain

Porcelain is the term used to describe white-vitrified ceramic ware, translucent in thin layers, impermeable to fluids, and manufactured from a fine mixture of kaolin, quartz, feldspar, and plastic white-firing clay. Porcelain is the most noble of ceramic products: the fired ware is usually white, always translucent and of very low porosity (0.01-6 per cent closed pores). The densification is due to the use of feldspar as a flux. The clay substance incorporated is nearly always in the form of kaolin, and quartz is never absent.

As a technical material, porcelain possess a number of valuable properties - high mechanical and electric strength, good chemical resistance and spalling resistance. Household porcelain has exceptional decorative quantities. The combination of these properties in the material made from commonly found crude minerals has resulted in the effective use of porcelain for a great variety of purposes in present-day science, engineering, and every-day life.

A distinction is made between 'hard' and 'soft' porcelain. Mixtures for hard porcelain contain more kaolin and less feldspar and are fired at higher temperatures than the mixtures used for soft porcelain.

Hard porcelain exhibits high mechanical strength, good dielectric characteristics, and high chemical and spalling resistance.

Porcelain is highly resistant to the action of all acids except hydrofluoric. In cases of prolonged action of phosphoric acid or alkalis, it is advisable to use unglazed porcelain.

Hard porcelain is made into chemical apparatus and laboratory vessels, thermocouple tubes, and such electric-insulation parts as high voltage insulators and installation electric porcelain.

The mechanical strength, spalling and chemical resistance of porcelain increase as the amount of mullite phase in its structure is increased. This can be done by using a greater content of kaolin in the mixture. However, kaolin can only be added within certain limits, since the mixture loses its plasticity and the firing temperature for the ware is increased when the amount of kaolin is increased.

The most outstanding properties of porcelain for domestic and artistic uses are whiteness of the fired body, its translucency, impermeability to gases and liquids, hardness and comparatively high resistance to mechanical and thermal shock; for technical purposes, in addition to the last four, there is high dielectric strength.

### 2.3 Electrical Porcelain

A large proportion of the porcelain manufactured does not serve household or laboratory purposes but is used for insulating electric equipment. The so-called electrical porcelain industry has become a large-scale producer for both low-tension and high-tension purposes.

For electrical insulation, completely vitrified ceramic products have the advantage over porous products that no spark path which might lead to localized melting and disruption can form in their interior. Maximum possible densification is therefore essential. Biscuit firing is often dispensed with, the green shapes being dipped air-dry and fired glost directly. Dielectric strength is much improved if the alkalis in porcelain are replaced by alkaline earths; it is only approximately proportional to porosity.

Pore spaces in porcelain lower the loss factor and the dielectric constant, provided that moisture is rigidly excluded: the slightest trace of water causes both to increase. Fine grinding of the raw materials lowers the sintering temperature and increases the mechanical and electrical strength (breakdown resistance).

Only from the practical but not from the scientific point of view porcelain may be regarded as an insulator since, apart from a perfect vacuum, there are no perfect insulators. Among refractory insulators the pure oxides,  $\text{SiO}_2$  and  $\text{Al}_2\text{O}_3$  in particular, are known to satisfy the most rigorous demands. In proportion as they contain other oxides, especially alkalis, their electrical strength deteriorates. Porcelain consists of an acidic glass and crystals, and it is the glass that mainly determines the properties. In glasses part of the alkali content is present in the form of ions, which even at  $200^\circ\text{C}$  have



considerable mobility in an electric field. Glass thus conducts current in the same way as salt solutions and, in fact, may be regarded as a supercooled liquid.

Electrical porcelain differs from domestic hard porcelain in containing considerable quantities of plastic clay, used to substitute part of the kaolin and feldspar. Bleininger and Riddle<sup>1</sup> advocated replacing feldspar by aluminosilicates of magnesium, beryllium or the alkaline earths. The dimensional accuracy of the products is said to be increased by replacing quartz by calcined kaolin, alumina, zirconium oxide or sillimanite.

#### **2.4 Chemical Composition of Ceramic Insulating Materials**

Clay materials do not have strong bonding capacity when fired. Some clays do not have proper vitrification characteristics, that is, they are not plastic. Some clays show extensive plasticity. Plastic clays show excellent bonding characteristic but their linear coefficient of thermal expansion is very poor for the electrical porcelain ware. Since a steady dimensional property of the ceramic insulator material is must for every engineering application, a variety of clays with plastic and non plastic property are mixed to get the highest possible stable form. On the other hand, clay product only does not show the required strength for certain electrical application. In electrical power transmission system, the insulator materials not only withstand the electrical energy but also the line tension. Mullite, the only crystalline phase responsible for high strength, appears from clay materials at higher temperature, i.e., 1500-1600°C. Commercially this high temperature is not economical for the production of the insulators. A variety of fluxing materials can be added to the clay material to get not only the higher mechanical bonding strength but also lower the temperature at which mullite can form. Commercially added fluxing materials are usually potash feldspar. This feldspar not only produces the dense product but also lower down the firing temperature of the material. If adequate  $\text{SiO}_2$  is not present in the clays, some quartz can be added. Actually silica and alumina are the basic constituent of the conventional ceramic insulator materials. Other oxides which are present in the raw materials act as impurities, i.e., lower down the firing temperature of the material.

Figure 2.2 shows how mechanical and electrical strength and thermal shock resistance depend on the composition of the body. It is evident that the best possible values of these three technically important properties cannot be attained in one and the same body. Fineness of grinding of the raw materials has a marked influence on the properties of porcelain, as has been confirmed by numerous detailed studies.

A typical proportion of the raw materials of the conventional BLSF insulator body is given in Table 2.1.

## 2.5 Mechanism of Formation of Porcelain

Porcelain ware shows an almost complete lack of open pores (water absorption not greater than 0.5%) and has high strength, good spalling resistance, and chemical inertness.

Various types of porcelain are obtained through the physical and chemical interaction of the argillaceous matter, quartz, and feldspar at high temperatures. In Fig. 2.3, showing the ternary system kaolin-quartz-feldspar, the areas of formation of different types of porcelain are indicated by the sintering isotherms for different mixtures at 1160, 1200 and 1280°C. The degree of sintering changes sharply as a function of the firing period and the degree of pulverization of the materials.

Individual structural elements in the porcelain have varying effects on its strength, whiteness, translucence, and certain other qualities. Study of the formation of porcelain has revealed the effect of technological factors on the development of special structural characteristics associated with the basic properties of a given type of porcelain product (the high mechanical and electric strength of insulators, the high chemical and spalling resistance of laboratory porcelain vessels etc.).

The phase composition and properties due to it depend on the kaolin and plastic clay, quartz, and feldspar content in the porcelain mixture, on the chemical composition of these materials and degree of pulverization, and also on the temperature and period of firing. Improvement of a particular property is often brought about at the expense of another; for example, an improvement in translucence is accompanied by reduction in mechanical strength and by an increase in the number of deformed items produced during firing. In such cases the problem arises of selecting a composition and firing conditions that will make it possible to obtain products with the right combination of properties for the given purpose.

The texture of porcelain and its most important properties are determined by the quantitative relationship between the crystalline and vitreous phases. The amount and quality of the vitreous phase in the porcelain depend, in turn, on the composition of the mixture, the fineness of grinding of the initial materials, and the firing conditions.

Extensive microscopic research has shown the following principal structural elements in porcelain:

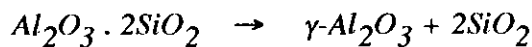
1. a vitreous isotropic mixture consisting of feldspar glass with different degrees of saturation by  $Al_2O_3$  and  $SiO_2$ ;
2. fused quartz particles which have not dissolved in the glass;
3. mullite crystals ( $3Al_2O_3 \cdot 2SiO_2$ ), distributed mainly in the silica-feldspar glass melt;
4. pores;

The formation of porcelain is shown schematically in Fig. 2.4. The drawings represent the phenomena occurring at different stages of the process (I-V) between the grains of kaolinite, quartz, and feldspar, the basic components of the porcelain mixture. Small additions of other oxides finding their way into the mixture with the basic raw material are not taken into account in the diagram because of their negligible effect on the process. As shown in the diagram, the feldspar grains 3 are located between the aggregates of clay particles 1 and the quartz grains 2.

During the first stage of firing, principally within the temperature range 500-550°C, as can be seen from the thermogram Fig. 2.5, dehydration of the kaolin occurs in accordance with the following reaction:

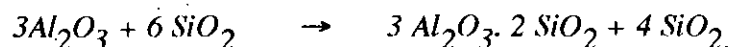


with a corresponding endothermal effect. Between 800 and 900°C the metakaolinite decomposes into oxides, the initial shape of the kaolinite platelets being preserved:



Within the range 950-1000°C, crystallization of  $\gamma-Al_2O_3$  occurs, accompanied by a considerable exothermal effect.

When the oxides are further heated, the  $Al_2O_3$  and  $2SiO_2$  interact between 1150 and 1250°C, accompanied by the formation of mullite and free silica in the form of cristobalite or tridymite (when the temperature is further raised) as follows:



The dissolving of the quartz and decomposition products of the kaolinite in the feldspar glass occur to a more or less complete extent, depending on the temperature and firing

period; thus, the amount and composition of the feldspar glass in the porcelain vary within wide limits.

On the basis of theoretical calculations as well as the study of different samples, it can be stated that porcelain contains about 50 volume per cent feldspar glass.

As the content of feldspar is increased, the translucence of the porcelain is improved. Increasing the temperature and prolonging the firing period, keeping all other things being equal, help to increase the amount of glass in the porcelain and also further enriches the  $\text{SiO}_2$  and  $\text{Al}_2\text{O}_3$  content.

The properties of porcelain are determined to a considerable extent by the mullite content, the amount and properties of the feldspar glass, and also the volume of sealed pores. The technical properties of feldspar glass are improved as the amount of  $\text{Al}_2\text{O}_3$  is increased. As the quartz and the residue left from other impurities dissolve in the glass, the porcelain skeleton becomes weaker and there is more deformation. Depending on the fineness of the grinding of the quartz, the composition of the mixture, the temperature and the period of the firing, 15 to 40% of the total amount of quartz added to the mixture enters the vitreous phase. The mullite crystals forming in the porcelain improve the structural toughness of the product during firing.

An equally important structural component of porcelain is the quartz particles that have not dissolved in the feldspar glass; these particles, together with the mullite crystals, form the porcelain skeleton.

Mullite possesses a number of valuable properties, such as a high melting point, high mechanical and electrical strength, chemical resistance, a low coefficient of thermal expansion, and, consequently, high spalling resistance. The nucleation of mullite crystals even occurs at temperatures of about  $1200^\circ\text{C}$ . But at comparatively low temperatures the crystals grow extremely slowly. At the firing temperature an intensive growth of the crystals, and the feldspar glass becomes abundantly inter grown with mullite needles.

An increase in the amount of fusible in the porcelain and a higher firing temperature help to increase the amount of vitreous phase and help it to fill up the pores. However, firing porcelain at temperatures above the norm for the given mixture results in the liberation of gas from the feldspar glass, bloating of the porcelain, and a decline in quality. The pores reduce the mechanical and electrical strength of porcelain, its chemical resistance, translucence, and certain other valuable properties. Thus for critical parts the porosity should not exceed 0.1-0.3% ( in terms of water absorption).

Raising the firing temperature and increasing the amount of vitreous phase above 45% slightly reduces the mechanical strength of the porcelain. The electrical strength increases with an increase in the firing temperature or in the length of the period for which the ware is held at the final temperature (Fig. 2.6 and 2.7 curve 2). The curve showing the variation in mechanical strength as a function of the final holding period (Fig. 2.8 curve 1) reveals that holding for 3-6 hours at the final temperature during the "maturation" period produces porcelain with maximum strength. If the holding period at the final firing stage is prolonged, the mullite crystals partly dissolve in the feldspar glass, as a result of which the dielectric characteristics of the vitreous phase and the porcelain are improved.

A great effect on the mechanical, and particularly on the electric resistance of the porcelain, is exerted by the porosity of the products. In high-grade high-voltage insulators, there are usually no open pores at all. If the porcelain is held for a long enough period at the final firing temperatures, the pores become spherical in shape due to the increased viscosity of the vitreous phase. Thus loses its electrical breakdown strength.

## 2.6 Ceramic Phase Equilibrium Diagram

At equilibrium a system is in its lowest energy state for the composition, temperature, pressure, and other conditions imposed on it. The time that it takes to reach this equilibrium state from any arbitrary starting point depends on other factors in addition to the final state that is eventually attained. Consequently, equilibrium conditions are only part of the story in determining what the actual structure of any real ceramic will be. However, it is always useful to have a clear understanding of what this final state is.

Phase equilibrium diagrams provide a clear and concise method of graphically representing what the equilibrium situation is for given conditions of concentration, temperature, and pressure. As such they are an invaluable tool, being used for recording the number of phases present, the composition, and the relative amounts of each phase present at equilibrium. In the following paragraphs, some important phase diagrams of one, two, three components systems is discussed which will be helpful in describing this present interest.

### 2.6.1 One component system - The $\text{SiO}_2$ system

Fig. 2.9 shows the pressure - temperature equilibrium diagram of most common one component system, i.e., silica. There are five condensed phases which occur at

equilibrium  $\alpha$ -quartz,  $\beta$ -quartz,  $\beta_2$ -tridymite,  $\beta$ -cristobalite, and liquid silica. The transition temperatures at 1-atmosphere pressure are also shown in the diagram. The  $\alpha$  to  $\beta$  quartz transition at  $573^\circ\text{C}$  is rapid and reversible. The other transformations shown are sluggish, so that long periods of times are required to reach equilibrium. The vapor pressure shown in the diagram is a measure of the chemical potential of silica in different phases. The same kind of diagram can be extended to include the metastable forms of silica which may occur (Fig. 2.10). The phase with lowest vapor pressure (the darker lines on the diagram) is the most stable at any temperature, hence called the equilibrium phase.

However, once formed the transition between cristobalite and quartz is so sluggish that  $\beta$ -cristobalite commonly transforms on cooling into  $\alpha$ -cristobalite. Similarly,  $\beta_2$ -tridymite commonly transforms into  $\alpha$ - and  $\beta$ -tridymite rather than into the equilibrium quartz forms. Similarly, when cooled, the liquid forms silica glass which can remain indefinitely in that state at room temperature.

At any constant temperature there is always a tendency to transform a phase into another phase of lower free energy (lower vapor pressure), and the reverse transition is thermodynamically impossible. It is not necessary, however, to transform into the lowest energy form. For example, at  $1100^\circ$  silica glass could transform into  $\beta$ -cristobalite,  $\beta_2$ -tridymite or  $\beta$ -quartz. Which one of these transformations actually takes place is determined by the kinetics of these changes. In practice, when silica glass is heated for a long time at this temperature, it crystallizes, or devitrifies, to form cristobalite which is not the lowest energy form but is structurally the most similar to silica glass. On cooling,  $\beta$ -cristobalite transforms into  $\alpha$ -cristobalite.

The form with the lowest vapour pressure at a given temperature is the most stable. The diagram contains curves for quartz, tridymite, cristobalite and silica-glass. Part of each curve is in full line, part in broken; the former represents the stable, the latter the unstable region. The line for quartz is full up to  $870^\circ\text{C}$ , where it is cut by the curve for tridymite. This means that quartz is the stable form up to  $870^\circ\text{C}$ ; within this range it undergoes an enantiomorphic transformation from  $\beta$ - to  $\alpha$ -quartz at  $573^\circ\text{C}$ . The quartz curve is continued in the form of a broken line up to  $1600^\circ\text{C}$ , the melting point of  $\alpha$ -quartz. Tridymite, like cristobalite and silica glass, is thus unstable up to  $870^\circ\text{C}$ , even though its conversion to quartz below this temperature may not take place in finite time. At  $117^\circ\text{C}$  ( $100^\circ$ - $118^\circ\text{C}$ )  $\gamma$ -tridymite inverts to  $\beta$ -tridymite, at  $163^\circ\text{C}$  ( $140^\circ$ - $165^\circ\text{C}$ ) to  $\alpha$ -tridymite<sup>2-4</sup>. This is stable only upto  $1470^\circ\text{C}$ , at which point it inverts to cristobalite. Tridymite melts at higher temperature than quartz, namely at  $1670^\circ\text{C}$ .

Cristobalite has an inversion point<sup>5</sup> at 230°C (180°-260°C), is stable above 1470°C and has the highest melting point of all crystalline forms of silica (1728°C). Above this temperature only the melt is stable. If cooled rapidly below the melting point of cristobalite it remains in its amorphous condition and forms silica glass. Silica glass has the highest vapour pressure of all forms of silica and the largest internal energy content. On de-vitrifying (crystallizing) it liberates some of its internal energy in the form of heat of crystallization.

### 2.6.2 Two component system - The $\text{Al}_2\text{O}_3$ - $\text{SiO}_2$ system

The  $\text{Al}_2\text{O}_3$  -  $\text{SiO}_2$  diagram is of fundamental importance in ceramics. The diagram which is shown in Fig. 2.11 has been repeatedly studied, in view of its exceptional importance in the interpretation of the physicochemical processes which are involved in the firing, melting and crystallization of different aluminosilicate ceramics, and in the understanding of the effects resulting from the interaction of these ceramics with corrosive substances.

In this system, there is one compound present, mullite, which is shown as melting congruently. The eutectic between mullite and cristobalite occurs at 1595°C and contains about 94%  $\text{SiO}_2$ . The solidus temperature between mullite and alumina is at 1840°C.

Factors affecting the fabrication and use of several ceramic products can be related to this diagram. They include refractory silica brick (0.2-1.0%  $\text{Al}_2\text{O}_3$ ), clay products (35-50%  $\text{Al}_2\text{O}_3$ ), high-alumina brick (60-90%  $\text{Al}_2\text{O}_3$ ), pure fused mullite (72%  $\text{Al}_2\text{O}_3$ ), and pure fused or sintered alumina (>99%  $\text{Al}_2\text{O}_3$ ). Table. 2.2 shows the invariant points of the system  $\text{Al}_2\text{O}_3$ - $\text{SiO}_2$ .

### 2.6.3 Three component systems

Many ternary systems are of interest in ceramic science and technology. The  $\text{K}_2\text{O}$ - $\text{Al}_2\text{O}_3$ - $\text{SiO}_2$  system is illustrated in Fig. 2.12. This system is important as the basis for many porcelain compositions. The eutectic in the subsystem potash feldspar-silica-mullite determines the firing behavior in many compositions. Porcelain compositions are adjusted mainly on the basis of (a) ease in forming (b) firing behavior. Although real systems are usually somewhat more complex, this ternary diagram provides a good description of the compositions used.

Very often constant temperature diagrams are useful. These are illustrated for subsolidus temperatures in Fig. 2.12 by lines between the forms that exist at equilibrium. These lines form composition triangles in which three phases are present at equilibrium,

sometimes called compatibility triangles. Constant-temperature diagrams at higher temperatures are useful, as illustrated in Fig. 2.13, where the 1200° isothermal plane is shown for the  $K_2O-Al_2O_3-SiO_2$  diagram. The liquids formed in this system are viscous; in order to obtain vitrification, a substantial amount of liquid must be present at the firing temperature. From isothermal diagrams the composition of liquid and amount of liquid for different compositions can be determined easily at the selected temperature. Frequently it is sufficient to determine an isothermal plane rather than an entire diagram, and obviously it is much easier.

## **2.7 Heat Treatment of Clays**

As clays are the most important part of the raw materials of the ceramic products, their behavior during firing in different ranges must be discussed. This will provide a valuable key rule in determining the firing schedule when the product are fired.

### **2.7.1 Phase changes which occur on heating kaolin clays**

The method of differential thermal analysis, when applied to kaolin minerals and to clay deposits containing principally kaolin minerals, shows a prominent endothermic effect in the region of 550-700°C, due to the dehydration of the mineral (the precise temperature depends on the particular kaolin mineral), followed by two exothermic reactions, the first at roughly 950-1000°C and the second between 1150° and 1250°C, which correspond to the formation of new minerals (Fig 2.5).

#### **2.7.1.1 Heat treatment in the range 600-800°C**

It is generally misleading to regard the structural breakdown purely as a function of the temperature. The time of heating is also important and (when the temperature is variable) the rate of heat-treating. This applies equally to the exothermic processes at higher temperatures, and for this reason it is difficult to make precise comparisons between results obtained under very different thermal conditions. Extreme cases are those in which the mineral is soaked for a long period, e.g. 24 hours, at a fixed temperature, and in which it is brought quickly to give temperature and then immediately cooled.

The water of constitution remaining in the clay after drying is not completely expelled below some temperature between 450° and 600°C. Water is slowly given up, however, below this temperature, and its loss is initially accompanied by a slight contraction. The contraction following the removal of moisture on drying in the air or heating at 110°C



must be regarded as due to shrinkage of the gel films on the clay particles accompanying loss of gel water. This finding may be regarded as furnishing experimental support for the view that the plasticity of clays depends in part on the existence of swollen gel layers surrounding the clay particles. Slowly heated clays show that kaolin and most clays undergo expansion up to about 500-600°C, followed by contraction.

Water of constitution is not expelled from the clay substance uniformly and gradually, but within a narrow temperature interval between 450° and 600°C. This has been clearly demonstrated for kaolin by Le Chatelier<sup>7</sup> who embedded a thermocouple junction in a sample which was then heated in an electric oven, the temperature being raised steadily. As shown in the Fig. 2.14, there was a retardation in the temperature rise registered by the thermocouple at about 550°C and a marked acceleration at about 1000°C. This indicates an absorption of heat, i.e. an endothermic reaction, at about 550°C and a strong development of heat, i.e. an exothermic reaction, at about 1000°C. Le Chatelier and many investigators<sup>7</sup> after him confirmed this observation with all kinds of clays. The similarity in the changes in the curves indicates that they are due to material changes common to all clays. Where the composition differs from  $\text{Al}_2\text{O}_3 \cdot 2\text{SiO}_2 \cdot 2\text{H}_2\text{O}$ , the clays will have other characteristic temperature.

The rate of heating has a pronounced effect on this endothermic reaction and subsequently different decomposition temperatures have been given for clays by different research workers. At a rate of heating of 1000°C/h, decomposition starts at about 550°C but with the slower rate of 200°C/h it starts at about 460°C. By heating in vacuo the temperature of expulsion of water can be strongly depressed, as Mellor and Holdcroft<sup>8</sup> demonstrated.

### ***The product formed by dehydrating kaolin minerals***

After dehydration the kaolin minerals become practically amorphous and cease to give an X-ray pattern of lines Weiss and Rowland<sup>9</sup>. Earlier workers stated that after dehydration a very diffuse band only is obtained on powder photographs. Whether or not this band corresponds to a strictly amorphous state has been much discussed; a further question is whether the material, if it is amorphous, is a mixture of alumina and silica or is an aluminium silicate. The dehydrated material is almost certainly not a normal mixture of the two components and various names have been given to it, such as metakaolin and pro-mullite. From an early investigation Hyslop and Rooksby<sup>10</sup> thought they had found a crystalline dehydrated product, but this was subsequently shown by Insley and Ewell<sup>11</sup> to have been a mica impurity which became more prominent in the X-ray diagram after the removal of the kaolinite pattern by heat treatment. Hyslop<sup>12</sup> considered

that the diffuse band given by metakaolin (the term now being used simply to signify a kaolin mineral heated beyond the dehydration stage) was characteristic of amorphous silica, but Comeforo, Fischer, and Bradley<sup>13</sup> consider the band "is more distinct than such bands from strictly amorphous solids" and from electron microscope studies have shown that the characteristic kaolin (hexagonal) plates persist "far above the dehydration temperature of kaolinite".

### *Hypothesis of breakdown into oxides*

After discussing the release of water from clay it is appropriate to consider the residual solid. The question arises whether this product is an anhydride of the formula  $\text{Al}_2\text{O}_3 \cdot 2\text{SiO}_2$  or whether it decomposes further. Light was thrown on to this problem first by the finding of Sachsse and Becker<sup>14</sup> that the whole of the alumina in kaolin can be dissolved in dilute hydrochloric acid (5 per cent conc.) after heating at a dull red heat, whereas ignition at a bright red heat renders it insoluble again. The  $\text{SiO}_2$  produced on ignition is soluble in dilute alkali. More exact studies were subsequently made by Sokolov<sup>15</sup> and he concluded that the clay substance on decomposing broke down into the free oxides  $\text{Al}_2\text{O}_3$ ,  $\text{SiO}_2$  and  $\text{H}_2\text{O}$ ; the alumina can be dissolved in 5 per cent HCL, the  $\text{SiO}_2$  in dilute caustic alkali. This view was later supported by Mellor and Holdcroft<sup>16</sup>, Keppeler<sup>17</sup>, Tammann and Pape<sup>18</sup>, and Rooksby<sup>19</sup> who added that the alumina in calcined kaolin behaves in exactly the same way as the corresponding amount of free alumina. For example, on heating above  $900^\circ\text{C}$  both become difficultly soluble, evolve appreciable and equal amounts of heat, increase in density and both lower the dissociation temperatures of the carbonates of the alkaline earths by the same amount, namely  $220^\circ\text{C}$ . Furthermore, on heating mixtures of alumina and silica the same exothermic effect is observed at  $940^\circ\text{C}$  as occurs with kaolin. Krause<sup>20</sup> believed that he had obtained proof of the breakdown of kaolin into the oxides from X-ray studies. Further support for the theory was provided by Biltz and Lemke<sup>21</sup>.

### *Hypothesis of silicate formation*

In contrast to the above views, a theory first propounded by Vernadsky<sup>22</sup> assumes that kaolin does not break down into free oxides on dehydration but yields a silicate with the formula  $\text{Al}_2\text{O}_3 \cdot 2\text{SiO}_2$ . The low density of dehydrated kaolin ( $2.32\text{-}2.38 \text{ g/cm}^3$ ) was adduced as proof, for a mixture of the oxides ought to have the density 3.08, the silica being assumed to be present as cristobalite. It should be borne in mind, however, that the high density of corundum cannot be ascribed to  $\text{Al}_2\text{O}_3$  in this form. It was found impossible by bromoform flotation to separate finely powdered dehydrated kaolin into

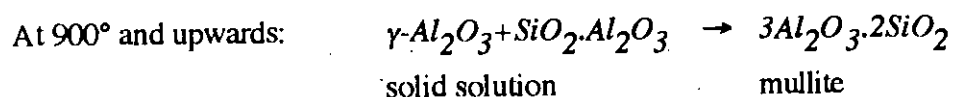
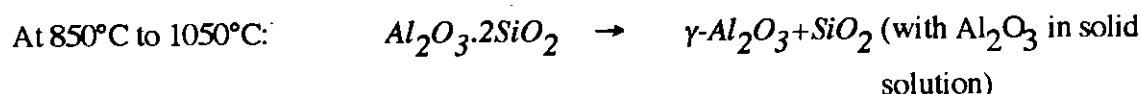
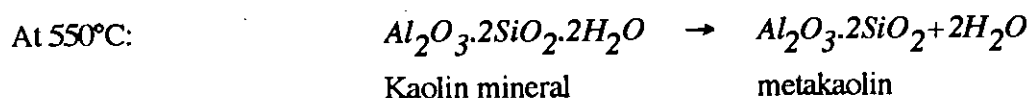
the free oxides according to their different specific gravities, as might have been expected. From this Agafonov and Vernadsky<sup>22</sup> concluded that they did not exist free but in combination as a silicate. Against this argument the objection must be raised that no comminution process known could separate a molecular mixture of oxides into the individual species. Even if kaolin decomposes into the oxides, comminution will only yield particles consisting of a mixture. For the same reason all other comparisons between the physical properties of dehydrated clay or kaolin, on the one hand, and artificial mixtures of the oxides, on the other, are invalid.

The homogeneity of dehydrated kaolin is reflected in its behavior under attack by chemicals. Caustic potash and hydrofluoric acid dissolve alumina and silica in the ratio 1:2<sup>23-24</sup>. Vesterberg<sup>25</sup> endeavored to clarify the nature of the oxides by attempting to extract the silica with a caustic soda solution, which will dissolve finely divided silica alone readily but leaves alumina unaffected. No silica could be dissolved from dehydrated kaolin by this means, which appears to support the conclusion that the two oxides are combined. The solubility experiment of Sachsse and Becker yields quite different results when carried out with dilute hydrochloric acid, as was first demonstrated by Von Fuchs<sup>26</sup> in 1821. On warming with this acid the whole of the alumina in the dehydration product goes into solution, provided the kaolin has been heated at 750-800°C for 3 hour or more.

X-ray spectrography has been applied to this problem by Rinne<sup>27</sup>, who argued that if free oxides are present in dehydrated kaolin, interfaces corresponding to one of the crystalline modifications of silica, i.e. quartz, tridymite or cristobalite, should be observed. He obtained no sharply defined line spectra, however, but only two diffuse bands and concluded that kaolin transforms into a silicatic dehydrated product 'metakaolin'. Hyslop<sup>10</sup> at first made the same deduction from an identical finding but later modified<sup>28-29</sup> his conclusions in the light of new X-ray spectra. In these the formation of a silicatic dehydration product was assumed but a transformation resulting in two new solid phases was observed at 870°C. One of these yielded the same line spectrum as  $\gamma$ -alumina which had been studied just previously by Hansen and Brownmiller<sup>29</sup>. By this observation the presence of free alumina in clays heated above 870°C was considered to be proved. Attempts to clarify the position microscopically must be less successful, since the minuteness and ill-defined structure of the clay particles frustrate observation. Spangenberg and Rhode<sup>30</sup> deduced from the ready solubility of the alumina and the insolubility of the silica a greater mobility of the alumina molecules in the lattice, the silica portion of which holds together even after dissolution of the alumina and yields a silica metamorphosis after metakaolin. This, in turn, constitutes a pseudo-

metamorphosis after kaolin, from which it differs morphologically in nothing more than a thickening of the individual lamellae. In their view the firm bonding of the silica in the lattice constitutes an argument against the presence of free oxides. They regard both oxide types as being arranged in sheets in the lattice. Even after removal of the alumina the silica remains behind in a structure of superimposed sheets loose enough to permit liquids to pass through.

Hyslop<sup>12</sup> assumed the following reactions to take place on heating kaolinite:



The conclusions reached may now be summarized as follows: all kaolinitic clays, after giving up their water, break down into an anhydride, 'metakaolin', which is a labile, reactive, amorphous quasi-compound with the formula  $\text{Al}_2\text{O}_3 \cdot 2\text{SiO}_2$ . The alumina in the lattice is mobile and can be dissolved out. At  $550^{\circ}$ - $830^{\circ}\text{C}$  metakaolin decomposes with formation of  $\gamma$ -alumina.

Eitel and Kedesdy<sup>31</sup>, using the electron microscope and electron diffraction, showed that the lamellar form of kaolin remains up to  $700^{\circ}\text{C}$ , though there is no true lattice. Metakaolin is able to absorb alkali hydroxide<sup>2</sup>. On further heating the  $\text{AlO}_6$  octahedral form  $\gamma$ -alumina. It appears that this starts at  $825^{\circ}\text{C}$  or higher according to grain size. The exothermal reaction at  $900^{\circ}$ - $1050^{\circ}\text{C}$  has been ascribed by some workers<sup>32</sup> to this  $\gamma$ -alumina formation, by others to the reaction of  $\gamma$ -alumina with  $\text{SiO}_2$  to form mullite<sup>33</sup>: if metakaolin is held at  $900^{\circ}\text{C}$  for 200 h, the lines of mullite appear. Then, however, there is no further exothermic reaction on heating rapidly to  $1000^{\circ}\text{C}$ .

### 2.7.1.2 Heat treatment in the range $800$ - $1400^{\circ}\text{C}$

From a survey of published data it is difficult to arrive at any final conclusion. The conflicting conclusions of different workers, all of whom identified the phases present by X-ray methods, may perhaps be partly attributed to a number of causes, such as (i) the effect of impurities associated with the clay mineral, (ii) the variety of heat treatments employed. As an illustration of (ii), the following may be quoted: Insley and Ewell<sup>110</sup>

heated specimens of kaolinite and dictite at 6°C per minute and then air-quenched from 925°C and 985°C, temperatures corresponding to the beginning and the maximum of the first exothermic reaction, and also from 1000°C and 1200°C. They also examined the effect of pre-heating at constant temperature for various temperatures between 840° and 910°C. Hyslop<sup>12</sup> examined one Scottish clay which was heated for 15 hours at 800°C followed by 20 hours at 1050°C or 20 hours at 1150°C.

### 2.7.1.3 The exothermic reaction at 900-1050°C

The heating curves of clays depicted in figure 2.15 exhibit sharp rises at 900 to 1000°C. This points to an exothermic reaction taking place in the material. Two reactions may be considered as possible causes of the evolution of heat: conversion of alumina from the  $\gamma$  to the  $\alpha$  form and a combination of  $\gamma$ -alumina and silica to form sillimanite or mullite. The first has often been studied on heating curves of pure specimens. It takes place with strong evolution of heat but does not invariably occur with all forms of alumina. Exceptions are, for instance, diaspore,  $\text{Al}_2\text{O}_3 \cdot \text{H}_2\text{O}$ , and hydrargillite,  $\text{Al}_2\text{O}_3 \cdot 3\text{H}_2\text{O}$ , but it is found with precipitated alumina, bauxite and  $\gamma$ -alumina<sup>30</sup>. Zwetsch<sup>28</sup> also observed the lines of alumina in X-ray spectra taken at 1000°C. On the basis of these observations, the formation of silicates from clay must be limited to higher temperature regions. The second reaction is theoretically possible, since the exothermic character of sillimanite formation from the oxides has been proved by Klever<sup>3</sup>:  $\text{Al}_2\text{O}_3 + \text{SiO}_2 = \text{Al}_2\text{O}_3 \cdot \text{SiO}_2 + 45.95 \text{ kcal}$ . He originally gave the temperature of formation as 1100-1200°C, but it may be assumed to start several hundred degrees lower with the intimate mixture of extremely fine, molecularly dispersed reactants present in mildly calcined kaolin. In this connection the statement of Hyslop and Rooksby<sup>10</sup> that sillimanite or mullite formation starts at 870°C deserves to be mentioned. Accordingly, we may attribute the exothermic reaction in this temperature range to the conversion of  $\gamma\text{-Al}_2\text{O}_3$  to  $\alpha\text{-Al}_2\text{O}_3$  and to aluminium silicate formation.

The specific surface,  $S$ , as determined by absorption of  $\text{N}_2$  or  $\text{O}_2$ , remains almost unchanged after heating to 800°C. It is practically uninfluenced by loss of water of constitution, although the 'holes' left in the lattice by the water lost are large enough to accommodate  $\text{H}^+$  ions. Nevertheless, the dehydrated kaolin shrinks and its lattice is in disarray. Above 900°C the apparent density increases markedly, and  $S$  decreases<sup>4</sup>.

### 2.7.2 Mullite formation and effect of alloy additions

No less than three naturally occurring silicates of alumina are known. They all have the formula  $Al_2O_3 \cdot SiO_2$  but differ in crystalline habit and physical properties. They are called sillimanite, andalusite and kyanite.

Owing to their importance in mineralogy and ceramics these three minerals have been intensively studied. Of prime importance in ceramics are the conditions under which they are stable, under which they are mutually convertible and under which they may occur in industrial products. At normal temperatures and pressures only one of them can be stable, and within its range of stability the other two must convert into the stable form unless the conversion rate is too low. This question was tested by Eitel and Neumann<sup>5</sup> by comparing their energy contents: as is well known, among various forms having the same chemical composition, that which has the lowest energy content is the most stable. Strictly speaking, all other forms must change into this stable form with evolution of heat (energy), though the rate of conversion may be extremely slow. The energy contents of different polymorphous but chemically identical compounds in a system can be determined by comparing their heats of chemical reaction: the most unstable form has the highest, the most stable form the lowest value. Since, generally, the glass obtained by rapid cooling of the melt represents the most unstable form, a glass corresponding to the formula  $Al_2O_3 \cdot SiO_2$  should be the least stable form of this compound. Unfortunately, this glass cannot be made because of its strong devitrification (crystallization) tendency. As sillimanite has lowest energy content, it is a stable mineral. All of the other minerals become unstable, however, on heating to a white heat. They are then transformed into a new silicate,  $3Al_2O_3 \cdot 2SiO_2$ , called mullite<sup>6</sup>, and a glassy melt. Mullite is the most stable aluminium silicate at high temperatures. It is of industrial importance because it occurs in ceramic bodies and is formed on solidification of melts of a suitable composition containing alumina and silica.

Actually mullite forms in a variable temperatures scale, i.e. 1300-1600°C. The transformation takes place over a large temperature interval, and in all cases a silica-rich glass is formed together with mullite. Free silica in the form of cristobalite has often been demonstrated in the glass.

Silicates of alumina have aroused the interest of ceramists not merely as raw materials for incorporation in ceramic bodies but also as new materials often found in the fired wares, where they occur in the form of acicular crystals. They are usually felted together in a state of disorder and occur preferentially as local agglomerations.

There is most knowledge about those substance that are formed by solidification from melts. According to Bowen and Greig<sup>6</sup>, apart from the pure components only a single compound can crystallize out from a melt of alumina and silica on solidification, namely mullite,  $3\text{Al}_2\text{O}_3 \cdot 2\text{SiO}_2$ , but neither silimmanite nor its polymorphic modifications, andalusite and kyanite. The two-component system ( $\text{Al}_2\text{O}_3 + \text{SiO}_2$ ) is characterized by a minimum melting point mixture with 5.5 per cent  $\text{Al}_2\text{O}_3$  - a so called eutectic - at  $1545^\circ\text{C}$  and a slight inflexion in the liquidus curve at about  $100^\circ\text{C}$ , a so called masked maximum indicating the presence of a compound which melts with decomposition (incongruently). This compound is mullite. From the melt the following minerals may crystallize out, depending on the contents of the two oxides: cristobalite, mullite, corundum. On further cooling and solidification from the melt there remains finally only mullite, intermingled with varying amounts of silica or corundum (Fig. 2.11).

Mullite produced by heating up to  $1400^\circ\text{C}$  for 1 hour appears under the microscope pseudomorphic with kaolinite. Its formation is catalyzed by the presence of only 1 per cent  $\text{ZnO}$ ,  $\text{Li}_2\text{O}$ ,  $\text{MgO}$ ,  $\text{Fe}_2\text{O}_3$ ,  $\text{MnO}$ ,  $\text{Ce}_2\text{O}_3$  and  $\text{MeO}_3$ ;  $\text{B}_2\text{O}_3$  and  $\text{CaO}$  are less effective,  $\text{Na}_2\text{O}$ ,  $\text{K}_2\text{O}$ ,  $\text{TiO}_2$  and  $\text{SnO}_2$  least of all. Their catalytic action varies with temperature;  $\text{Li}_2\text{O}$  and  $\text{MgO}$  are active at both high and low,  $\text{ZnO}$  only at high temperatures<sup>34</sup>. Catalysts containing 4-5 components are the most effective, e.g. a mixture of 2  $\text{MnO}$ , 1  $\text{MgCl}_2$ , 2  $\text{TiO}_2$  and 4  $\text{CaF}_2$ <sup>35</sup>.

The changes which take place in kaolin on heating may be readily followed in the electron microscope. Not until  $1100^\circ\text{C}$  is breakdown of the hexagonal lamellae observable; then fine needles begin to separate, the first nuclei of mullite. Particles heated still further exhibit only these formed needles, which are scattered in disorder throughout the fired body<sup>13,31</sup>.

Owing to the high proportion of silica in fired clay its presence in the free, crystalline state [ $3(\text{Al}_2\text{O}_3 \cdot 2\text{SiO}_2) = 3\text{Al}_2\text{O}_3 \cdot \text{SiO}_2 + 4\text{SiO}_2$ ] must always be expected beside mullite. The silica can be demonstrated by X-ray methods. The dilatometer, furthermore, occasionally discloses a well developed cristobalite effect at its conversion temperature of about  $230^\circ\text{C}$ , more rarely the tridymite effect at  $117^\circ\text{C}$ . It is remarkable that with many fired clays both these effects are absent, and the microscope then also fails. From clays that have been fired at  $1000^\circ\text{C}$  silica can no longer be dissolved out by alkalis alone, irrespective of whether the clays are ignited subsequently at lower or higher temperatures<sup>36-39</sup>.

The formation of mullite from clay is not quantitative, because part of the theoretically possible amount dissolves in the glass formed from the fluxes. The presence of mullite in ceramic materials is nearly always regarded favorably, because it improves the properties of the product owing to its great hardness and low coefficient of expansion. The main production of mullite takes place between 1000° and 1200°C, i.e. after production of a glassy melt, and it increases further between 1200 and 1500°C. The mullite content found was 7-9 per cent less than the amount calculated from the chemical composition of the raw materials; the rest had probably entered the glassy phase. Mullite is not stable above 1550°C. The formation of corundum in mullite blocks is evidently due to this decomposition. One per cent of alkali is sufficient to bring it about above 1400°C. The instability of mullite is indicated by the concealed maximum in the liquidus curve in the system alumina-silica, which has been studied by Gad and Barrett<sup>40</sup>. They found that, in the presence of 2-4 per cent Na<sub>2</sub>O, mullite is decomposed into corundum and a melt with surprising rapidity (e.g. 40 h); K<sub>2</sub>O is less and Li<sub>2</sub>O more effective than Na<sub>2</sub>O. Addition of silica hinders decomposition, that of Al<sub>2</sub>O<sub>3</sub> increases it. CaO and MgO were without effect. At 1150-1170°C, decomposition was incomplete even after 540 h, but was more nearly complete the higher the temperature.

### 2.7.3 Firing of Porcelain

#### 2.7.3.1 Firing of Clays, Feldspar and Quartz

Of major technical interest is a knowledge of raw mixtures of the materials which sinter earliest and are therefore the most suitable ones for making porcelain. It is usual to characterize the extent of sintering by porosity, and porcelain can be considered densified only when its water absorption is less than 1 per cent. In figure 2.16 the temperatures required for densification have been drawn in a triangular network representing compositions in the three-component system kaolin-quartz-feldspar. Wolf devised other three component diagrams from which the compositions of bodies can be determined. In figure 2.16 the composition 50 kaolin, 25 feldspar, 25 quartz, corresponding to hard porcelain, is indicated by a small circle; it should thus require only about S.C (seger cone) 9 for complete vitrification, whereas industrially S.C. 14 is required for the glost fire in order to ensure correct firing in all parts of the oven or kiln. Bodies to fire up at lower temperatures, such as soft porcelain, must contain more quartz and feldspar than hard-paste porcelain. Addition of small quantities of lime or magnesia lowers the finishing temperature appreciably.

The composition of the body is not solely determinant for densification on firing; the grain size of the constituents, especially quartz, also plays a part. Increasingly fine



grinding of quartz and feldspar increase shrinkage and decrease porosity, at any rate at high firing temperatures. Within limits, the same effect as changing the rational composition can be achieved merely by suitable choice and appropriate comminution of the non-plastics. The changes which take place in the properties of a porcelain body on firing are indicated in figure 2.17.

According to Gould<sup>41</sup>, the purpose of the reduction stage is not only to attain a white fired colour: it also constitutes the most suitable means for obtaining uniform top temperature everywhere in the oven or kiln and for avoiding of over-firing which would cause discoloration and bloating. He assumes that complex carbides and deposits of carbon form in the body at medium temperatures and remain unchanged under reducing conditions but, in an oxidizing fire, are decomposed with liberation of gases. The presence of up to 3 per cent C in the fired body has little effect on the colour. Opposed to this the view of Odelberg<sup>42</sup> that in an oxidizing fire it is also possible to obtain a pitcher practically free from closed pores and at the same time avoid localized ferruginous melts in the body. In between these two views lies that of Larchevque<sup>43</sup> who advocates firing under reducing conditions up to 1320°C only.

### 2.7.3.2 Constitution of fired porcelain body and effect of heat treatment

The first scientific observation on the constitution of porcelain were made with the aid of the microscope and consisted in the establishment of the fact that the fired porcelain consists of glassy matrix permeated with crystallites and spherical cavities; the crystallites were formerly considered to be de-vitrification products of the glassy matrix. Opposed to this is the view that the crystalline material derives directly from kaolin, the skeleton of porcelain, by a chemical transformation. Similar beliefs were held by the ancient Chinese potters. Our present views on porcelain mainly stem from Mellor<sup>44</sup> and Zoellner<sup>45</sup>. The latter isolated the crystallites by the use of dilute hydrofluoric acid which dissolves feldspar, and found that these had the composition of sillimanite,  $\text{Al}_2\text{O}_3 \cdot \text{SiO}_2$ . This has recently been corrected, and they are now considered to have the composition of mullite,  $3\text{Al}_2\text{O}_3 \cdot \text{SiO}_2$ . His method of determining the mullite has frequently been checked since. It hardly allows the whole of the mullite to be obtained, as the finest grains will also dissolve in HF. X-ray analyses of mullite in the fired body usually give somewhat higher figures than the chemical analyses. Needles of mullite are observed under the microscope only in bodies fired above 1300°C. They grow larger at higher firing temperatures but, according to results of Mellor and Austin<sup>46</sup>, disappear again after twelve repeated firings, leaving behind a homogeneous glass. The deformation eutectic of the system  $\text{K}_2\text{O} - \text{Na}_2\text{O} - \text{Al}_2\text{O}_3 - \text{SiO}_2$  has the composition 0.78  $\text{Na}_2\text{O}$  - 0.22  $\text{K}_2\text{O}$  - 0.204 -  $\text{Al}_2\text{O}_3$  -

$3.43\text{SiO}_2$ ; this is not a true eutectic, since it has not been formed from a cooling melt. When many needles of mullite are formed they are smaller in size and form a crystalline conglomerate. According to Ponomarov<sup>47</sup>, the glass containing the maximum amounts of dissolved  $\text{SiO}_2$  and  $\text{Al}_2\text{O}_3$  has the composition  $\text{K}_2\text{O} - 1.15 \text{Al}_2\text{O}_3 - 12 \text{SiO}_2$ . When all components of porcelain are present simultaneously, solubility is higher, for hard fired porcelain contains only a small proportion of crystalline silica and less mullite than corresponding to the amount of kaolin in the body formula. The glassy content of fired porcelain may thus be assumed to be much more than half, probably 60-94 per cent by weight; in soft, especially fritted, porcelain it is higher than that present in hard porcelain. Incidentally, an observation of Navratil and Fessler<sup>48</sup>, that a highly siliceous glass throws out more mullite, is noteworthy, since it indicates a means of influencing the crystallization of mullite. According to Krause and Keetman<sup>49</sup>, feldspar begins to melt at  $1100^\circ\text{C}$  but a feldspar-quartz eutectic forms already at  $1000^\circ\text{C}$ ; they state that the feldspar melt dissolves less mullite than earlier workers claimed, namely only 5-6 per cent, but more quartz. This agrees with the finding that hard-fired laboratory porcelain consists solely of mullite and glass. Naturally, the glass dissolves not only quartz and kaolin but also mullite, which was proved convincingly by Mellor and Austin<sup>46</sup> observing mullite needles to disappear by twelve repeated firings. Under laboratory conditions Schwarz and Merck<sup>50</sup> found that 9 per cent of mullite dissolved in feldspar glass. When the silica content of the melt was high, i.e. when more quartz had dissolved, part of the mullite crystallized out again, subject to the high viscosity of the melt; on reducing its viscosity by adding fluxing oxides, mullite crystallized out in large needles. Discrepancies in the results of these workers are probably referable to differences in the heat treatment and content of fluxing oxides.

The first series of experiments (for hard porcelain) showed that at firing temperatures of  $1200^\circ$  and  $1400^\circ\text{C}$  the glassy phase amounted to  $2/3$  of the fired body. On prolonging the fire, and still more on firing at higher temperatures, the quartz content is reduced and the mullite increased. As little as 2 per cent added limestone suffices for the formation of 70 per cent glass at  $1200^\circ\text{C}$ . On prolonged heating at this temperature 16.3 per cent of the glass crystallizes in the form of mullite. The almost complete absence of cristobalite is surprising. At  $1400^\circ\text{C}$  no less than 94 per cent glass is formed. Owing to the presence of the small amount of lime the viscosity of the glassy phase is reduced to such an extent that the body may be too soft to be friable. On the other hand,  $\text{MgO}$  additions render the glassy phase more viscous. Figure 2.18 shows schematically the various phases existing in porcelain fired at  $1400^\circ\text{C}$ . On repeated firing, the strength rises initially and thermal expansion falls, but the thermal shock resistance is lowered at the same time, probably owing to cooling stresses in the very glassy porcelain. Because of the danger of cooling

cracks or dunting it is customary in the porcelain industry to cool the fired ware very slowly over the range 800°-700°C, i.e. in the region of the transformation point of feldspar - glass. In this region Hoborn and Gruneisen<sup>51</sup> found a change in the expansion coefficient, which is also observed in normally cooled glasses; a discontinuity corresponding to this transformation also appears in the conductivity-temperature curve. From the amount and properties of the glassy phase in porcelain Kraner<sup>52</sup> concluded that it was a more important constituent of the fired body than mullite. It is apparent from the discussion that the constituents of the porcelain body (glass, cristobalite, mullite) are not in a state of equilibrium, since on prolonged firing the crystalline materials re-dissolve, especially cristobalite which rapidly disappears. The failure to reach equilibrium is due to the high viscosity of the feldspathic glass. For the same reason Ponomarov<sup>47</sup> concluded that the melt must be inhomogeneous: in the immediate neighborhood of the crystallites it would be enriched in respect of their constituent elements, and consequently it must have different properties in different regions. The crystalline development of mullite is, in general, more pronounced with kaolins than with other clays, owing to the coarser grain size. This presumes that mullite is formed directly from clay substance by the latter yielding up its excess of combined silica to the feldspathic glass.

The properties of porcelain are influenced by these crystalline inclusions and by the homogeneity of the glassy phase. Accordingly, Budnikov<sup>53</sup> advocates prolonging the firing schedule at top temperatures (soaking) sufficiently to achieve homogeneity; only then can the necessary diffusions be completed. At the same time a more uniform distribution of the crystallites will result, especially those of quartz, which will form the coherent framework on which the characteristic mechanical properties of the porcelain primarily depend.

Attempts have recently been made to replace the feldspar in porcelain and stoneware by frits. This represents a transition stage to fritted porcelain which is compounded with high percentages of frit. According to Collins<sup>54</sup>, addition of even small amounts of frit will often allow the firing temperature to be lowered, with satisfactory formation of mullite.

Much importance is also attached to influencing the glassy phase as the major component of porcelain. Navratil and Fessler<sup>48</sup> studied the influence of various added fluxes on the amount of glass or mullite formed (Fig. 2.19). They found that addition of alkalis resulted in the formation of more glass and less mullite than other metallic oxides. ZnO and talc are also used as additives in porcelain formulations.

The presence of soda and lime in the feldspar affects all the properties. This was demonstrated by Chilcote<sup>55</sup> who introduced potash, soda and lime feldspars systematically into the body and examined the effect on the most important properties. Glass formation and, with it, translucency were greatest when a eutectic mixture of all three feldspars was used.

#### 2.7.4 The Modifications of silica during heating

After clay, free silica is the most important raw material and constituent of ceramic bodies. It occurs in several modifications, all of which are important industrially. Silica in the free state is usually found in the form of quartz, and until a few decades ago it was not known that there are two other independent crystalline species of silica, tridymite and cristobalite<sup>10,28</sup>. These three crystalline forms may exist in several modifications, each of which is stable over a different temperature range. A modification of a particular crystalline species, for instance of quartz, immediately changes into another when the inversion point is passed in the course of a temperature change; for example,  $\beta$ -quartz changes into  $\alpha$ -quartz at 573°C. Much more difficult to achieve are the transformations of quartz, tridymite and cristobalite into one another, although each of these species has a more or less well defined temperature range of stability. In these conversions the rearrangement of the atoms in the crystal lattice involves a considerable expenditure of work. Pure monotropic transformations of silica are not known, but the difficult transformation of quartz into tridymite at 870°C may be regarded as pseudomonotropic; only the transformations of the  $\alpha$ - $\beta$ - $\gamma$ -modifications of the same crystalline species can be said to be truly enantiotropic ( $\alpha$  refers in all cases to the form stable at high temperatures).

Besides the three main crystalline species and their modifications, there is also an amorphous variety, silica glass, often wrongly called quartz glass.

The phase diagram of silica, which affords one an insight into these complicated relationships, has been determined by Fenner<sup>56-57</sup>. The stability ranges for the different modifications are given in Fig. 2.10, in which the vapour pressure has been plotted against temperature.

An important deduction from the phase diagram is that, on long heating at high temperatures, quartz must necessarily convert into one of the other two crystalline species. It is remarkable, however, that this transformation does not proceed according to the diagram, i.e. quartz does not change directly into tridymite above 870°C, but the lattice primarily breaks down completely, probably as far as the formation of an

amorphous form from which the less stable form, cristobalite, is first formed, and this finally transforms to tridymite. This strange order of transformations is known as Ostwald's rule of stages<sup>58-59</sup>. It states that the transformation of a phase into the form most stable under the conditions ruling does not take place directly, but the less stable forms arise first and the stable form last. Ostwald's<sup>58</sup> rule apparently holds only for the pseudomonotropic transformations of the three main crystalline species among themselves (conversions), but not for the enantiotropic transformations within the three main forms (inversions).

The simplest way of distinguishing between the three crystalline species is to determine the specific gravity, though tridymite and cristobalite are less easy than quartz to differentiate by this means. The consequences of the decrease in specific gravity from quartz, 2.65, to the two other modifications are important industrially. This conversion is, indeed, inescapably bound up with a volume change of 14.4 per cent, i.e. it is the cause of the 'growth' on firing of ceramic bodies containing quartz. Table. 2.3 shows the different densities of different phases of quartz.

The transformation of one form of silica into another does not occur instantaneously at a certain temperature. It had formerly been assumed that this was the case for the  $\beta$ - $\alpha$ -quartz inversion, but different workers gave different values for the inversion temperature<sup>37-38</sup>. It usually occurs at 573-575°C, but by the aid of the differential thermometer method variation of up to 38°C have been observed in the course of an examination of 250 different specimens; in 95 per cent of the cases examined, however, the temperature variations did not exceed 2.5°C. With synthetic quartz variations up to 160°C have been observed. This was considered to be due to the presence of other ions in the lattice: thus with Ge present the inversion temperature was 40°C higher, with Li and Al 120°C lower.

According to Florke<sup>60</sup>, irregularities in the transformation temperatures and other properties of cristobalite and tridymite are solely due to unidimensional lattice defects. Single crystals of pure cristobalite can be produced at 1650°C, but of tridymite only if foreign ions are present. These exhibit superstructures of high periodicity but not the two-layer structure hitherto assumed after Fenner<sup>61</sup>, which could not be prepared. The effect of the lattice defects is to displace the transformation temperatures, etc. and render them less sharp.

According to Fenner<sup>61</sup>, the inversion may take place during heating somewhere between 201° and 270°C, and during cooling somewhere between 198° and 241°C; it is not as sudden a change as the  $\beta$ - $\alpha$ -quartz change at 573°C. According to Weyl<sup>62</sup> natural

crystalites invert at temperatures between 175° and 250°C<sup>41-42</sup>. Inversion temperatures on cooling are often found to be lower than those observed on heating, and the volume change observed on cooling ranges between 4 and 8 per cent. Incidentally, the expansion of cristobalite between 200 and 1000°C was found to be not always reversible. If  $\alpha$ -cristobalite is perfectly pure, it can be stable even below 230°C. The type of mineralizer also affects the inversion temperature. Plumat<sup>63</sup> found that the internal stresses set up in cristobalite by the fluxes present are the cause of the depression of the inversion point by up to 100°C occasionally reported. Similarly, observed irregularities in the inversion of tridymite are, in his view, due to differences in heat treatment. Dietzel<sup>64</sup> throws doubt on the existence of some crystalline modifications of tridymite, ascribing their apparent existence to the effect of foreign atoms in the lattice.

In products containing clay, tridymite occurs only when the product has been maintained at 1300-1400°C for long period. Cristobalite usually occurs in such a small size that the individual crystals cannot be observed under the microscope, owing to their smallness and low birefringence.

#### 2.7.5 Quartz conversion and effect of alloy addition

Very pure quartz, especially in the form of large, single crystals, hardly converts or does so with extreme slowness<sup>51</sup>. Small crystal size favours conversion, which apparently proceeds from the outer surface and is promoted by impurities, if present. In accordance with Ostwald's rule tridymite is not formed directly, but via cristobalite. Hirsch<sup>65</sup> studied the extent of conversion using various raw materials. Since complete conversion of quartz is nearly always desired for industrial purposes, the catalytic effect of impurities has often been studied. The catalytic effect of many chemicals has been studied by Van Niewenburg and De Nooyer<sup>66-67</sup> who measured the diminution in specific gravity of quartz heated with 1 per cent of the additive for one hour at 1300°C. This interesting series of experiments shows clearly that only the alkalis are effective as catalysts, lithium most, followed by potassium and sodium. With salts a moderate catalytic effect is observable only when they contain dissociable alkali. Conversion is poor with firmly bound sodium, e.g. NaCl. The catalytic effect of iron oxide and the other substances studied, including phosphates which have often been recommended, can only be described as moderate. Furthermore, increasing the amount of catalyst has but little effect on the conversion (Table 2.4).

Quartz conversion is only locally affected by solid-state catalysts (CaO, MgO, TiO<sub>2</sub>), while those that form melts (alkalis, FeO) spread over the surface and penetrate fissures,

thus acting more effectively<sup>68</sup>. Addition of  $\text{AlPO}_4$  to quartz accelerates the conversion to cristobalite, but above  $1600^\circ\text{C}$  softening commences.  $\text{SiO}_2$  and  $\text{AlPO}_4$  do not, however, form solid solution. Above  $1600^\circ\text{C}$   $\text{P}_2\text{O}_5$  vaporizes and the phases of the system  $\text{Al}_2\text{O}_3\text{-SiO}_2$  appear<sup>69</sup>.

Parmelee and Chesters<sup>70</sup> measured the reaction velocity,  $V$ , by studying the expansion of silica and spinel bodies in the course of firing. They plotted the reciprocal of the absolute firing temperature,  $T$ , against  $\log V$  and obtained a straight line.

According to Ostwald's<sup>58</sup> rule the primary conversion product of quartz is not tridymite but cristobalite. It may be that amorphous silica is formed as transient intermediate phase. This transformation depends only on the extent of surface and temperature. Whereas an individual piece of rock crystal is only changed superficially on firing, when finely ground it converts completely in a single fire. Even with the finest powder the conversion does not start below  $1000^\circ\text{C}$ ; it proceeds extremely slowly, and is still not rapid at  $1400^\circ\text{C}$ . At  $1360^\circ\text{C}$ , 66 per cent is converted in 90 h, at  $1500^\circ\text{C}$ , 85 per cent in 4 h, at  $1570^\circ\text{C}$  conversion is complete in one hour. According to Mellor and Campbell<sup>71</sup> the conversion velocity of pure quartz is related exponentially to the absolute temperature, as in other first-order reactions.

The transformation of cristobalite to tridymite proceeds still more slowly than the conversion of quartz to cristobalite. It can be accelerated by admixture of  $\text{FeO}$ . This enters the cristobalite lattice, so that  $2\text{Si}^{4+}$  is replaced by  $(2\text{Al}^{3+} + \text{Fe}^{2+})$  or by  $(2\text{Fe}^{3+} + \text{Fe}^{2+})$ . Such cristobalite converts rapidly at  $1320^\circ\text{C}$ <sup>72</sup>. Even easily convertible quartzite containing suitable fluxes and grain sizes of  $\text{SiO}_2$  have to be fired ten times in ceramic ovens before all the free crystalline silica has been converted to tridymite. With unsuitable raw materials complete conversion takes much longer: a coke oven has been known to collapse suddenly after a year in use, because the conversion of the quartz in the silica bricks took so long to complete. On the other hand, the conversion of tridymite to cristobalite above  $1470^\circ\text{C}$ , i.e. in the region of stability of the latter, proceeds rapidly.

## 2.8 Phase Analysis by X-ray Diffraction

A given substance always produces a characteristic diffraction pattern, whether that substance is present in the pure state or as one constituent of a mixture of substances. This fact is the basis for the diffraction method of chemical analysis, i.e., phase analysis. Qualitative analysis for a particular substance is accompanied by identification of the pattern of that substance.

The particular advantage of diffraction analysis is that it discloses the presence of a substance as that substance actually exists in the sample, and not in terms of its constituent chemical elements. For example, if a sample contains the compound  $A_xB_y$ , the diffraction method will disclose the presence of  $A_xB_y$  as such, whereas ordinary chemical analysis would show only the presence of elements A and B. Furthermore, if the sample contained both  $A_xB_y$  and  $A_xB_{2y}$ , both of these compounds would be disclosed by the diffraction method, but chemical analysis would again indicate only the presence of A and B. Another rather obvious application of diffraction analysis is in distinguishing between different allotropic modifications of the same substance: solid silica, for example, exists in one amorphous and six crystalline modifications, and the diffraction patterns of these seven forms are all different.

The powder pattern of a substance is characteristic of that substance and forms a sort of fingerprint by which the substance may be identified. If we had on hand a collection of diffraction patterns for a great many substances, it could be identified an unknown by preparing its diffraction pattern and then locating in the field of interest of known patterns one which matched the pattern of the unknown exactly. The collection of known patterns has to be fairly large, if it is to be at all useful, and then pattern-by-pattern comparison in order to find a matching one becomes out of the question.

What is needed is a system of classifying the known patterns so that the one which matches the unknown can be located quickly. Such a system was devised by Hanawalt in 1936. Any one powder pattern is characterized by a set of line positions  $2\theta$  and a set of relative line intensities  $I$ . But the angular positions of the lines depend on the wavelength used, and a more fundamental quality is the spacing  $d$  of the lattice planes forming each line. Hanawalt therefore decided to describe each pattern by listing the  $d$  and  $I$  values of its diffraction lines, and to arrange the known patterns in decreasing values of  $d$  for the strongest line in the pattern. This arrangement made possible a search procedure which would quickly locate the desired pattern.

## 2.9 Texture Analysis by Neutron Diffraction Technique

Textures in materials have been studied extensively since the 1930s following the pioneering work of Wassermann<sup>73-74</sup>. The modern era of texture measurement started in 1949 with the development of the x-ray pole figure technique for texture measurement by Schultz<sup>75</sup>. Finally, modern texture analysis was initiated with the publication by Bunge<sup>76</sup> and Roe<sup>77</sup> of a mathematical method of pole figure inversion. In recent years



scientific communities have paid ever more attention to problems of applied science. This holds also for people working in the field of neutron scattering.

### 2.9.1 Introduction

The microstructure of a crystalline material is defined by multitude of parameters, such as dislocation structure (density and stacking fault energy), grain structure (size, size distribution, and shape), second phase content (volume fraction, size, and distribution) and interface characteristics (grain boundaries and inter phase boundaries). An additional attribute of the microstructure is the aggregate orientation distribution of individual grains. The orientation of each individual grain is defined by a set of orthogonal axes fixed on that grain and referenced to an external coordinate system. When the distribution of grain orientations in a polycrystalline material deviates from random, the material has said to have a 'texture'. All crystalline materials are capable of developing a texture during synthesis or processing. The simplest example is a single crystal, where only one orientation is present. The more interesting case is polycrystalline materials, where some distribution of orientations is present. Numerous examples are available for any type of crystalline material (e.g., metals, ceramics, polymers, and semiconductors). Proceedings from the triennial International Conference on textures of Materials (ICOTOM) are excellent sources<sup>78-79</sup>.

The study of texture is important to numerous applications in research and quality control. A quantitative knowledge of texture is a prerequisite for phase fraction determination in a multiphase alloy<sup>80</sup>, for residual stress measurement in bulk materials<sup>81</sup>, strength of materials which are extruded for processing. Since texture evolution occurs during processing, texture measurement documents an important aspect of microstructural development along the processing path. Finally, physical and mechanical properties depend on texture; so both the correlation of many aspects of material behavior and the prediction of properties are consequences of texture analysis.

The concept of symmetry is important in texture analysis which consists of two elements. The crystal structure imposes some degree of symmetry, the highest being the cubic structures. Sample symmetry is a consequence of the fabrication operations. An extensive literature base, too large to reference here, documents all aspects of texture analysis and applications. In addition to the aforementioned ICOTOM proceedings, the interested reader is referred to a series of European conference proceedings<sup>82-85</sup>, the journal *Textures and Microstructures*, and several excellent books dedicated to textures<sup>86-88</sup>.

### **2.9.2 Processing and properties**

A wide range of properties depends on the crystallographic direction which the property is being measured. In a polycrystalline workpiece where all crystals are randomly distributed, the differences in properties present at the grain-size scale are averaged out, and the material properties are isotropic. However, most processing introduces a texture in the fabricated material, resulting in an anisotropy of properties of the finished product.

Each processing step in a production path leaves its individual fingerprint in the texture of the material. The texture evolution during processing begins with the solidification of the material. Solidification occurs in specific crystallographic directions. If the growth of the crystals is unhindered, a specific (fiber) texture is developed. Typically, the fiber texture forms an angle with respect to the solidification direction. The magnitude of this angle is determined by the rate of the heat extraction. Texture evolution continues with the deformation of the processed material. Deformation of a polycrystalline solid is restricted to a number of active slip systems, which are responsible for the development of textures and are characteristic for each rolled, extruded, forged or pugged material. For metals annealing after deformation typically results in recrystallization of the material. Depending on the active recrystallization mechanism, the annealing texture is either very strong and composed of preferred orientations different from the former rolling texture, or, in other cases, the recrystallization texture is weak and can be described as a randomized version of the texture from the previous processing step. In either case, the annealing texture are characteristic to the individual process. Production steps have no impact on the texture evolution if they are intended to redistribute solute or to precipitate hardening phases, such as preheating or aging. Thus, the final texture is the product of all texture changes during processing. From this, it can be concluded that texture changes in upstream processes can have significant influence on the properties of the final product and should be monitored carefully.

### **2.9.3 Neutron Diffraction for Texture Analysis**

Texture determination by neutron diffraction is essentially similar to its measurement by x-ray diffraction. However, the experimental apparatus and quantitative data corrections are significantly different. Neutron scattering is preferable to x-ray techniques when information on the bulk is needed when large grains are present in the material or when magnetic properties are studied. Neutron sources are only available at nuclear research centers.

Thermal neutrons have a continuous spectrum of wavelength ranging from 0.5 Å to 4.0 Å. Typically, a wavelength of 1.2 Å at the maximum of the spectrum is selected with a monochromator crystal. Most of the scattering of neutrons occurs from the atomic nuclei. The consequence is that, in contrast to x-rays, the atomic form factor does not change with the Bragg angle  $\theta$  and the atomic scattering is similar in magnitude for both light and heavy elements, and it does not vary systematically with atomic number. These attributes make texture analysis by neutron diffraction suitable for samples with low crystal symmetry, where a large number of pole figures is required, such as minerals, as well as for materials containing light elements, such as polymers. Additionally, the scattering amplitude of neutrons is significantly smaller than for x-rays, which results in a much lower absorption of the neutrons than the x-rays. In the majority of materials, the penetration depth for neutrons is typically in the centimeter range, while the penetration depth for x-rays is in the micrometer range. This makes neutron diffraction especially useful for the texture measurement of coarse grained materials such as metals, alloys, ceramics etc. It also provides a high sensitivity for the texture analysis of small volume fractions of second phases. While it is difficult to measure the texture of second phases having volume fractions of less than ten percent by x-ray diffraction, neutron diffraction allows texture studies in second phases with a volume fraction as small as one percent.

The function which is needed for describing the studied problem is the distribution of scattered neutron intensity for monochromatic ingoing neutrons fulfilling Bragg's law for a particular scattering plane of the crystal in question. The function can be measured by fixing the detector at an angle satisfying the law

$$2d \sin\theta = n\lambda_0$$

where  $d$  is the distance between the selected planes,  $\theta$  is the scattering angle,  $\lambda_0$  is the ingoing neutron wave-length and  $n = 1, 2, 3, \dots$ , while the sample is being rotated into all possible directions. The process of texture analysis for ceramic material was followed according to the technical document issued by the International Atomic Energy Agency, Vienna, 1977. N.Kroo and I.Vizi, set up the technique by which they analyzed texture in materials made of steel by neutron scattering method.

## **2.10 Thermal Analysis of Ceramic Insulator**

### **2.10.1 Introduction**

The currently accepted definition of thermal analysis, as given by Mackenzie<sup>89-90</sup> and the International Confederation for Thermal Analysis (ICTA) is: a group of techniques in which a physical property of a substance and/or its reaction products is measured as a function of temperature whilst the substance is subjected to a controlled temperature program. This definition implies that before a thermal technique can be regarded as thermoanalytical, three criteria must be satisfied:

1. A physical property has to be measured.
2. The measurement has to be expressed (directly or indirectly) as a function of temperature.
3. The measurement has to be made under a controlled temperature program.

Failure of any method to meet these criteria would exclude it as a method of thermal analysis. Actually the most widely used techniques are Thermo Gravimetry (TG), Differential Thermal Analysis (DTA). Inorganic materials are most widely studied by thermal analysis techniques, followed by high polymers, metals and metallic alloys, and organic substances. It should be noted that, in many cases, the use of only a single thermal analysis technique may not provide sufficient information about a given system. As with many other analytical methods, complementary or supplementary information, as can be furnished by other thermal analysis techniques, may be required. For example, it is fairly common to complement all DTA data with thermogravimetry.

### **2.10.2 Thermogravimetric analysis (TGA)**

#### **2.10.2.1 Basic principles**

The method of thermogravimetry is basically quantitative in nature in that the mass change can be accurately determined. However, the temperature ranges in which the mass-changes occur are qualitative in that they depend on the instrument and sample characteristics. With the wide use of commercial thermobalances, TG data of a sample can be correlated from laboratory to laboratory if similar conditions of pyrolysis are employed.

Thermogravimetry is widely used in almost all of the areas of chemistry and allied fields. In the early 1950s it caused a revolution in inorganic gravimetric analysis. Equally important has been the application of TG techniques to applied sciences problems such as

the characterization of various materials used in road construction, determination of moisture contents in a wide variety of materials, and determination of mass loss of ceramic materials. Actually TG is almost universally applied to a large number of analytical problems in the fields of metallurgy, paint and ink science, ceramics, mineralogy, food technology, inorganic and organic chemistry, polymer chemistry, biochemistry, geochemistry, and others.

The application of thermogravimetry to a particular problem is possible if a mass-change is observed on the application of heat. If no mass-change is observed, then other thermal techniques such as DTA, DSC, TMA, and so on, may have to be employed. If the mass change is very small ( $< 1\%$ ), then perhaps other techniques may be more useful.

Some of the many application of TG are listed as follows:

1. Thermal decomposition of inorganic, organic, and polymeric substances.
2. Corrosion of metals in various atmospheres at elevated temperatures.
3. Solid-state reactions.
4. Roasting and calcining of minerals.
5. Distillation and evaporation of liquids.
6. Pyrolysis of coal, petroleum, and wood.
7. Determination of moisture, volatiles, and ash contents.
8. Rates of evaporation and sublimation.

#### **2.10.2.2 Applications to clays and allied materials**

Dunn<sup>91</sup> has summarized the major areas of application of TG and other TA techniques to clays and accessory minerals. These applications include:

1. Assessment of raw material deposits through characterization, classification, and analysis.
2. Investigation of the changes in the raw materials resulting from industrial processing.
3. General problem-solving techniques used when difficulties are encountered through changes in raw material, new technology, or new specifications.

TG has the capability of providing accurate quantitative determinations, provided that a single stoichiometric reaction of the clay or mineral occurs in the temperature range of interest. Thus, the mass-loss due to the dehydroxylation of clays (Fig. 2.20) can be used

to determine the clay content of a mixture. When overlapping mass-losses occur, isothermal intervals can be employed to resolve the separate reactions, as in the determination of alunite and kaolinite in alunite clays<sup>92</sup> and  $\text{MgCO}_3$  and  $\text{CaCO}_3$  content in dolomites.

The TG curves of a kaolinite standard, as determined by Earnest<sup>93</sup>, is shown in fig. 2.20. Sorbed water is evolved at temperatures up to 200°C; in this case, the amount is 0.2% of the total sample mass. The dehydroxylation reaction occurs in the temperature range of 400-700°C, resulting in a mass-loss of 13.8%.

The decomposition curves of most soils showed horizontal mass levels starting at 150-180°C and extending to 210-240°C, indicative of either hygroscopic moisture or hygroscopic moisture plus easily volatile organic compounds. In general, the mass-loss values fell between those obtained by the Karl Fischer method and oven drying at 105°C. The organic matter started to burn off between 210 and 240°C and was usually completely burned off at 500°C. In organic soils and those containing less than 15% clay, a relatively close estimate of the organic matter could be made from the mass-loss curve. When the clay content varied from 15-40%, the loss in mass at 500°C usually gave an estimate of the organic matter, which was in satisfactory agreement with dry-combustion and wet-oxidation data. When the clays contained more than 40% clay, it was not possible to distinguish between mass-losses due to decomposition of organic matter and those due to the elimination of the lattice water of clays. This work also suggests that the lattice water in the pure clay samples can be quantitatively determined. Because the lattice water came off at different temperatures with different clays, it may be possible to use these temperatures as an additional means of identification and characterization.

### **2.10.3 Differential thermal analysis (DTA)**

#### **2.10.3.1 Basic principles**

Differential thermal analysis (DTA) is a thermal technique in which the temperature of a sample, compared with the temperature of a thermally inert material, is recorded as a function of the sample, inert material, or furnace temperature changes in the sample due to endothermic or exothermic enthalpic transitions or reactions such as those caused by phase changes, fusion, crystalline structure inversions, boiling, sublimation, and vaporization, dehydration reactions, dissociation or decomposition reactions, oxidation and reduction reactions, destruction of crystalline lattice structure, and other chemical reactions. Generally speaking, phase transitions, dehydration, reduction, and some

decomposition reactions produce endothermic effects, whereas crystallization, oxidation, and some decomposition reactions produce exothermic effects.

The temperature changes occurring during these chemical or physical changes are detected by a differential method, such as is illustrated in Fig. 2.21. If the sample and reference temperatures are  $T_s$  and  $T_r$ , respectively, then the difference in temperature,  $T_s - T_r$ , is the function recorded. Perhaps a better name for this technique would be differential thermometry; the term 'differential thermal analysis' implies that it has something to do with analysis, which, as with any other analytical technique, may or may not be the case. In thermal analysis, the temperature of the sample  $T_s$ , is recorded as a function of time and a heating or cooling curve is recorded. Small temperature changes occurring in the sample are generally not detected by this method. In the differential technique, since the detection thermocouples are opposed to each other, small differences between  $T_s$  and  $T_r$  can be detected with the appropriate voltage amplification devices. Thus, small samples (down to several  $\mu\text{g}$  in mass) may be employed and are, as a matter of fact, more desirable.

A comparison between the two techniques is shown in Fig. 2.22. In parts (a) and (b), the sample temperature is recorded as a function of time as the system temperature is increased at a linear rate. However, the difference between the curves in (a) and (b) is that no enthalpic transition takes place in the sample in (a), while in (b) exothermic and endothermic changes occur. Since no other temperature changes take place in the sample in (a), no deviation from the linear temperature rise is detected in the sample temperature. However, in (b), deviations occur at the procedural initial reaction temperature,  $T_i$ , due to temperature changes caused by endothermic or exothermic changes. These changes are essentially completed at  $T_f$  and the temperature of the sample returns to that of the system. In the curves in (c), the difference in temperature,  $T_s - T_r$ , is recorded as a function of system temperature,  $T$ . At  $T_i$ , the curve deviates from a horizontal position to form a peak in either the upward or the downward direction, depending on the enthalpic change. The completion of the reaction temperature,  $T_f$ , does not occur at the maximum or minimum of its curve but rather at the high-temperature side of the peak. Its exact position depends on the instrumental arrangement. Thus, in the differential method, small temperature changes can be easily detected and the peak area is proportional to the enthalpic change ( $\pm\Delta H$ ) and sample mass.

A typical DTA curve is illustrated in Fig. 2.23. Four types of transitions are illustrated:

1. Second-order transition in which a change in the horizontal baseline is detected;
2. An endothermic curve peak caused by a fusion or melting transition;
3. Endothermic curve peak due to a decomposition or dissociation reaction;
4. An exothermic curve peak caused by a crystalline phase change.

The number, shape, and position of the various endothermic and exothermic peaks with reference to the temperature may be used as a means for the qualitative identification of the substance under investigation. Also since the area under the peak is proportional to the heat change involved, the technique is useful for the semiquantitative or, in some cases, quantitative determination of the heat of reaction. Since the heat of reaction is proportional to the amount of reacting substance, DTA can be used to evaluate quantitatively the amount of substance present if the heat of reaction is known. Thus, the technique finds much use in the qualitative and semiquantitative identification of organic and inorganic compounds, clays, metals, minerals, fats and oils; polymeric materials, coal and shales, wood, and other substances. Quantitatively, it can be used for the determination of a reactive component in a mixture, or the heat of reaction involved in physical or chemical changes.

### 2.10.3.2 Applications to clays and minerals

One of the early fields of application of DTA was in the area of clays and minerals. These compounds which gave birth to the theory and instrumentation of the technique, have been widely investigated. DTA was used to identify clays from various locations throughout the world and was widely used to determine the free quartz content of the minerals. Numerous other applications were made of DTA. The application of DTA to these materials is discussed by Mackenzie et al.<sup>94</sup> and many others.

One of the first clays to be studied by DTA was kaolinite, and it still is being investigated by modern DTA and other TA techniques. A typical DTA curve of kaolinite, as determined by Earnest<sup>95</sup>, is shown in Fig. 2.24. In general, the DTA curve peaks are due to the following processes:

*Desorption of Water* - Ambient to 110°C, Endotherm - Minor. Seldom observed by DTA except in highly disordered species. Easily observed by TG and DTG.



*Dehydroxilation of Crystal Lattice* - 450 to 700°C, Endotherm - Major. The main endothermic peak. Observed in all members of the group except alophanc. Peak temperature, symmetry, and magnitude are diagnostic tools.

*Structural Organization* - 900 to 1000°C, Exotherm - Major.

*Structural Organization and Reaggangement* - 1150°C and above, Exotherm - Minor (Variable). This represents the formation of mullite and cristobalite. The intensity varies with impurities or additives as well as particle size.

Many studies have been concerned with the effect of particle size on the DTA curve peaks. In general, the smaller the particle size is, the lower will be the  $\Delta T_{\min}$  for a given peak, and the narrower will be the peak.

Crystalline quartz, when heated undergoes a solid<sub>1</sub> → solid<sub>2</sub> phase transition ( $\alpha \rightarrow \beta$  quartz) at about 573°C. Keith and Tuttle<sup>96</sup> found that in a study of 250 quartz samples, the inversion temperature range was 38°C in natural quartz, although most of the samples were within 573±25°C. This inversion temperature was attributed to solid solution of varying amounts of other ions in the quartz. Since the amount of solid solution is influenced by the temperature during formation, the inversion temperature can be used as a criterion of formation temperature for samples crystallized under similar chemical environments.

#### 2.10.4 Thermal expansion analysis

A differential dilatometer is an expansion apparatus in which the material under examination is heated together with a reference specimen of another material of known (preferably low) and uniform expansion (quartz glass or Invar metal). Both specimens press against a mirror which moves in accordance with the difference in expansion. A ray of light reflected from this mirror traces on light-sensitive paper a curve recording the differential expansion of the two materials.

##### 2.10.4.1 Application of Dilatometer

Characteristic of all differential thermal expansion curves for clays is a rising branch from 20-100°C, followed by a contraction which finishes at about 250°C. Even if the clay has been pre-heated for 2 hours at 100°C, contraction persists though to a lesser extent; there may be a second expansion before the final firing shrinkage sets in.

The contraction following the removal of moisture on drying in the air or heating at 110°C must be regarded as due to shrinkage of the gel films on the clay particles accompanying loss of gel water. This finding may be regarded as furnishing experimental support for the view that the plasticity of clays depends in part on the existence of swollen gel layers surrounding the clay particles. Slowly heated clays show that kaolin and most clays undergo expansion up to about 500-600°C, followed by contraction.

Remarkable differences in the behaviour of the different modifications of silica can be observed using dilatometer. Fig. 2.25 shows how the length of specimens changed on raising the temperature: quartz expanded uniformly up to its inversion at 573°C, at which temperature a sudden increase in length of about 0.2 per cent occurred, but at 600°C the increase in length ceased. The corresponding contraction on cooling took place quite suddenly.

Tridymite undergoes two sudden changes in length at 117°C and 150°C. Together they amount to about 0.3 per cent, although the total increase in length up to 600°C is less than that of quartz. In addition to these two inversions, a third has been observed by several research workers at about 450°C; its effect is, however, slight<sup>57,97</sup>.

The expansion behaviour of cristobalite is quite different. At about 230°C it undergoes an increase in length of about 1.13 per cent; the total increase, completed by 500°C, is 50 per cent greater than for tridymite. Accordingly, cristobalite is dangerous in ceramic bodies intended to pass repeatedly through the temperature range from ambient to red heat. It is a cause of peeling in earthenware when the glaze cannot follow the sudden contraction of the body. Apparently, quartz is responsible for these faults only to a limited extent, for its sudden length change is relatively small in amount. In the case of earthenware the quartz change also takes place at a temperature at which the glaze is not completely rigid and can therefore adjust itself more readily to length changes in the body. Generally speaking, tridymite is the most suitable type of silica to have in ceramic bodies because of its small total length change and the comparatively small jumps associated with its inversions. On the other hand, the 'pinch effect' due to the low-temperature inversion of cristobalite on cooling is claimed to improve the crazing resistance of glazed earthenware by causing additional compression in the glaze.

The position of the  $\beta$ - $\alpha$  inversion point of cristobalite on the temperature scale and the shape of the thermal expansion curve depend on the degree of order in the crystal lattice. A well ordered cristobalite inverts at 270-275°C, and the thermal expansion curve

exhibits a sharp jump. Cristobalites with lattice defects invert at lower temperatures, according to Florke<sup>60</sup>, and the thermal expansion curve rises less steeply.

### **2.11 Scope of the Present Work**

In view of the foregoing discussion, the main subject of the present work will be to investigate the effects of the addition of different alkaline earth oxides on the properties of the main BISF ceramic insulator body. Important mechanical, thermal and textural properties will be examined using modern methods and instruments and, finally, a better body composition and firing sequence are expected to be obtained and be suggested for future use.

### **3. EXPERIMENTAL**

#### **3.1. Introduction**

The study was undertaken for the structural characterization of the ceramic insulator material. To perform the study a verity of samples were prepared. The samples were prepared conforming to the same chemical composition used in Bangladesh Insulator and Sanitary ware Factory Ltd. (BISF); some additives were mixed with the raw materials of the BISF body and their effects were studied. Although the BISF technology (Fig. 3.1) used for the commercial manufacture of ceramic insulator product was followed to process the sample, certian steps in the process was omitted. After processing, the structural characterization was carried out by x-ray diffraction technique, the textural defect was identified by the neutron scattering method and the thermal analysis was done by Differential Thermal Analyser (DTA), Thermo Gravimetric Analyser (TGA) and Dilatometer. Some physical characteristics i.e., bending strength, density were also measured to establish the adaptability of the products with the additives.

#### **3.2. Sample Preparation**

##### **3.2.1. Raw material selection**

The raw materials used to prepare BISF body sample are listed below:

1. China Clay
2. China Clay (Rajmahal)
3. Ball Clay (White)
4. Bejoypur Clay (Grade 1)
5. Washed Bejoypur Clay
6. Ball Clay (Black)
7. Feldspar

Table 3.1 and 3.2 show the grain size distribution and the chemical analysis of each raw materials respectively. The detailed description about these raw materials is available in the Technological Report on "Evaluation of Raw Materials from Bangladesh"<sup>98</sup>.

The percentage of raw materials added to prepare the BISF body is shown in the Table 3.3, and the resultant final BISF body composition is shown in the Table 3.4 (a). A

second set of samples were prepared using a higher percentage of  $\text{TiO}_2$  and the chemical composition is shown in table 3.4 (b).

### 3.2.2 Chemical analysis

The basic requirement of the quality product is its chemical analysis in a considerable range and for this reason chemical analysis of the raw materials is mandatory in every batch. The analysis of the raw material was done by conventional volumetric method. Determination of  $\text{K}_2\text{O}$  and  $\text{Na}_2\text{O}$  were carried out by Flame Photometry.

### 3.2.3 Crushing

Many raw materials need to have the size of their lumps, aggregates, grains, particles, etc., reduced before they can be used in ceramic manufacture. In general, crushing refers to reduction of large lumps to a convenient size for secondary reduction. Actually in the processing of ceramic insulator materials the raw materials used were clays, feldspar and some additives. The only component to be crushed is the feldspar. The jaw crushers are used to perform this operation.

### 3.2.4 Ball milling or pot milling

Clays and feldspar with different percentages are mixed in the pot mill and the mills were rotated at a speed at which the balls, etc., are carried up the side and then roll over each other to the bottom. The grinding is therefore effected by impact and rubbing. Water was added with the clays with the ratio of 1: 1 so that a proper consistency of the mixing was resulted. The duration of milling, one of the determination factors of the particle size of the raw materials was 6 to 8 hours. The final particle size after milling was about 50 to 60 $\mu\text{m}$ .

### 3.2.5 Magnetic particle separation

Certain minerals can be purified by magnetic methods although they are not ferromagnetic. The susceptibility to intense magnetic fields of such feebly magnetic materials is insufficient to attract them against the force of gravity, as is done in the removal of strongly magnetic material. But by applying a very high magnetic field intensity horizontally to a falling stream the more susceptible particles can be deflected sufficiently to effect a separation.

The raw material was crushed and ground to a size where the minerals to be separated were no longer mechanically bound together. The particle size was less than 60 $\mu\text{m}$ . The

magnetic separation was carried out by applying strong magnetic field when the material is in the wet condition. The raw material was passed through the field and the separation was carried out.

### **3.2.6 Reservoir**

After grinding and milling, many materials are stored for short or long periods. Clay slips, mixed body slips may be stored in arks which are kept agitated just enough to prevent separation. They operate much like blungers, but less vigorously.

In the present research, the need of reservoir was limited. Actually the slip was produced and the material was cast directly as the amount of the material was small. But for the large scale production the reservoir is must.

### **3.2.7 Filter press or casting in plaster of paris mould**

In the large scale production the clay slurries and slips used for purifying and mixing can be dewatered by a number of ways. The commonest method is filter pressing. Actually filter clothes are used with applying pressure mechanically in the dewatering process. This process is rapid and economical.

In the present research wok, no filter press was used. As the amount of material required to produce samples was small, the slip was cast directly into the plaster of paris mould. The slurry was processed to lower down the moisture content to 18-20% in the plaster of paris mould. The dry plaster mould will suck the water down to 18-20%. The slurry was kept in the mould for 5-6 hours.

### **3.2.8 Pug milling**

The function of pugmills is to improve the uniformity of a plaster clay body giving it greater workability because of the proper coation of clay particles with water. The vacuum machines that is fixed with the pug mill do this more throughly as they also remove any air bubbles.

The materials under study were pugged with the pug mill and rod type samples of 10 mm in diameter and 135 mm in length were prepared.

### **3.2.9 Drying**

The humidity was first increased to 60 to 70% so that the initial drying rate was low while at the same time the temperature was raised. The humidity was kept high to control

the rate of drying during the critical period of drying-shrinkage. Subsequently the humidity could be reduced so that drying in the later stages was rapid. This allowed the overall process to be carried out rapidly without causing defects in the ware. Drying temperature in the tunnel dryers was kept at 120-130°C and the duration of drying was 24 hours.

### **3.2.10 Firing**

Ceramic samples were fired in tunnel kilns. In tunnel kilns, ware passed through the kiln on a car and the temperature distribution along the kiln was kept constant. Air for combustion was heated by the cooling ware, and the combustion gases passed over the entire length of the kiln and heated all the ware entering. In this way the heat content of the combustion process was utilized with great efficiency. The firing curves for the production of the samples is shown in Fig 3.2(a). The deviation of this curve can be compared with the standard firing cycle curve in Fig 3.2(b). An irregularity in the firing cycle used to prepare ceramic insulators at the BISF is clearly noticeable. The cooling cycle is too fast to introduce serious residual stresses in the fired product. Also, the heating cycle was not uniform and may cause warpage or crack in the product.

## **3.3 Additives and Composition**

2 to 4% alkaline earth oxides were added to the mother body (the BISF insulator body) as the fluxing agents for the samples. These are called additives. These additives acted as fluxing agents for the samples. The prime aim of addition of such additives were to enhance the growth rate of crystalline mullite and development of tridymite or cristobalite phases.

A complete data of parent body and the additives are listed in Table 3.5.

## **3.4 Physical Properties Measurements**

### **3.4.1 Bending strength measurement**

High demands are made on commercial ceramic insulator in respect of mechanical strength. For this reason it is tested for bending strength. On bending a rod, the lower layers are stressed in compression, the upper layers in tensions. For ceramic products cross-breaking strength is usually more important than crushing or tensile strength, but

bodies with the highest crushing strength usually also have the highest cross-breaking strength.

Bending strength measurements were carried out for the samples prepared. The machine that was employed for bending test measurements is called Bending strength tester. Here a static load was employed at the center of the specimen. The specimen was held by supports at the both end. The load employed was recorded by a scale which was not the direct reading. This reading then converted into actual reading ( $\text{Kg/cm}^2$ ). A formula was employed to convert the machine reading which is presented below:

$$\sigma_{bB} = (F_B \cdot L_S) / 4.M$$

where,

$F_B$  = Breaking load in N (Scale value)

$L_S$  = Width between supports in mm

$M$  = Moment of resistance in  $\text{mm}^3$  (Dependent on the cross section shape of the specimen)

=  $\pi d^3/32$ , where  $d$  is the diameter of the sample

$\sigma_{bB}$  = Ultimate breaking end bending stress ( $\text{N/mm}^2$ )

### 3.4.2 Density measurement

Average length and diameter of each sample were measured to calculate the average volume ( $V$ ) of each sample. The weight ( $W$ ) of the sample was taken and the density of the sample was calculated using the formula,

$$D = W/V$$

### 3.5 Optical Metallography

Ceramic materials are extremely hard materials requiring different procedures than those used for metals. Although some samples were sectioned with special abrasive cutoff wheels; however, diamond wheels are preferred in other cases. Grinding with emery or silicon carbide paper was not used because very little material would be removed before the paper wears out. Diamond abrasives were used, almost exclusively, for all stages of preparation.



Hand grinding is a very tiring chore; automatic devices are definitely preferred. Several procedures were used to hold the diamond abrasives during rough and fine grinding, such as diamond on cast-iron or cerad wheels, rosewood rods, and resin- or metal-bonded diamond laps. Depending on the smoothness of the cut, preparation commenced with 60-, 45-, or 30- $\mu\text{m}$  diamond discs. With automatic devices, relatively high pressures and short times (1 to 2 min) were used with a wheel speed of about 300r/min and copious water cooling. Coarser grits were required to grind an as-sintered surface.

Rough polishing was conducted using 6- or 3- $\mu\text{m}$  diamond paste on nylon, Texmet, or Pellon cloths. Polishing times of 1 to 2 min were used with very high pressure and low (150 rpm) wheel speeds. Final polishing was performed using 1- $\mu\text{m}$  diamond paste on a low-nap or napless cloth with high pressure for about 1 min, although some prefer to finish samples with 1/4  $\mu\text{m}$  diamond paste on Microcloth. These procedures are necessary to minimize stress relief in ceramic materials.

The etching were performed by immersing the samples in 2 % hydrofluoric acid for 10-15 minutes.

After etching the samples were observed under optical microscope at high magnification (x500) and micrographs were taken as necessary.

### 3.6 Phase Analysis by X-ray Diffraction

Phase analysis by X-ray diffraction was carried out by Hanawalt method. 2 to 3 g of the powdered samples were put in a slide and pressed so that these were attached with the surface of the slot of the slide. Then x-ray patterns were recorded. The powder was characterized by a set of line positions  $2\theta$  and a set of relative line intensities  $I$ . The angular positions of the lines depended on the wavelength used, and a more fundamental quality was the spacing  $d$  of the lattice planes forming each line. Thus by listing the  $d$  and  $I$  values of its diffraction lines, and to arrange the known patterns in decreasing values of  $d$  for the strongest line in the pattern. This process identified the phases present in the samples.

### 3.7 Texture Analysis

Texture analysis of the sample was made using neutron diffraction technique and an experimental set-up was organized at the Atomic Energy Research Establishment, INST, Savar, Dhaka.

The detector of the neutron spectrometer was fixed at the angle (Bragg's angle) of the x-ray pattern at which the intensity of the mullite phase was highest at the plane 210. The sample was then rotated at its own axis. The position of the sample rotation was shown in Fig. 3.3.

Three samples were taken for the study to compare the textural characteristics. Two samples were fired and one was non fired. Sample no. 1 was non fired. The fired samples were sample no. 1 and 7.

In order to study the expected changes in the texture of the ceramic materials, the diffracted neutron were recorded for each corresponding rocking angle and then counts versus rocking angle curve was plotted.

### 3.8 Thermal Analysis

Thermal analysis of the samples prepared were carried out by the following procedure:

1. By differential thermal analyser (DTA)
2. By thermogravimetric analyser (TG)
3. By dilatometer

#### 3.8.1 Differential thermal analysis

Differential thermal analysis of the ceramic insulator samples were made using Rigaku Thermal Analyser TAS 100 with basic unit TG 8110. 5 to 6 mg each of unfired powered samples were put into a furnace which was connected to the machine. The rate of heating used was 15°C per minute and the maximum temperature raised was 1000°C. The results were reported in the form of  $dT$  versus  $T$  curve.

#### 3.8.2 Thermogravimetric analysis

Powered samples were taken 5-6 mg each for differential thermal analysis. For this test the samples should be unfired. The main objective of this analysis was to find out the

chemical decomposition of the material at a definite temperature. The samples were put into a furnace which was connected to the machine. The rate of heating was 15°C per minute. Temperature raised upto 1000°C. The model number of the machine used was Rigaku Thermal Analyser TAS 100 with basic unit TG 8110.

### 3.8.3 Dilatometar

This machine is very important in glazing point of view. If the coefficient of thermal expansion does not match with that of the glaze material, the product will lose its electrical properties as well as its other quality. For this machine fired samples were taken whose dimensions are given below:

Length of the sample = 5 cm (max)

Width of the sample = 3 to 12 mm (min).

The samples under study was put into a furnace chamber in which the rate of heating was 5°C per minute. The experiment was carried out up to 400°C.

The coefficient of thermal expansion was measured by using the following formula:

$$\text{Coefficient of thermal expansion} = \Delta L / L.(400-T).M$$

Where,  $\Delta L$  = Expansion from graph

L = Length of the specimen

T = Room Temperature in °C

M = Magnification power of the graph

## 4 RESULTS AND DISCUSSION

### 4.1 Bending Strength

Table 4.1 and figures 4.1 to 4.6 show the bending strength of different samples. From the figures it is clear that the addition of alkaline earth oxide improves the bending strength of the BISF main body and amongst all alkaline earth oxides zirconium silicates and zinc oxides were appeared to have the best results.

From Table 4.1 it is clear that  $ZrSiO_4$  and  $ZnO$  showed the best results. But  $ZrSiO_4$  showed the best results when 3 per cent were added. Both  $ZrSiO_4$  and  $ZnO$  act as fluxing agent for the porcelain material i.e., these oxides lower down the firing temperature. On the other hand these oxides act as the nucleating sites for formation of mullite. Mullite increases the toughness and strength of the material. Again, if these fluxing material are added more than the required, a reverse action can be resulted. When 2 per cent  $ZrSiO_4$  was added, the strength of the material was slightly increased and the strength reached the highest value when added 3 per cent. Finally when 4 per cent was added the strength decreases. This shows that if  $ZrSiO_4$  is to added to the raw materials of the insulator, 3 per cent will be the optimum to get the best result. For  $ZnO$ , when added 2 per cent, the strength was increased. But when added 3 per cent the strength lowered down and showed the best result when added 4 per cent. This is a irregular picture for the materials added. Because if the added oxides are increased, the body showed the highest strength at a certain adding point. If more oxides are added, mullite will be dissolved and the material will lose its strength. So no definite conclusion can be drawn for this alloy oxides. On the other hand a mixture of oxides were added to the insulator raw material to observe the combined effect. But more or less in every case the data obtained from the experiment showed that the strength decreased. If the chemical analysis is observed it is clear that some  $TiO_2$  is always present in the raw clay materials. Now if intentionally some  $TiO_2$  and  $ZnO$  or  $ZrSiO_4$  or  $MnO_2$  are added to the clay materials, the total  $TiO_2$  will be increased and the effect will be lower strength.

To examine these effect few other samples were prepared using the BISF body containing a higher percentage of  $TiO_2$  and the bending strength data is shown in table 4.2. It is clear that, for samples no.8 where 2 per cent  $MnO+TiO_2$  are added, the bending strengths of the samples containing 0.57 , 0.71, 2.24 and 2.38 per cent  $TiO_2$  are 683.46, 698.79, 837.79 and 773.67  $Kg/cm^2$  respectively. So roughly at about 2 per cent  $TiO_2$  addition, the peak value of the bending strength will be observed.

## 4.2 Density Measurement

The density data of the studied samples is shown Table 4.3. It is shown that sample no. 8 (2% MnO<sub>2</sub> and TiO<sub>2</sub>), 3 (3% ZrSiO<sub>4</sub>), 7 (4% ZnO) were of higher density. This indicated that the presence of higher percentage of mullite and tridymite or cristobalite in the sample. The higher amount of crystalline phases supports the addition of catalytic oxides, i.e., zinc oxide, zirconium silicates. On the other hand sample no. 6 which was not modified, i.e., original BISF body, showed lower density compared to the modified samples. Sample no. 13 (4% ZrSiO<sub>4</sub> and TiO<sub>2</sub>) showed lowest density. Here fluxing oxides were higher and this dissolved the crystalline phases and formed the glassy phase and lowered down the density of the material. The samples that were prepared for the tests had no porosity.

## 4.3 Texture Analysis

The graphical representation of the textural effects in the form of an intensity count versus rocking angle curve are shown in figures 4.7 to 4.9. If the degree of periodicity of the curve is 0, that is if a straight line is explored with respect to intensity observation, the material is said to be texture free and has higher mechanical strength.

The non-fired samples show a straight line in the counts versus rocking angle graph, because crystalline growth of the phases were not occurred in the non-fired sample. The individual crystal of different oxides may have some definite directions. Thus textural indication may not be shown in these non-fired pattern. In the fired samples, however, the presence of crystalline phases (mullite, etc.) would cause some diffraction of the neutron particles and show some definite texture. The presence of alkaline oxides acted as nucleating sites for the growth and development of the crystalline phases and, hence, influence the textural properties.

Sample no. 1 (original BISF body), non-fired, (Fig. 4.7) showed a straight line in the counts versus rocking angle curve. This signifies the absence of texture upto angle 360°. For the fired specimen of the same sample, textural absence was observed upto 300° - rocking angle at the vertical directional rotation (Fig. 4.8). But after 300° rocking angle a periodicity was observed and the presence of texture could be identified at this rotational direction. These places were weak for the ceramic sample in the quality point of view.

For the fired sample no. 7 (4% ZnO), a straight line in the counts versus rocking angle curve was detected (Fig. 4.9) indicating no texture at the vertical directional rotation of

the sample. In this sample additives were used to increase the growth rate of the crystalline mullite. The direction of the growth of mullite may also been changed during the process.

#### 4.4 Thermo-Gravimetric Analysis

The thermo-gravimetric data for the sample studied are shown in Figs. 4.10 to 4.12.

During heating a differential heat loss was identified from the dilatometer TG analyser. Table 4.4 shows the percentage of weight loss on heating of the samples from room temperature to 1000°C at a rate of 15°C per minute.

For sample no. 1 (BISF body) the percentage of weight loss is minimum. Approximately at 550°C a sudden weight loss in the TG curve is shown in Fig 4.10. This is because of the breakdown or decomposition of chemically bonded water, which is obligatory for the property of the material. This abrupt nature of decomposition may cause rupture or place of weakness in the electrical porcelain.

Sample no. 7 (4% ZnO) showed the similar behaviour. Here the weight loss is about 11 percent and the sudden weight loss due to decomposition of water also appears at about 525°C, a somewhat lower temperature than that found for sample 1.

For sample no. 3 (3% ZrSiO<sub>4</sub>), however, although the percentage of weight loss is maximum (i.e. 16 %), no sharp decomposition of chemically bonded water was observed. Only a very weak decomposition temperature could be detected at 550°C. So the sample is appeared to be more safe on thermal rupture point of view.

#### 4.5 Differential Thermal Analysis

Fig. 4.10 to 4.12 showed the differential thermal analysis for BISF normal body (sample no. 1), modified sample with 3 per cent zirconium silicate (sample no. 3) and with 4 per cent zinc oxide (sample no. 7)

A wide peak indicating an exothermic reaction can be observed in all of these curves at temperatures between 100 and 500°C. This is because of the transformation of excess silica (besides feldspar and kaolinitic clays) from quartz phase to cristobalite phase. The degree of widening or the area under the exothermic portion of the curve for sample 1

clearly indicates the presence of a higher portion of silica phase and, consequently, a lower portion of mullite phase in the structure. The narrowness of this portion of the curve for sample 7 confirms the presence of a higher portion mullite phase and, hence, the higher mechanical properties. Sample 3 stands in between these two samples.

The endothermic reaction due to the breakdown of chemically bonded water, also indicated in the TG curves, is also confirmed in these DTA curves.

The most important case (i.e. the formation of mullite which occurs at temperatures between 1100 to 1300°C), however, cannot be studied because of the limitation of the instrument used.

#### **4.6 Co-Efficient of Thermal Expansion**

Five samples were examined under the Dilatometer and the length change versus temperature curves for these samples are shown in Figures 4.13 and 4.14. From these curves the linear coefficient of thermal expansion were calculated (Table 4.5).

From Table 4.5 it is clear that the modified samples were somewhat better than the unmodified sample i.e., original BISF body (sample 1) in respect to the coefficient of thermal expansion except the modified sample with 4 per cent zinc oxide (sample no. 7). The sample nos. 3 (3 per cent zirconium silicate), 13 (4 per cent zirconium silicate and titanium oxide) and 8 (2 per cent manganese oxide and titanium oxide) were denser and for porcelain production these samples were appeared to have a better quality.

#### **4.7 Optical Metallography**

The heterogencous nature of the product is observed in the Fig. 4.15 to 4.27 where quartz grains are surrounded by a solution rim of high-silica glass. The outlines of glass-mullite areas corresponding to the original feldspar grains and the unresolved matrix corresponding to the original clay can be clearly distinguished. Pore (dark) are also seen to be present. Although mullite is the crystalline phase in both the original feldspar grains and in the clay matrix, the crystal size and development are quite different. Here the dark matrix shows the presence of mullite, though it is not visible as separate mullite crystal. From the microstructures, the quartz grains are the only phase to be cared about. The grain size, shapes are also to be considered. A quartz grain and the surrounding solution

rim of silica-rich glass is shown in the microstructures. Usually the quartz forms only the glass phase, but for some compositions fired at high temperature, there is a transformation into cristobalite or tridymite which starts at the outer surface of the quartz grains. Typical microstress cracks were seen; the cracks were caused by the greater contraction of the quartz grains compared to that of the surrounding matrix.

The microstructure of the normal body of BISF (sample 1) shows the quartz grains and the surrounding solution rim of silica-rich glass (Fig. 4.15). This sample shows larger quartz grains which could be a reason for lower strength.

The microstructure of the modified samples based on zirconium silicate additions showed (Fig. 4.16, 4.17) more or less same grain size, when the additions were 2 and 3 per cent. The grains were fine and well distributed. When 4 per cent zirconium silicate (Fig. 4.18) was added, some change in microstructure was observed. The grains of quartz were larger compared to the samples containing 2 and 3 per cent alloy oxides.

The microstructure of the modified samples based on zinc oxide addition were shown in Figs. 4.19 to 4.21. The figures showed the variation of structure due to additions of 2, 3 and 4 per cent alloy oxides. The interesting part of these figures is the formation of larger grains of quartz due to the addition of 3 per cent zinc oxide (Fig. 4.20). But an addition of higher or lower amount shows a finer grains of quartz.

Figures 4.22 to 4.24 show the microstructures of the ( $\text{MnO}_2 + \text{TiO}_2$ ) modified samples. The quartz grains are more or less same sized irrespective of the amount of alloy oxide addition.

The microstructures of the modified samples based on ( $\text{ZrSiO}_4 + \text{TiO}_2$ ) addition are shown in the figures 4.25 to 4.27. The figures show the variation of structure due to additions of 2, 3 and 4 per cent alloy oxides. The interesting part of these figs were formation of larger grains of quartz due addition of 3 per cent ( $\text{ZrSiO}_4 + \text{TiO}_2$ ). But addition of higher amount i.e., 4 per cent (Fig. 4.27), showed finer grains of quartz. Addition of 2 per cent alloy oxide showed finer grains of quartz.



#### 4.8 Phase Analysis by X-ray Diffraction

X-ray diffraction technique (Henawalt Method) was carried out on the samples prepared for this study. The phases observed and their corresponding planes and arbitrary intensities were recorded. The data thus obtained were presented graphically and in Tables 4.6 to 4.18.

The normal BISF body shows only mullite phases in the x-ray records. When 2, 3, 4 percent zirconium silicate were added to the BISF body composition presence of some tridymite were observed. This tridymite phase not only imparts light weightness to the body but also shows lower co-efficient of thermal expansion. Addition of 2, 3 percent zinc oxide to the BISF body composition shows mullite and tridymite phases. But when 4 per cent zinc oxides were added to the BISF body, no tridymite but mullite phase was observed. Here addition of 4 percent zinc oxide dissolves out the tridymite phase. Combined effect of 2, 3 and 4 per cent manganese dioxide, zirconium silicate, zinc oxide and titanium oxide in the x-ray diffraction pattern shows both mullite and tridymite phases. Here one thing is to be remembered that though zirconium silicate were added 2, 3 and 4 per cent to the BISF body composition the tridymite phase remains in the structure. But when 4 per cent zinc oxide were added to the body the phase disappeared. Thus for light weight and lower co-efficient of thermal expansion of the material, zirconium silicate is the best to add compared to 4 per cent zinc oxide. The x-ray diffraction patterns are shown in the Figs. 4.28 to 4.40.

## 5 CONCLUSIONS

The study finally reached to the following conclusions:

1. The addition of alkaline earth oxides lower down the firing temperature of the ceramic body and thus gives enough time for the growth of the crystalline phases.
2. The growth of tridymite is observed by x-ray diffraction for material with alkaline earth oxides which ensures the materials stability.
3. The grains size of the fused quartz becomes finer with addition of these catalytic oxides.
4. Additions of alkaline earth oxides eliminates the textural defects of the materials.
5. The addition of alkaline earth oxides increases the growth of mullite and, hence, improve the mechanical properties of the material. Zirconium silicate and zinc oxide are appeared to have the best effects in increasing the strength of the ceramic materials.
6. The density of the material decreases with 3 per cent addition of zirconium silicate and increases with 4 per cent zinc oxide addition. Addition of 4 per cent zirconium silicate plus titanium dioxide extensively lowers down the density of the material.
7. Though the weight loss of the materials increases with addition of alkaline earth oxides during heating, but among them addition of 3 percent zirconium silicate showed uniform weight loss which ensures thermal stability at the range of 500 to 600°C. But the original BISF body and 4 per cent zinc oxide added samples showed sudden weight loss at the range of 500 to 600°C.
8. Additions of alkaline earth oxides lowers the coefficient of thermal expansion of the materials and 3 per cent zirconium silicate shows the best result followed by 4 per cent zinc oxide.
9. Amongst all the alkaline earth oxides added to the original BISF ceramic insulator body, a 3% addition of zirconium silicate was appeared to have resulted the best combination of properties, and can be suggested to use extensively in the commercial manufacture of ceramic insulators.

## 6 SUGGESTIONS FOR FUTURE WORK

The topic just described here requires a great deal of research to find out more information about it. The present author experienced a lot of experimental difficulties to carry out certain important tests such as finding out the electrical breakdown voltage, performing thermal analyses at higher temperatures, etc. These tests are of fundamental importance for a ceramic insulator materials and the author regrets of not having the opportunity of carry out these tests. Besides these tests, the future works that can be carried out in conjunction with the part which is already done here are summarized below:

1. Use of scanning electron microscope for the quantitative identification of the mullite and tridymite phases.
2. The firing temperature should be varied from about 1000 to 1300°C at a 5°C interval to observe the effects of the addition of individual alkaline earth oxide. This will indicate the presence of sufficient mullite at such a lower temperate and ensures a cut in the fuel consumption.
3. The addition of zinc oxide shows an unusual picture (i.e., strength decreases up to 3 per cent addition and increases beyond this point) in the present work which does not comply with the general theoretical belief and the findings of other oxide addition. This needs a further clarification.

## 7 BIBLIOGRAPHY

1. Bleininger, A. V. and Riddle, F.H., J. Amer. Ceram. Soc. 2 (1919) 564
2. Zerfoss, S. and Utter, B. A., J. Amer. Ceram. Soc. 29 (1946) 205
3. Klever, E., Glastechn. Ber. 7 (1929/30) 85
4. Gregg, S. J. and Stephens, M. J., J. Chem. Soc. (Dec., 1953) 3951
5. Eitel, W. and Neumann, B., Neues Jb. Min. Geol. Palaont. 53, Suppl. I (1925) 1
6. Bowen, N. L. and Greig, J. W., J. Amer. Ceram. Soc. 7 (1924) 238
7. Chatelier, H. LE, Z. Phys. Chem. I (1887) 396
8. Mellor, J. W. And Holdcroft, A.D., Trans. Brit. Ceram. Soc. 10 (1910/11) 94
9. Weiss, E. J., and Rowland, R. A., 1956. "Oscillating-heating X-ray diffractometer studies of clay mineral dehydroxylation", Amer. Min, 41, 117-126
10. Hyslop, J. F. and Rooksby, H. P., Trans. Brit. Ceram. Soc. 27 (1927/28) 93, 29912. Hyslop, J. F., Trans. Brit. Ceram. Soc. 43 (1944) 49
11. Insley, H., and Ewell, R. H., 1935. "Thermal behaviour of kaolin mincrals", J. Res. nat. Bur. Stand. 14, 615-627
13. Comeforo, J. E., Fischer, R. B. and Bradley, W. F., J. Amer. Ceram. Soc. 31 (1948) 254
14. Sachse and Becker, Landw. Versuchsw. 40 (1892) 245
15. Sokolov, A. N., Tonindustr Ztg 36 (1912) 1107; Sprechsaal Arch. (1912) No. 9
16. Mellor, J.W. and Holdcroft, A.D., Reference 8 and ibid. (1911/12) 169
17. Keppeler, G., Reference 100 p. 447
18. Tammann, G. and Pape, W., Z. Anorg. Chem. 127 (1923) 43
19. Rooksby, H. P., J. Sci. Instrum. 18 (1941) 84
20. Krause, O., Glastechn. Ber. 10 (1931) 491

21. Biltz, W. and Lemke, A., Z. Anorg. Chem. 186 (1930) 373
22. Agafonov, V. and Vernadsky, W., C.R. Akad. Sci. U.R.S.S. 178 (124 I.) 1082
23. Iskull, W., Trans. Ceram. Res. Inst., Leningrad 2 (1925)
24. Jurganov, W. W. and Sussmanowitsch, M. W. , Trans. Ceram. Res. Inst., Moscow 21 (1929)
25. Vesterberg, K. A., Arch. Chem. Miner. Geol., Stockh., 9 (No. 14) 1
26. Fuchs, H. Von, Denkschr. Akad. Wiss. Munchen 7 (1821) 65
27. Rinne, F., Z. Kristallogr. 61 (1924/25) 119
28. Zwetsch, A., Reference 101 p. 6
29. Hansen, W. C. and Brownmiller, L. Z., Amer. J. Sci. 15 (1928) 225
30. Spangenberg, K. and Rhode, J., Keram. Rdsch. 35 (1927) 398
31. Eitel, W. and Kedesdy, H., Abh. preuss. Akad. Wiss. No. 5 (1943). 37
32. Colegrave, E. B. and Rigby, G. R., Trans. Brit. Ceram. Soc. 51 (1952) 355
33. Roy, R., Roy, D. M. and Francis, E. E., J. Amer. Ceram. Soc. 38 (1955) 198
34. Parmelee, C. W. and Rodriguez, A., J. Amer. Ceram. Soc. 25 (1942) 1
35. Budnicov, P.P. and Schmuckler, K.M., Zh. prikl. khim., Leninger. 19 (1946) 1029
36. Rhode, J., Keram. Rdsch. 35 (1927) 398
37. Navias, L., J. Amer. Ceram. Soc. 8 (1925) 296
38. Michr, W., Ber. dtsh. keram. Ges. 9 (1928) 339
39. Tuttle, M. A. and Cook, R. L., J. Amer. Ceram. Soc. 32 (1949) 286
40. Gad, G. M. and Barrett, L. R., Trans. Brit. Ceram. Soc. 49 (1950) 470
41. Gould, R. E., Reference 102 p. 84
42. Odelberg, A. S. W., Trans. Brit. Ceram. Soc. 38 (1939) 403

43. Larchevwque, M., Reference 103 vol. 2 p. 131
44. Mellor, J. W., J. Soc. Chem. Ind. 26 (1907) 375
45. Zoellner, A., Ph.D. thesis, Berlin, 1908
46. Mellor, J. W. and Austin, J. B., Trans. Brit. Ceram. Soc. 6 (1906) 129
47. Ponomarov, J., Keram. I Steklo (1929) No.1
48. Navratiel, H. and Fessler, A. H., Ber. Dtsch. Keram. Ges. 11 (1930) (a) 371; (b) 369
49. Krause, O. and Keetman, E., Sprechsaal (a) 68 (1935) 177; (b) 69 (1936) 45; (c) ib. 613
50. Schwarz, R. and Merck, K., Z. Anorg. Chem. 156 (1926) 1
51. Holborn, L. and Gruneisen, E., Ann. Phys. Lpz. 6 (1901) 136
52. Kraner, H. M., J. Amer. Ceram. Soc. 12 (1929) 383
53. Budnikov, P. P. and Gevorkyan, K. O., Glass & Ceramics, Moscow 8 No. 3 (1951) 15 (Brit. Ceram. Abstr. (1951) 380 A; Amer. Ceram. Abstr. (1951) 200)
54. Collins, P.F., J. Amer. Ceram. Soc. 15 (1932) 17; Ceramic Ind. 18 (1932) 294
55. Chilcoté, J. H., J. Amer. Ceram. Soc. 17 (1934) 203
56. Fenner, C. N. and Day, F., Jr., Z. Anorg. Chem. 85 (1914) 133
57. Nieuwenburg, C. J. Van, Rec. Trav. Chim. Pays-Bas 48 (1929) 402
58. Ostwald, W., Z. Phys. Chem. 22 (1897) 289
59. Cole, S. S., J. Amer. Ceram. Soc. 18 (1935) 149
60. Florke, O. W., Ber. Dtsch. Keram. Ges. 32 (1955) 369
61. Fenner, C. N., J. Amer. Ceram. Soc. 36 (1913) 331
62. Weyl, W. A., C. R. Acad. Sci., Paris 180 (1935) 1949
63. Plumet, E., Verre et Silic. Industr. 13 Suppl. (1948) 81

64. Dietzel, A., in Reference 99
65. Hirsch, H., Ber. Dtsch. Keram. Ges. 7 (1926) 49
66. Nieuwenburg, C. J. Van and De Nooyer, C. N. J., Rec. Trav. Chim. Pays-Bas 47 (1928) 627; Ber. Dtsch. Keram. Ges. 9 (1928) 493
67. Taylor, N. W. and Cho-Yuen-Lin, J. Amer. Ceram. Soc. 24 (1941) 57
68. Krause, O., Sprechsaal 70 (1937) 611, 648; 75 (1942) 276
69. Marzahl, H., Ber. Dtsch. Keram. Ges. 32 (1955) 203
70. Chesters, J. H. and Parmelee, C. W., J. Amer. Ceram. Soc. 17 (1934) 50
71. Mellor, J. W. and Campbell, A. J., Trans Brit. Ceram. Soc. 15 (1915/16) 77
72. Rath, G. Vom, Ann. Phys., Lpz. 133 (1868) 507
73. Wassermann, G., Texturen Metallischer Werkstoffe (Berlin: Springer, 1939)
74. Wassermann, G., and J. Grewen, Texturen Metallischer Werkstoffe, 2nd ed. (Berlin: Springer, 1962)
75. Schultz, L. G., "A Direct Method of Determining Preferred Orientation of a Flat Reflection Specimen Using a Geiger Counter X-Ray Spectrometer", J. Appl. Phys., 20 (1949), pp. 1030-1036
76. Bunge, H. J., "Zur Darstellung Allgemeiner Texturen," Z. Metall., Bd. 56 (1965), pp. 872-874
77. Bleininger, A. V. and Moore, J. K., Trans. Amer. Ceram. Soc. 10 (1908) 293; Sprechsaal 42 (1909) 644
78. Gottstein, G., and Lucke, K., eds., Texture of Materials, Proceedings of the Fifth International Conference on Texture of Materials, ICOTOM5 (New York: Springer-Verlag, 1978)
79. Bunge, H. J., ed., Textures of Materials, ICOTOM-10, Proceeding of the 10th International Conference on Textures of Materials (Aedermannsdorf, Switzerland: Trans Tech Publications, 1994), pp. 157-162

80. Brokmeier, H.-G., and Gertel, H., "Quantitative Phase Analysis in Textured Materials", *Advances and Applications of Quantitative Texture Analysis*, ed. H. J. Bunge and C. Esling (Oberursel, Germany: DGM informations gesellschaft, 1991), pp. 289-298
81. Brakman, C. M., "Application of the ODF to Residual Stress Analysis Problems of Textured Cubic Materials. Diffraction Strain Pole Figures. "Theoretical Methods of Texture Analysis, ed. H. J. Bunge (Oberursel, Germany: DGM informationsgesellschaft, 1987), pp. 377-390
82. Bunge, H. J., ed., *Experimental Techniques of Texture Analysis* (Oberursel, Germany: DGM informationsgesellschaft, 1986)
83. Bunge, H. J. , ed., *Theoretical Methods of Texture Analysis* (Oberursel, Germany: DGM informationsgesellschaft, 1987)
84. Bunge, H. J., ed., *Directional Properties of Materials* (Oberursel, Germany: DGM informationsgesellschaft, 1988)
85. Bunge, H. J. and Esling, C., eds., *Advances and Applications of Quantitative Texture Analysis* (Oberursel, Germany: DGM informationsgesellschaft, 1991)
86. Bunge, H. J., *Texture Analysis in Materials Science* (Boston, Butterworths, 1982)
87. Bunge, H. J. and Esling, C., eds., *Quantitative Texture Analysis* (Oberursel: DGM 1982)
88. Wenk, H. -R., ed., *Preferred Orientation in Deformed Metals and Rocks: An Introduction to Modern Texture Analysis* (New York, Academic Press, Inc., 1985)
89. Mackenzie, R.C., *Thermochem. Acta*, 28, 1 (1979)
90. Mackenzie, R. C., *Isr. J. Chem.*, 22, 203 (1982)
91. Dunn, J. G., *Tech. Inform. Sheet No. 130*, Stanton Redcroft, London
92. Pekenc, E., and J. H. Sharp, *Proc. 4th ICTA*, I. Buzas, ed., Vol. 2. Akademiai Kiado. Budapest, 1975, p. 585
93. Earnest, C. M., *Thermal Analysis Application Study 30*, Perkin-Elmer Corp., Norwalk, CT



94. R. C. Mackenzie, ed., Differential Thermal Analysis, Academic. New York. 1970.  
Chaps. 7-15
95. Earnest, C. M., Thermal Analysis Application Study 30, Perkin-Elmer Corp.,  
Norwalk, CT
96. Keith, M. L., and O. F. Tuttle, Am. J. Sci., Bowen, Vol., 203 (1952)
97. Zwetsch, A. and Buching, W., Ber. Dtsch. Keram. Ges. 11 (1930) 270
98. Hladecek, M., Pechacek, F., Zeman, D., Kleisner, J., Evaluation of Raw Materials  
from Bangladesh, Research Institute for Ceramics, Refractories and Non-Metallic  
Raw Materials, Pilsen, Czechoslovakia, 1988
99. Edelman, C. H., Landbouwk. Tijdschr., Groningen 49 (April/May, 1937)
100. Keppeler, G., Sprechsaal 46 (1913) 445
101. Zwetsch, A., Ber. dtsh. keram. Ges. 19 (1934) 2
102. Morey, G. W. and Chen, W. T., Amer. Min. 40 (1955) 995
103. Kerr, P. F., J. Amer. Ceram. Soc. 21 (1938) 268.

89285

## Tables

**Table 2.1 A typical proportion of the raw materials used to prepare conventional ceramic insulator body**

Bejoypur Clay	Ball Clay	Feldspar (Local)	Feldspar (India)	China Clay (Body)	China Clay (Highly plastic)	Total, %
32	8	30	11	8	11	100

**Table 2.2 Invariant points of the system  $Al_2O_3$ - $SiO_2$**

Point	Phases	Process	Wt. % of		Temp., °C
			$Al_2O_3$	$SiO_2$	
1	$Al_2O_3$ +liquid	Fusion	100	0	2050
2	$Al_2O_3$ +solid solution+ $3Al_2O_3 \cdot 2SiO_2$ +liquid	Eutectic	79.0	21.0	1850
3	$3Al_2O_3 \cdot 2SiO_2$ +liquid	Congruent fusion	71.80	28.2	1910
4	$3Al_2O_3 \cdot 2SiO_2$ + $SiO_2$ +liquid	Eutectic	5.5	94.5	1584
5	$SiO_2$ +liquid	Fusion	0	100	1713

**Table 2.3 Densities of different phases of quartz**

Phases	Crystal system	Sp. Gr.
$\beta$ -Quartz	Hexagonal (Trigonal)	2.65
$\gamma$ -Tridymite	Rhombic (pseudo-hexagonal)	2.27
$\beta$ -Cristobalite	Cubic (pseudo-isometric)	2.31
Silica glass	Amorphous	2.21

**Table 2.4 Effect of catalyst on the conversion of quartz**

Catalyst added (1 %)	Sp.Gr. after heating for 1 hour at 1300°C	Conversion due to catalyst (per cent)
No flux	2.265	-
CaO	2.585	12
CaF <sub>2</sub>	2.62	2
MgO	2.585	12
BaO	2.605	6
PbO	2.585	12
ZnO	2.61	5
Cr <sub>2</sub> O <sub>3</sub>	2.605	6
MnO <sub>2</sub>	2.58	14
CoO	2.61	5
Fe <sub>2</sub> O <sub>3</sub>	2.55	23
FeO	2.53	29
ZrO <sub>2</sub>	2.60	8
TiO <sub>2</sub>	2.625	0
Al <sub>2</sub> O <sub>3</sub>	2.615	3
B <sub>2</sub> O <sub>3</sub>	2.58	14
Na <sub>2</sub> WO <sub>4</sub> ·2H <sub>2</sub> O	2.55	23
WO <sub>3</sub>	2.60	8
MoO <sub>3</sub>	2.59	11
Na <sub>2</sub> B <sub>4</sub> O <sub>7</sub> ·10H <sub>2</sub> O	2.505	37
Na <sub>2</sub> HPO <sub>4</sub> ·12 H <sub>2</sub> O	2.545	25
(NH <sub>4</sub> ) <sub>3</sub> PO <sub>4</sub>	2.61	5
Na <sub>2</sub> SiF <sub>6</sub>	2.42	63
Na <sub>2</sub> SiO <sub>3</sub>	2.39	72
Na <sub>2</sub> CO <sub>3</sub>	2.35	85
K <sub>2</sub> CO <sub>3</sub>	2.325	92
Li <sub>2</sub> CO <sub>3</sub>	2.305	98

**Table 3.1 Grain size distribution of clayey raw material used in the insulator body**

Fraction $\mu\text{m}$	Yield, Wt %					
	China clay (imported)	China clay (Rajmahal)	Ball clay (White) local	Bejoypur clay (Grade-1) local	Bejoypur clay (Grade-1) washed local	Ball clay (black) Imported
> 63	0.8	1.2	0.2	46.6	8.4	2.6
20-63	0.0	4.0	0.0	7.5	11.9	12.7
10-20	9.9	14.8	5.0	9.1	18.3	21.4
5-10	20.8	11.9	13.5	7.5	18.3	17.5
2-5	28.8	20.7	28.9	7.5	17.4	12.7
1-2	9.9	10.9	10.0	4.3	11.0	10.7
< 1	29.8	36.5	42.4	17.5	14.7	22.4

**Table 3.2 Chemical analysis of the raw materials used to prepare samples**

	China Clay Highly Plastic (Imported)	China Clay Body (Imported)	Ball Clay White (Imported)	Bejoypur Clay (Grade-1) Local	Ball Clay (Black) Imported	Feldspar Local	Feldspar (India)
L.O.I	9.08	11.99	9.90	6.23	10.16	0.53	1.0
SiO <sub>2</sub>	50.18	51.86	54.43	72.09	61.27	74.98	67.0
TiO <sub>2</sub>	0.14	0.50	1.84	1.02	1.41	0.08	0.50
Al <sub>2</sub> O <sub>3</sub>	33.34	34.72	30.97	18.69	24.85	14.37	19.0
Fe <sub>2</sub> O <sub>3</sub>	1.88	0.57	1.37	1.01	0.71	0.83	0.50
MgO	1.05	0.07	0.34	0.14	0.26	0.08	0.40
CaO	0.94	0.07	0.17	0.10	0.65	0.68	0.75
Na <sub>2</sub> O	0.81	0.041	0.17	0.11	0.25	3.54	4.0
K <sub>2</sub> O	2.58	0.18	0.81	0.61	0.44	4.91	10.5

**Table 3.3 Typical Body Composition of Ceramic Insulator**

Bijoypur Clay	Ball Clay	Feldspar (Local)	Feldspar (India)	Broken body	China Clay (body)	China Clay (Highly Plastic)	Total, %
32	8	30	8	3	8	11	100

**Table 3.4(a) Chemical Analysis of the Unmodified Final Product**

L.O.I	SiO <sub>2</sub>	TiO <sub>2</sub>	Al <sub>2</sub> O <sub>3</sub>	Fe <sub>2</sub> O <sub>3</sub>	MgO	CaO	Na <sub>2</sub> O	K <sub>2</sub> O	Total, %
5.03	67.50	0.573	20.81	0.93	0.25	0.47	1.64	2.90	100

**Table 3.4(b) Chemical Analysis of the Raw Materials of 2nd set of samples**

L.O.I	SiO <sub>2</sub>	TiO <sub>2</sub>	Al <sub>2</sub> O <sub>3</sub>	Fe <sub>2</sub> O <sub>3</sub>	MgO	CaO	Na <sub>2</sub> O	K <sub>2</sub> O	Total, %
6.75	60.02	0.71	25.96	0.98	0.32	1.19	1.12	2.95	100

**Table 3.5 Samples prepared for the testing**

Sample No.	Composition
1	Normal (BISF) Body
2	BISF body + 2% Zirconium silicate
3	BISF body + 2% Zinc oxide
4	BISF body + 2% ( $\text{MnO}_2 + \text{TiO}_2$ ) (2 parts $\text{MnO}_2$ + 1 part $\text{TiO}_2$ )
5	BISF body + 3% Zirconium silicate
6	BISF body + 4% Zirconium silicate
7	BISF body + 3% $\text{ZnO}_2$
8	BISF body + 4% $\text{ZnO}_2$
9	BISF body + 3% ( $\text{MnO}_2 + \text{TiO}_2$ ) (2 parts $\text{MnO}_2$ + 1 part $\text{TiO}_2$ )
10	BISF body + 4% ( $\text{MnO}_2 + \text{TiO}_2$ ) (2 parts $\text{MnO}_2$ + 1 part $\text{TiO}_2$ )
11	BISF body + 2% ( $\text{ZrSiO}_4 + \text{TiO}_2$ ) (2 parts $\text{ZrSiO}_4$ + $\text{TiO}_2$ )
12	BISF body + 3% ( $\text{ZrSiO}_4 + \text{TiO}_2$ ) (2 parts $\text{ZrSiO}_4 + \text{TiO}_2$ )
13	BISF body + 4% ( $\text{ZrSiO}_4 + \text{TiO}_2$ ) (2 parts $\text{ZrSiO}_4 + \text{TiO}_2$ )
14	BISF body + 2% ( $\text{ZnO}_2 + \text{TiO}_2$ ) (2 parts $\text{ZnO}_2$ + 1 part $\text{TiO}_2$ )
15	BISF body + 3% ( $\text{ZnO}_2 + \text{TiO}_2$ ) (2 parts $\text{ZnO}_2$ + 1 part $\text{TiO}_2$ )
16	BISF body + 4% ( $\text{ZnO}_2 + \text{TiO}_2$ ) (2 parts $\text{ZnO}_2$ + 1 part $\text{TiO}_2$ )

**Table 4.1 Bending strength data of the samples**

Sample No.	Composition (2000gm)	Reading (Kg/cm <sup>2</sup> )	Mean Bending Strength (Kg/cm <sup>2</sup> )
1	Normal (BISF) Body	705.98 660.94	683.46
2	BISF body+2% Zirconium silicate	727.37 818.29	772.80
3	BISF body+3% Zirconium silicate	845.00 851.00	848.00
4	BISF body+4% Zirconium silicate	630.40 638.00	634.20
5	BISF body+2% ZnO <sub>2</sub>	794.23 805.30	799.77
6	BISF body+3% ZnO <sub>2</sub>	774.50 783.50	779.00
7	BISF body+ 4% ZnO <sub>2</sub>	853.50 848.50	851.00
8	BISF body+2% (MnO <sub>2</sub> +TiO <sub>2</sub> ) (2 parts MnO <sub>2</sub> + 1 part TiO <sub>2</sub> )	831.29 844.28	837.79
9	BISF body+3% (MnO <sub>2</sub> +TiO <sub>2</sub> ) (2 parts MnO <sub>2</sub> + 1 part TiO <sub>2</sub> )	710.20 699.20	704.70
10	BISF body+4% (MnO <sub>2</sub> +TiO <sub>2</sub> ) (2 parts MnO <sub>2</sub> + 1 part TiO <sub>2</sub> )	640.00 628.00	634.00
11	BISF body+2% (ZrSiO <sub>4</sub> +TiO <sub>2</sub> ) (2 parts ZrSiO <sub>4</sub> +TiO <sub>2</sub> )	775.00 789.00	782.00
12	BISF body+3% (ZrSiO <sub>4</sub> +TiO <sub>2</sub> ) (2 parts ZrSiO <sub>4</sub> +TiO <sub>2</sub> )	770.00 754.00	762.00
13	BISF body+4% (ZrSiO <sub>4</sub> +TiO <sub>2</sub> ) (2 parts ZrSiO <sub>4</sub> +TiO <sub>2</sub> )	860.00 841.60	850.80
14	BISF body+2% (ZnO <sub>2</sub> +TiO <sub>2</sub> ) (2 parts ZnO <sub>2</sub> +1 part TiO <sub>2</sub> )	690.50 686.30	688.40
15	BISF body+3% (ZnO <sub>2</sub> +TiO <sub>2</sub> ) (2 parts ZnO <sub>2</sub> +1 part TiO <sub>2</sub> )	740.50 743.50	742.00
16	BISF body+4% (ZnO <sub>2</sub> +TiO <sub>2</sub> ) (2 parts ZnO <sub>2</sub> +1 part TiO <sub>2</sub> )	710.60 699.40	705.00



**Table 4.2 Bending test data using 2nd set of samples**

Sample No.	Additives	% addition	Bending Strength (kg/cm <sup>2</sup> )	Mean Strength (kg/cm <sup>2</sup> )
1	(Original BISF body)		705.98	698.79
			700.10	
			690.30	
8	2 parts MnO <sub>2</sub> + 1 part TiO <sub>2</sub>	2	766.00	773.67
			775.00	
			780.00	
3	ZrSiO <sub>4</sub>	3	843.00	846.00
			850.00	
			845.00	
7	ZnO	4	870.00	866.00
			865.00	
			863.00	
13	2 parts ZrSiO <sub>4</sub> + 1 part TiO <sub>2</sub>	4	812.00	812.33
			815.00	
			810.00	

**Table 4.3 Density of the ceramic insulator materials**

Sample No.	% Oxide added	Average Density, gm/cc
01	BISF body	2.36
08	2% (MnO <sub>2</sub> +TiO <sub>2</sub> )	2.45
03	3% ZrSiO <sub>4</sub>	2.37
07	4% ZnO	2.45
13	4% (ZrSiO <sub>4</sub> +TiO <sub>2</sub> )	2.29

**Table 4.4 Percentage of weight loss on heating of sample**

Sample No.	% Oxide Added	% Wt. loss
01	BISF body	$(0.43/4.3)100=10.0\%$
03	3% ZrSiO <sub>4</sub>	$(0.40/2.5)100=16.0\%$
07	4% ZnO	$0.65/5.75)100=11.30\%$

**Table 4.5 Variation of coefficient of thermal expansion**

Sample No.	% Oxide Added	Coefficient of thermal expansion
01	BISF body	$4.5 \times 10^{-6}$
08	2% (MnO <sub>2</sub> +TiO <sub>2</sub> )	$4.0 \times 10^{-6}$
03	3% ZrSiO <sub>4</sub>	$3.7 \times 10^{-6}$
07	4% ZnO	$4.8 \times 10^{-6}$
13	4% (ZrSiO <sub>4</sub> +TiO <sub>2</sub> )	$3.8 \times 10^{-6}$

**Table 4.6 Normal BISF body**

Diffraction angle ( $2\theta$ )	d-spacing	$I/I_0$	Diffraction planes, hkl	Phases present
26.30	3.390	100.00	210	Mullite
33.40	2.680	15.00	220	Mullite
35.50	2.530	15.00	111	Mullite
39.40	2.280	10.00	210	Mullite
40.90	2.204	20.00	121	Mullite
57.50	1.600	5.00	041	Mullite
60.60	1.526	15.00	331	Mullite

**Table 4.7 Effect of 2% zirconium silicate addition**

Diffraction angle ( $2\theta$ )	d-spacing	$I/I_0$	Diffraction planes, hkl	Phases present
22.60	3.930	4.50	-	Tridymite
22.80	3.896	2.30	-	Tridymite
26.60	3.348	100.00	210	Mullite
33.10	2.704	14.00	220	Mullite
35.30	2.540	16.00	111	Mullite/Tridymite
39.10	2.301	2.30	021	Mullite/Tridymite
40.90	2.204	23.00	121	Mullite
42.60	2.12	4.50	230	Mullite
53.30	1.717	4.50	240	Mullite/Tridymite
60.50	1.528	4.50	331	Mullite
62.50	1.485	4.50	510	Mullite/Tridymite

**Table 4.8 Effect of 3% zirconium silicate addition**

Diffraction angle (2θ)	d-spacing	I/I <sub>0</sub>	Diffraction planes, hkl	Phases present
26.40	3.370	100.00	210	Mullite
27.00	3.299	8.33	-	Tridymite
33.10	2.700	8.33	220	Mullite
35.10	2.550	1.67	111	Mullite
35.50	2.530	1.67	-	Tridymite
40.70	2.214	16.67	121	Mullite
43.70	2.069	4.00	-	Tridymite
48.20	1.886	0.83	400	Mullite
53.50	1.711	12.50	240	Mullite
55.50	1.654	1.67	-	Tridymite
60.60	1.526	12.50	331	Mullite
64.40	1.445	2.08	002	Mullite
67.80	1.380	2.08	112	Mullite

**Table 4.9 Effect of 4% zirconium silicate addition**

Diffraction angle (2θ)	d-spacing	I/I <sub>0</sub>	Diffraction planes, hkl	Phases present
26.70	3.335	100.00	210	Mullite
31.10	2.873	11.36	001	Mullite
33.40	2.680	13.63	220	Mullite
35.80	2.506	40.91	111	Mullite
39.20	2.296	6.82	201	Mullite
40.80	2.209	27.27	121	Mullite
43.90	2.060	2.27	320	Mullite
47.60	1.908	3.41	-	Tridymite
50.00	1.822	1.14	-	Tridymite
52.30	1.747	1.14	330	Mullite
53.70	1.705	13.63	321	Mullite
57.70	1.596	1.14	041	Mullite
59.60	1.549	1.14	411	Mullite
60.70	1.524	6.82	331	Mullite
62.60	1.482	0.91	510	Mullite
64.50	1.440	1.14	002	Mullite

**Table 4.10 Effect of 2% zinc oxide addition**

Diffraction angle (2 $\theta$ )	d-spacing	I/I <sub>0</sub>	Diffraction planes, hkl	Phases present
26.50	3.360	100.00	210	Mullite
33.20	2.696	7.00	220	Mullite
35.00	2.560	7.00	111	Mullite
36.60	2.453	11.00	130	Mullite
40.80	2.209	22.00	121	Mullite/Tridymite
53.60	1.708	1.40	321	Mullite
59.30	1.557	3.60	141	Mullite
60.50	1.528	11.00	331	Mullite
64.20	1.449	3.60	002	Mullite/Tridymite

**Table 4.11 Effect of 3% zinc oxide addition**

Diffraction angle (2 $\theta$ )	d-spacing	I/I <sub>0</sub>	Diffraction planes, hkl	Phases present
20.70	4.287	33.33	-	Tridymite
23.80	3.735	0.66	200	Mullite
26.60	3.348	100.00	210	Mullite
31.20	2.864	23.33	001	Mullite
35.10	2.554	20.00	111	Mullite
36.60	2.453	40.00	130	Mullite
40.60	2.220	10.00	121	Mullite
42.60	2.120	1.33	230	Mullite
55.30	1.654	6.67	-	Tridymite
59.10	1.562	13.33	141	Mullite
60.60	1.526	16.67	331	Mullite
64.40	1.445	0.67	002	Mullite/Tridymite
65.00	1.433	20.00	-	Tridymite

**Table 4.12 Effect of 4% zinc oxide addition**

Diffraction angle ( $2\theta$ )	d-spacing	$I/I_0$	Diffraction planes, hkl	Phases present
26.50	3.360	100.00	210	Mullite
31.20	2.860	35.00	001	Mullite
36.80	2.440	65.00	130	Mullite
40.80	2.209	20.00	121	Mullite
50.00	1.820	10.00	311	Mullite
59.20	1.559	30.00	141	Mullite
60.80	1.522	15.00	331	Mullite
65.20	1.429	30.00	250	Mullite

**Table 4.13 Effect of 2% (manganese dioxide + titanium oxide) addition**

Diffraction angle ( $2\theta$ )	d-spacing	$I/I_0$	Diffraction planes, hkl	Phases present
26.40	3.370	100.00	210	Mullite
31.00	2.880	2.22	001	Mullite
33.50	2.670	8.33	220	Mullite
35.50	2.526	11.11	111	Mullite
37.10	2.421	2.80	130	Mullite
40.00	2.250	1.12	-	Tridymite
41.00	2.199	44.40	121	Mullite
42.50	2.125	5.60	230	Mullite
51.50	1.770	1.11	330	Mullite
54.30	1.687	2.80	420	Mullite
61.00	1.517	27.80	-	Tridymite
64.80	1.437	5.60	-	Tridymite

**Table 4.14 Effect of 3% (manganese dioxide+titanium oxide) addition**

Diffraction angle (2 $\theta$ )	d-spacing	I/I <sub>0</sub>	Diffraction planes, hkl	Phases present
26.30	3.385	100.00	210	Mullite
30.30	2.947	16.66	-	Tridymite
30.80	2.900	16.66	001	Mullite
31.90	2.803	16.66	-	Tridymite
33.30	2.688	22.22	220	Mullite
35.20	2.547	27.77	111	Mullite
39.20	2.296	16.66	201	Mullite
40.80	2.209	27.77	121	Mullite
49.70	1.832	2.77	311	Mullite
60.60	1.526	27.77	331	Mullite
64.50	1.443	5.55	002	Mullite/Tridymite

**Table 4.15 Effect of 4% (manganese dioxide+titanium oxide) addition**

Diffraction angle (2 $\theta$ )	d-spacing	I/I <sub>0</sub>	Diffraction planes, hkl	Phases present
26.60	3.348	100.00	210	Mullite
33.40	2.680	24.00	220	Mullite
35.50	2.526	9.50	111	Mullite
39.40	2.285	7.00	001	Mullite
41.00	2.199	14.00	121	Mullite
61.00	1.517	19.00	-	Tridymite

**Table 4.16 Effect of 2% (zirconium silicate+titanium oxide) addition**

Diffraction angle (2θ)	d-spacing	I/I <sub>0</sub>	Diffraction planes, hkl	Phases present
26.60	3.348	100.00	210	Mullite
33.10	2.704	22.22	220	Mullite
35.20	2.547	19.44	111	Mullite
40.80	2.209	25.00	121	Mullite
42.50	2.125	8.33	230	Mullite
56.60	1.624	1.00	041	Mullite/Tridymite
60.80	1.522	14.00	331	Mullite
64.50	1.443	6.00	002	Mullite
68.00	1.377	1.11	112	Mullite

**Table 4.17 Effect of 3% (zirconium silicate + titanium oxide) addition**

Diffraction angle (2θ)	d-spacing	I/I <sub>0</sub>	Diffraction planes, hkl	Phases present
26.70	3.335	100.00	210	Mullite
33.50	2.672	9.00	220	Mullite
35.50	2.526	13.00	111	Mullite
39.50	2.279	6.50	201	Mullite
41.00	2.199	22.00	121	Mullite
42.80	2.110	2.00	320	Mullite/Tridymite
53.60	1.708	9.00	321	Mullite
60.70	1.524	9.00	331	Mullite



**Table 4.18 Effect of 4% (zirconium silicate + titanium oxide) addition**

Diffraction angle (2 $\theta$ )	d-spacing	I/I <sub>0</sub>	Diffraction planes, hkl	Phases present
26.60	3.348	100.00	210	Mullite
35.20	2.547	5.00	111	Mullite
41.00	2.199	12.50	121	Mullite
48.00	1.893	1.04	400	Mullite
53.50	1.711	10.00	240	Mullite
57.70	1.596	0.50	041	Mullite
60.80	1.522	8.00	331	Mullite
64.60	1.440	2.00	002	Mullite/Tridymite

## Figures

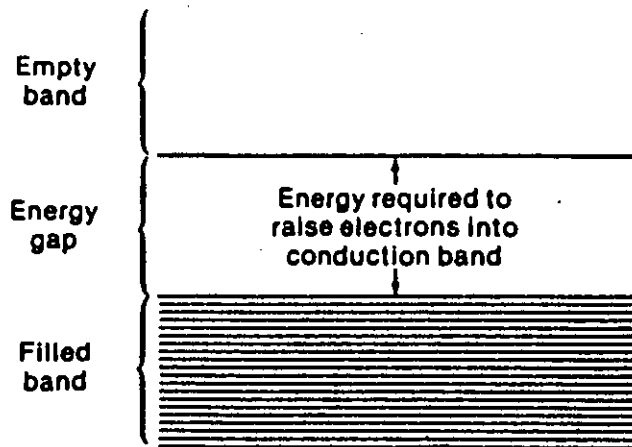


Fig. 2.1 Schematic of the energy bands in an insulator such as MgO or Al<sub>2</sub>O<sub>3</sub> showing the larger energy gap between the filled band and the next available empty band. (© ASM International)

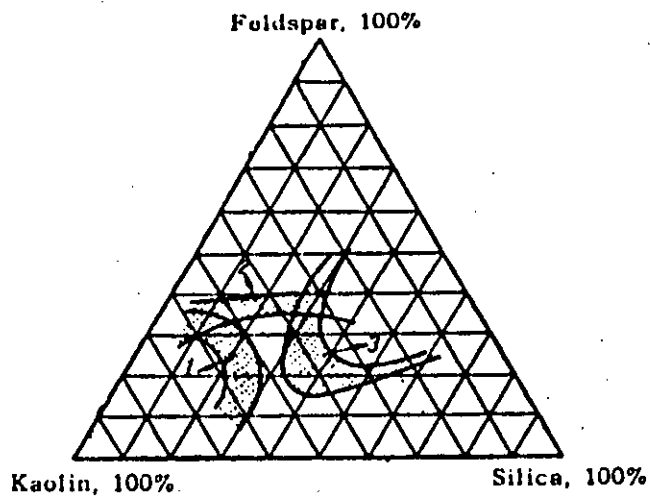


Fig. 2.2 Properties of porcelain as function of a mixture composition: 1-high heat resistance; 2-high electrical strength; 3-high mechanical strength

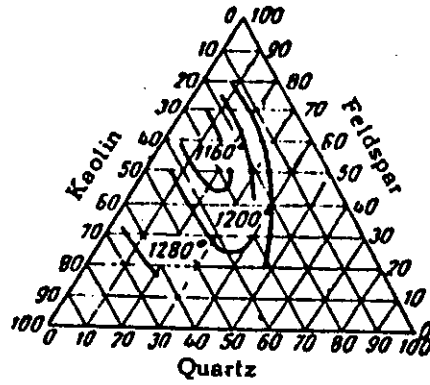


Fig. 2.3 Sintering isotherms

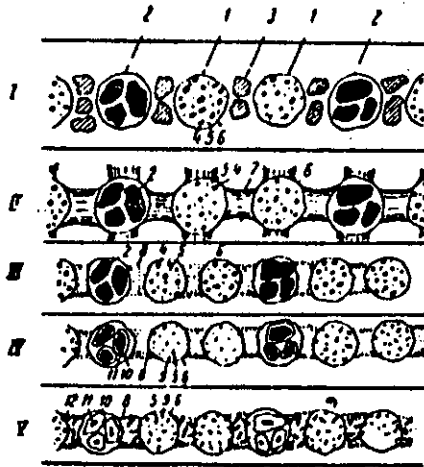


Fig. 2.4 Diagram showing formation of porcelain: 1-kaolinite; 2-quartz; 3-feldspar; 4-amorphous  $\text{SiO}_2$ ; 5-primary mullite in kaolinite residue; 6-outline of kaolinite along interaction boundaries with feldspar; 7,8-feldspar melt; 9-silica and feldspar melt within kaolinite residue; 10-fused edge of quartz; 11-residue quartz; 12-mullite within feldspar melt (diffusion); I-V-phases of process

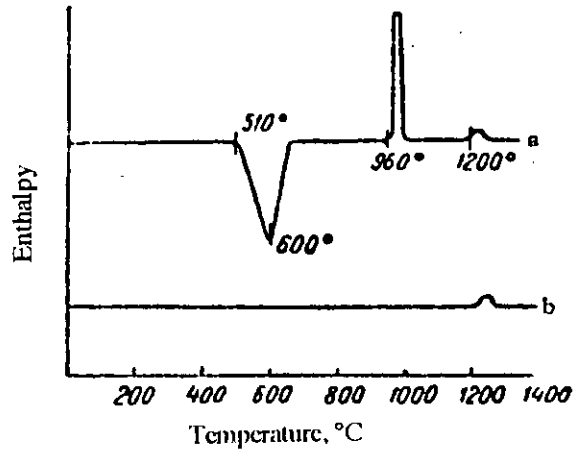


Fig. 2.5 Thermogram for kaolin : a-raw; b-calcined at 950°C. After Belyankin, D. S. and Ivanov, B. V. Materials on the study of dinas and its raw-material bases in the USSR. Acad. Sci. Press, Moscow, 1938

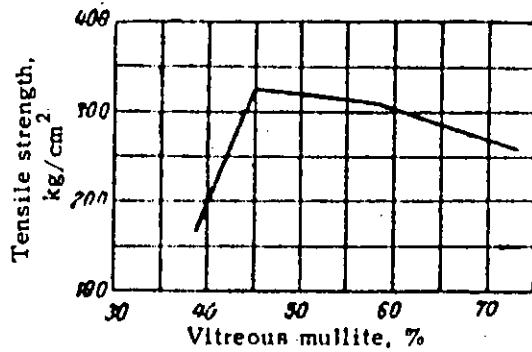


Fig. 2.6 Mechanical strength of porcelain as function of the amount of vitreous phase

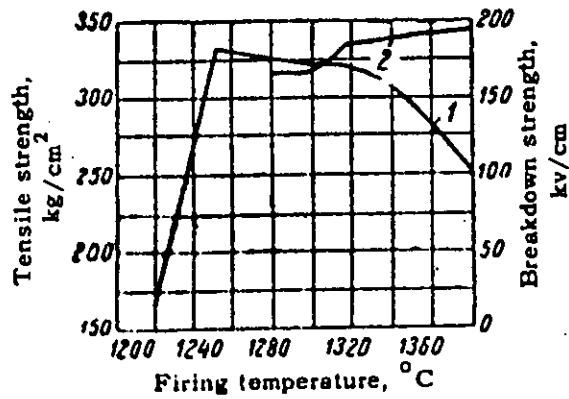


Fig. 2.7 Effect of firing temperature and dielectric strength of porcelain: 1-mechanical strength; 2-breakdown voltage

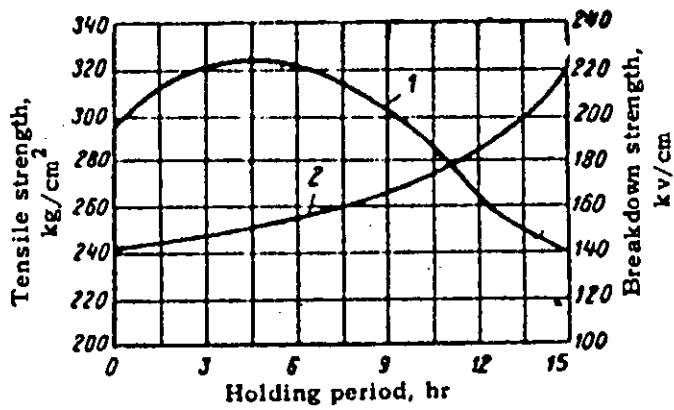


Fig. 2.8 Mechanical and dielectric strength of porcelain as a function of length of period ware is held at final firing temperature: 1-mechanical strength; 2-breakdown voltage

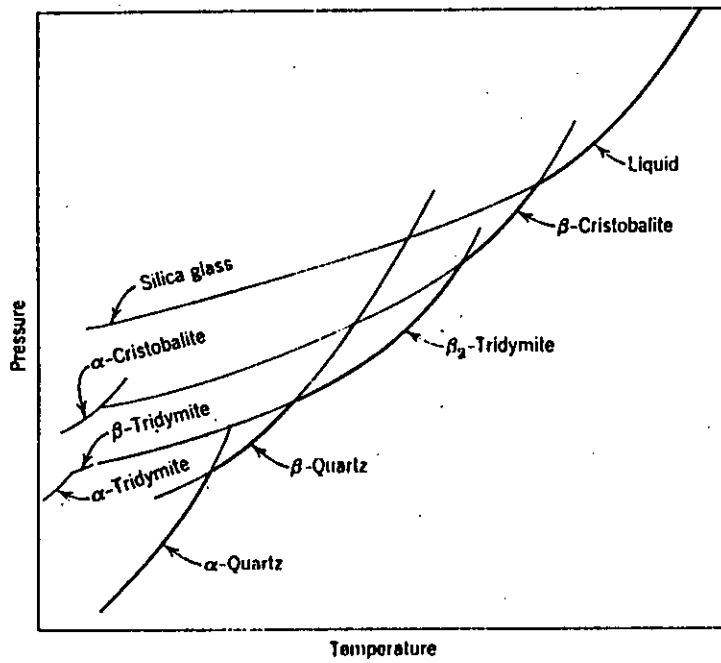


Fig. 2.9 Equilibrium diagram for SiO<sub>2</sub>

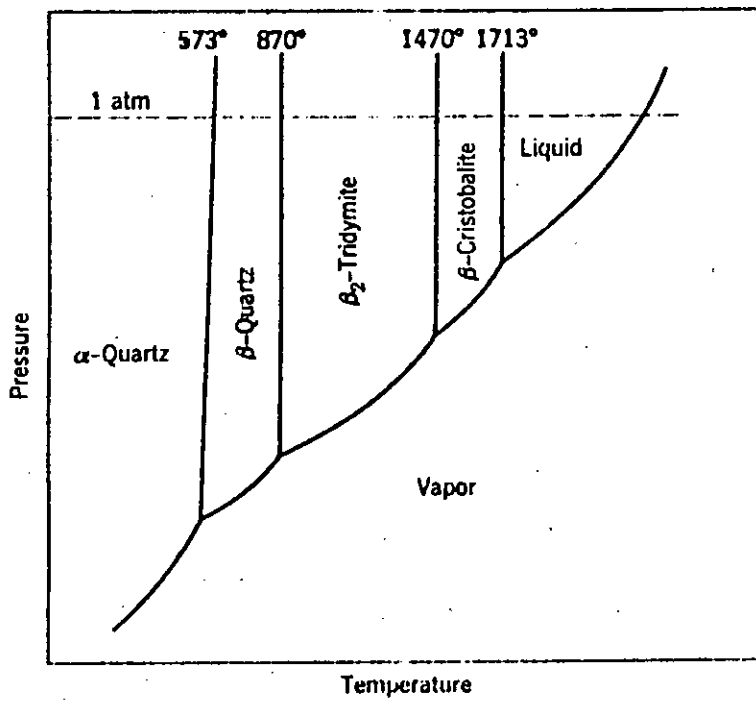
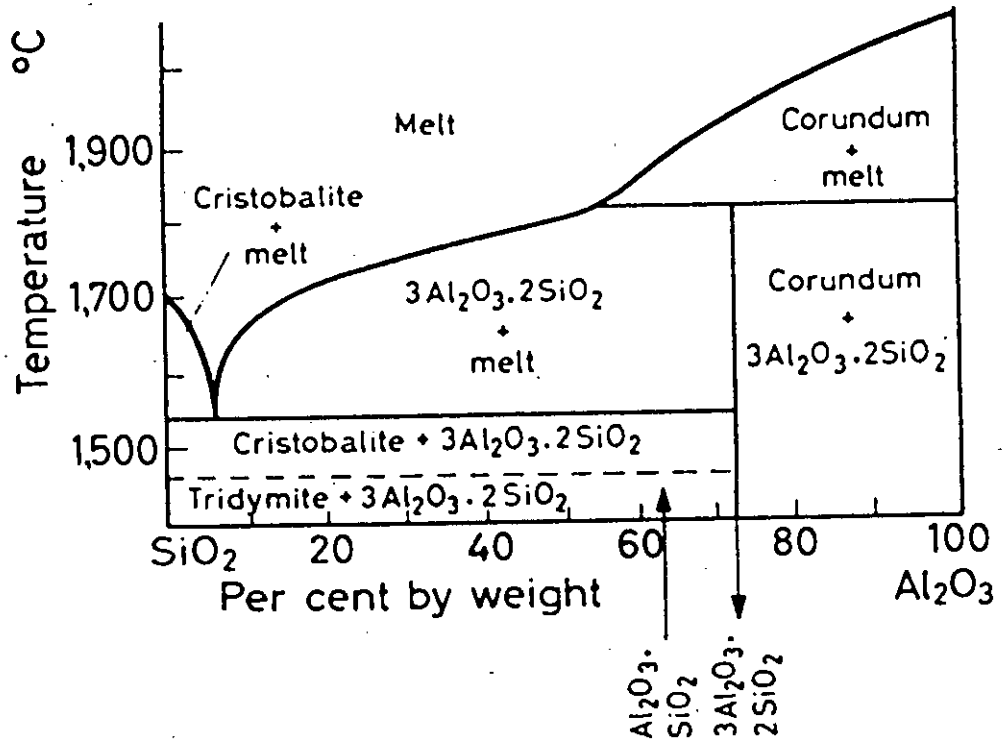


Fig. 2.10 Diagram including metastable phases occurring in the system SiO<sub>2</sub>



**Fig. 2.11** The binary system  $\text{Al}_2\text{O}_3$ - $\text{SiO}_2$ .  
 After Bowen, N. L. and Greig, J. W., J.  
 Amer. Ceram. Soc. 7 (1924) 238



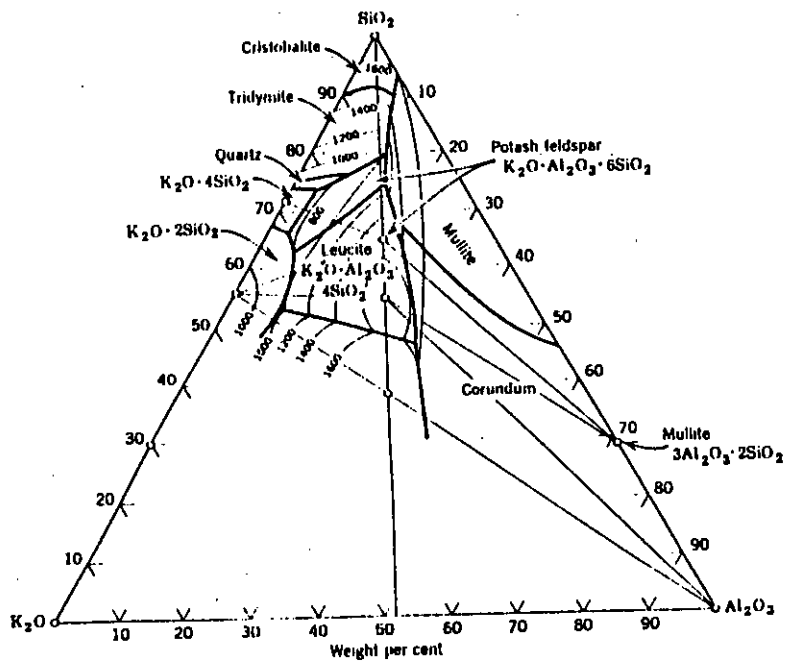


Fig. 2.12 The ternary system  $K_2O-Al_2O_3-SiO_2$ . After J. F. Schairer and N. L. Bowen, *Am. J. Sci.*, 245, 199 (1947)

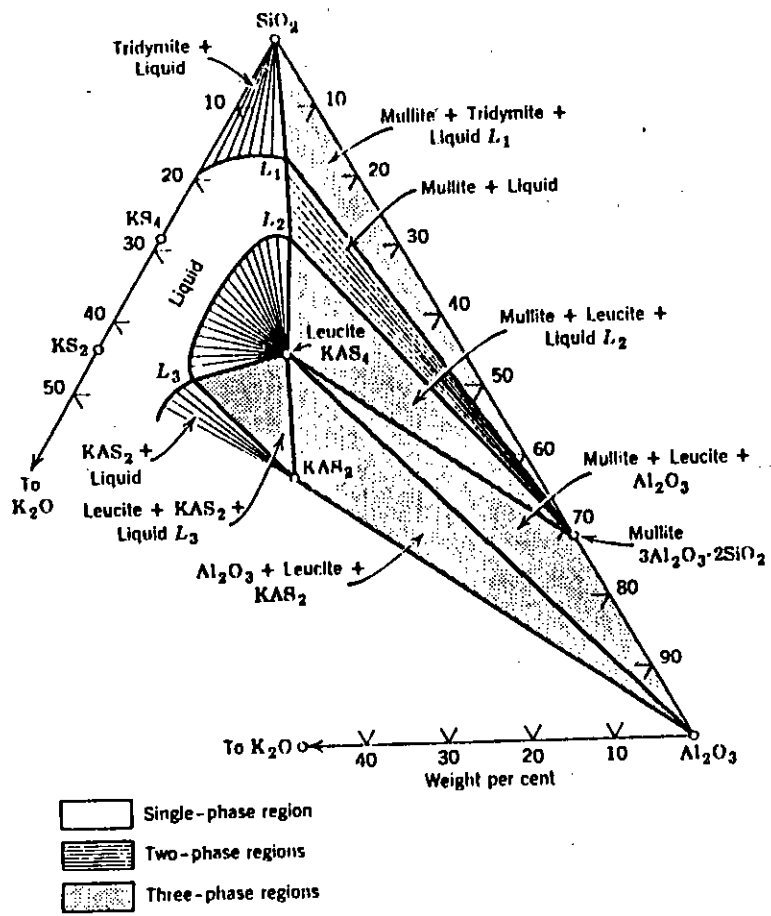


Fig. 2.13 Isothermal cut in the  $K_2O-Al_2O_3-SiO_2$  diagram at  $1200^\circ C$

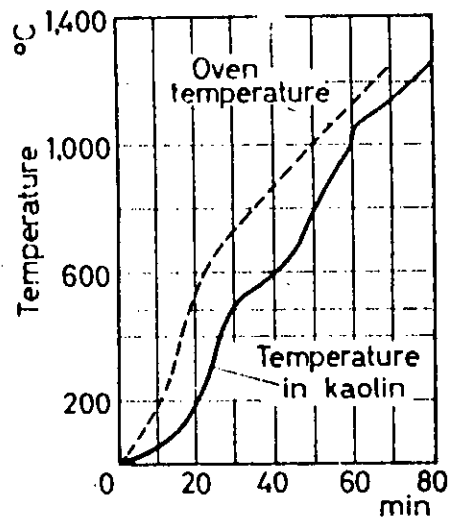
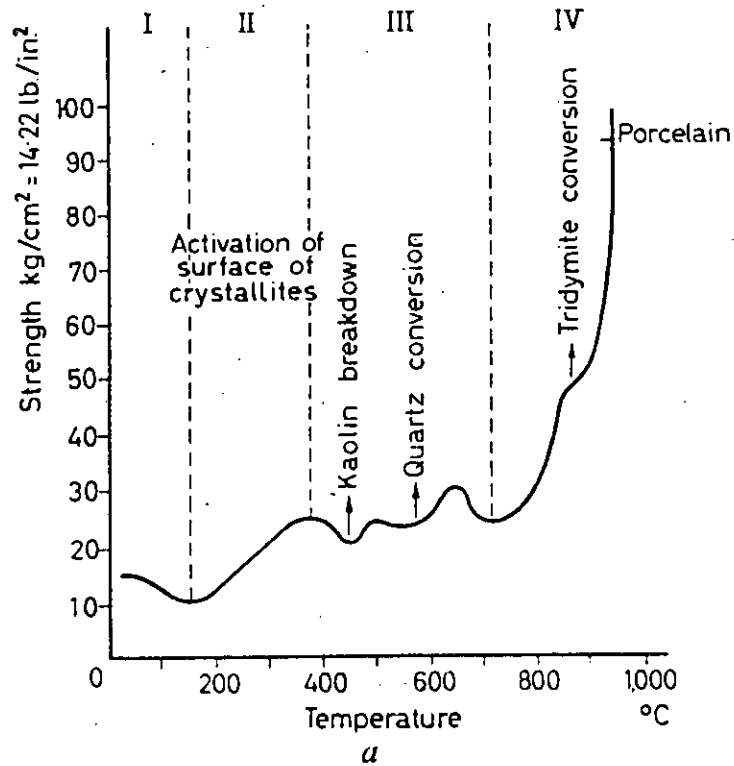


Fig. 2.14 Heating curve of a kaolin from Halle. After Chatelier, H. LE, Z. Phys. Chem. 1 (1987) 396



- I First reaction phase: evaporation of water envelopes surrounding the crystallites  
 II Second reaction phase: diffusion of water vapour to exterior  
 III Third reaction phase: de-activation of surface of crystallites  
 IV Fourth reaction phase: interlattice diffusion

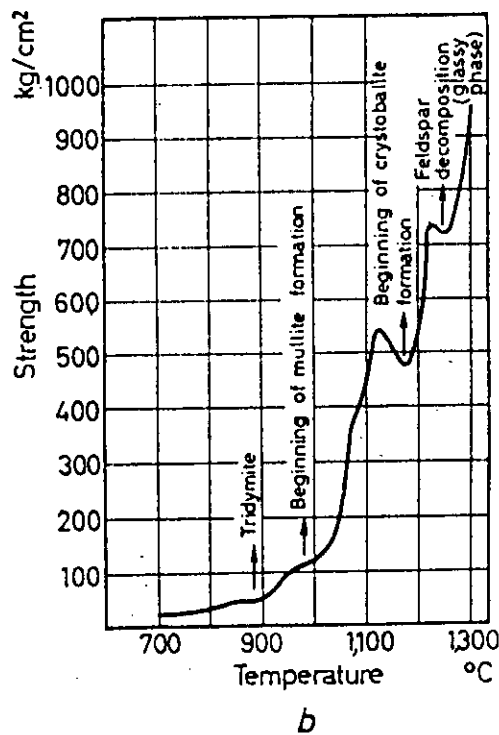


Fig. 2.15 a and b. Strength of porcelain body after firing at different temperatures. After Mehmel, M. F., Ber. dtsh. keram. Ges. 28. (1951) 696

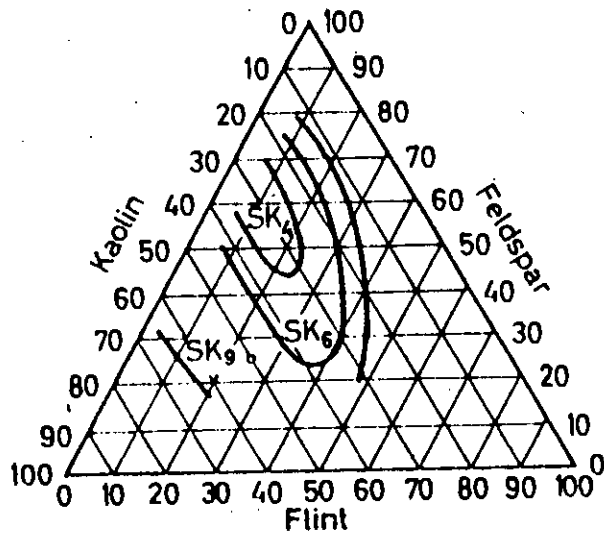


Fig. 2.16 Vitrification isothermals of porcelain bodies. After Bleininger, A. V. and Moore, J. K., *Trans. Amer. Ceram. Soc.* 10 (1908) 293; *Sprechsaal* 42 (1909) 644

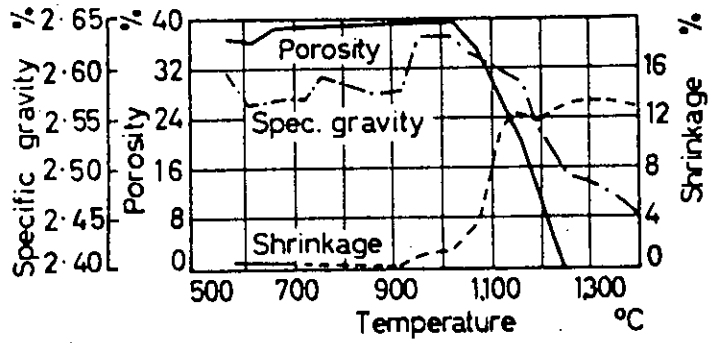


Fig. 2.17 Changes in properties of porcelain body in course of firing. After Rieck, R., *Sprechsaal* 60 (1927) No. 43; 65 (1932) 175

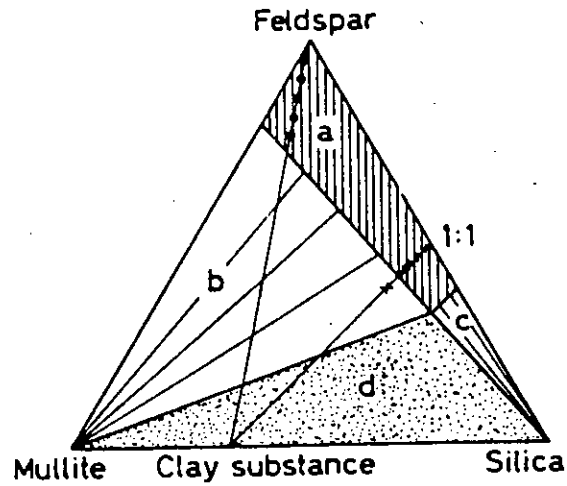


Fig. 2.18 Phases present in porcelains of different composition after firing at 1400 C. From Navratiel, H. and A. H. Fessler, A.H., Ber. Dtsch. Keram. Ges. 11 (1930) (a) 371; (b) 369

- - - - - Solubility of kaolin in feldspar

x-x-x-x-x Solubility of kaolin in feldspar-quartz mixture (1:1)

+ Saturation point of kaolin (separation of mullite)

a Area of glasses

b Area of glass and mullite

c Area of glass and cristobalite

d Area of glass and cristobalite and mullite

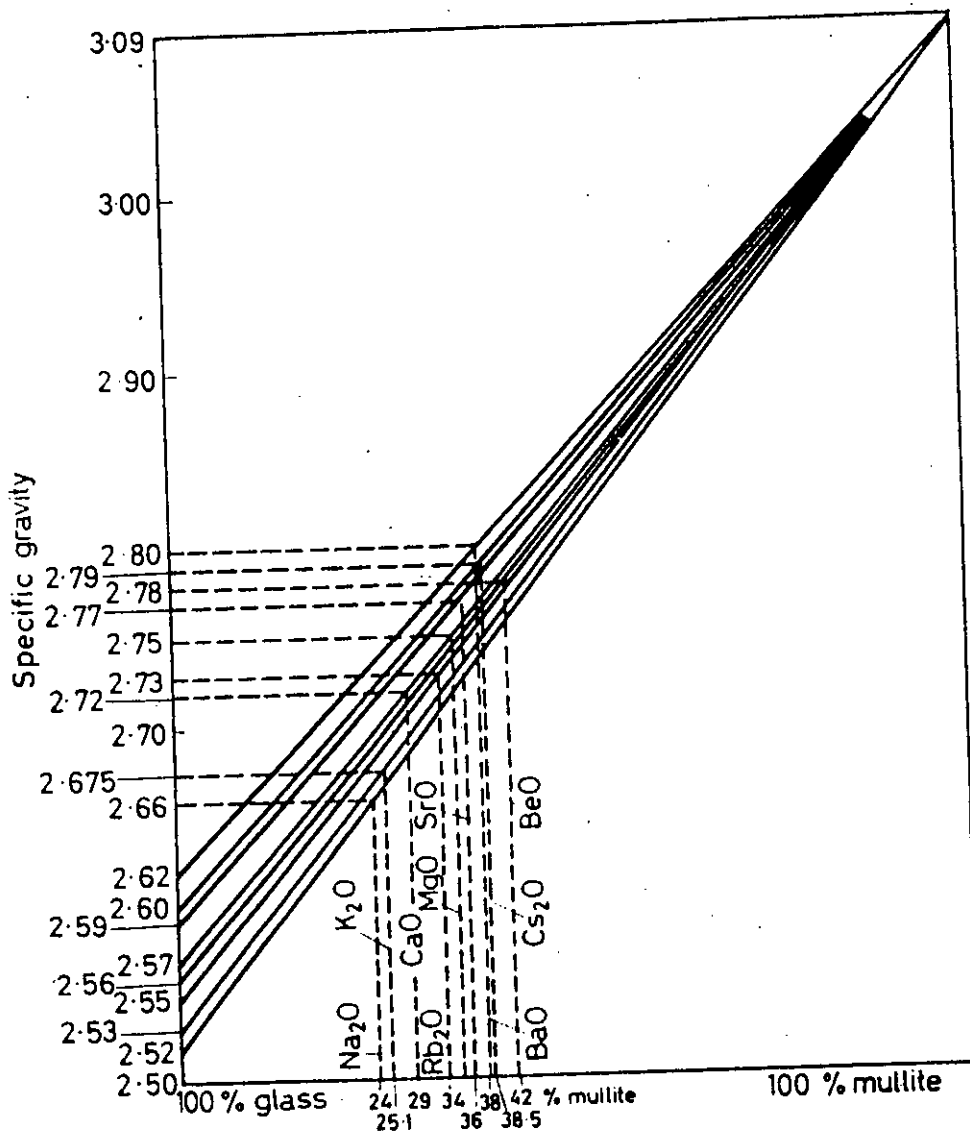


Fig. 2.19 Effect of additions of fluxes on glass formation, crystallization of mullite and density in porcelain. From Navratel, H. and A. H. Fessler, A.H., Ber. Dtsch. Keram. Ges. 11 (1930) (a) 371; (b) 369

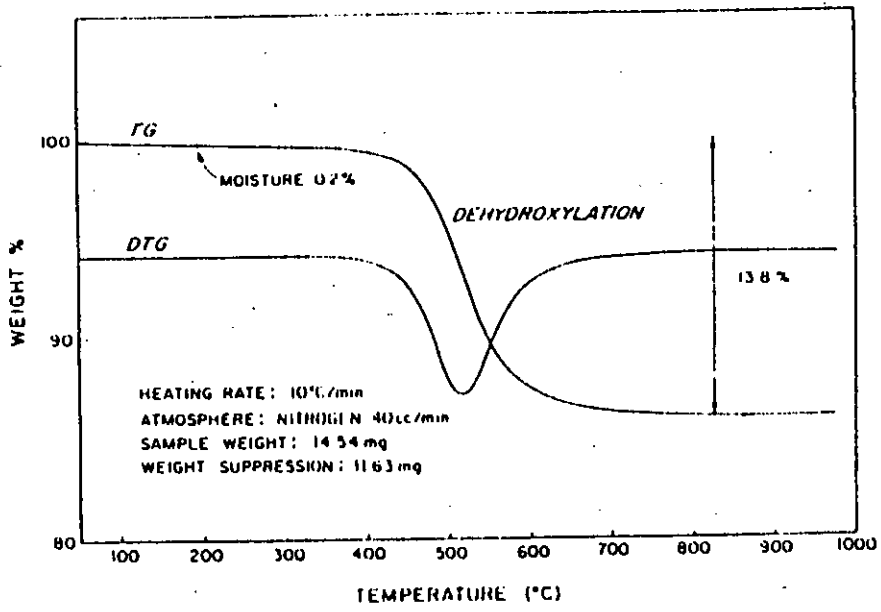


Fig. 2.20 TG curve of kaolinite standard

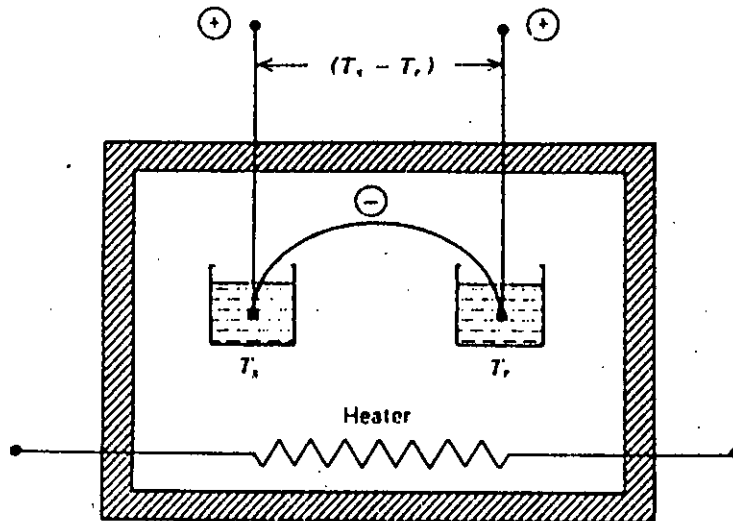


Fig. 2.21 Basic DTA system



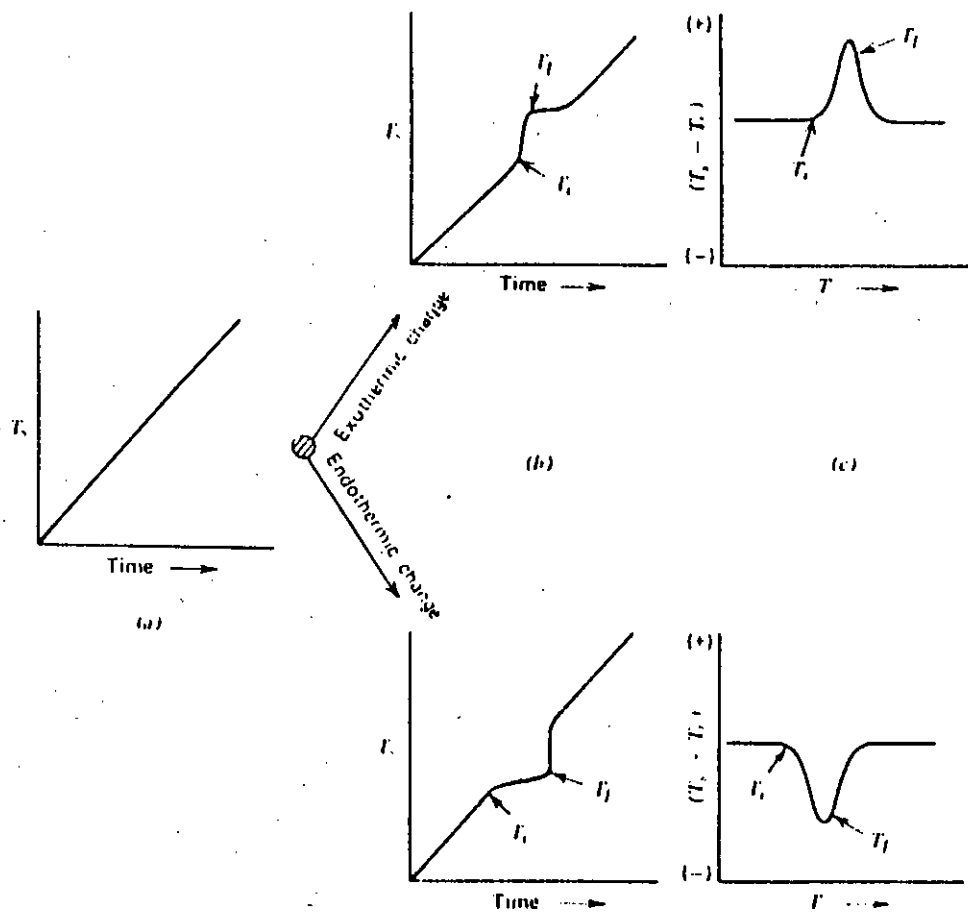


Fig. 2.22 Comparison between thermal analysis and differential thermal analysis

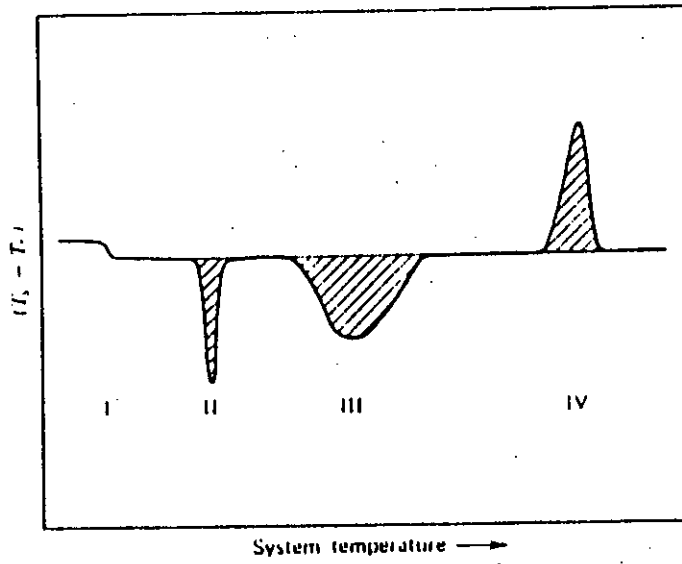


Fig. 2.23 Typical DTA curve

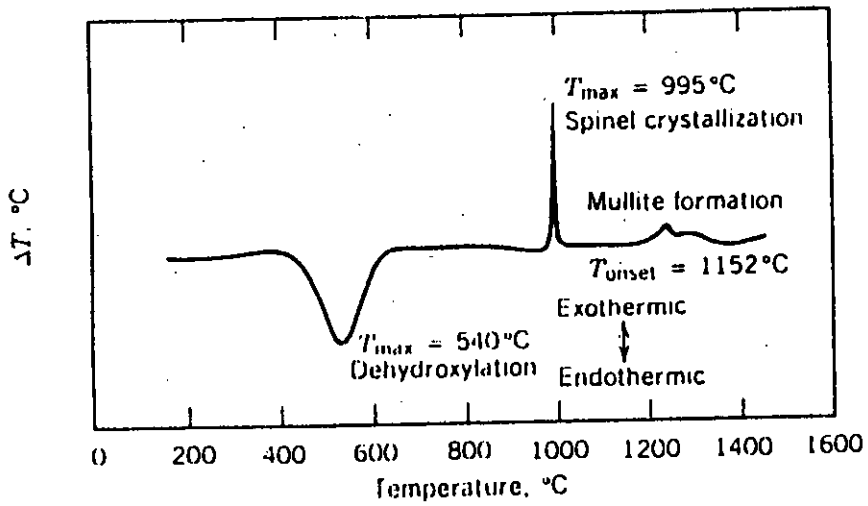


Fig. 2.24 Typical DTA curve of kaolinite

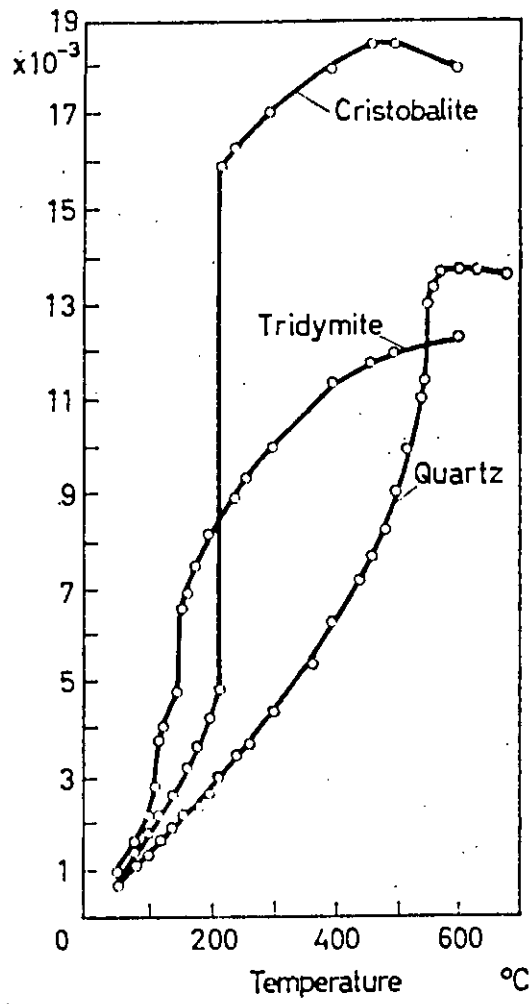
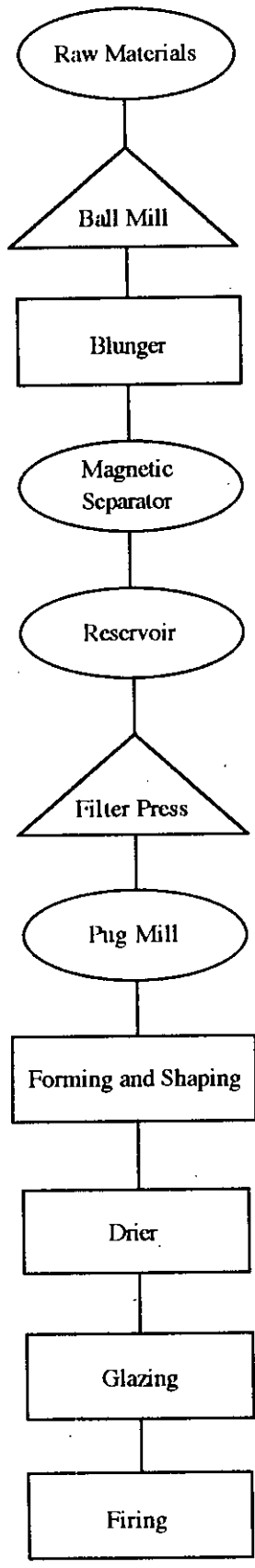
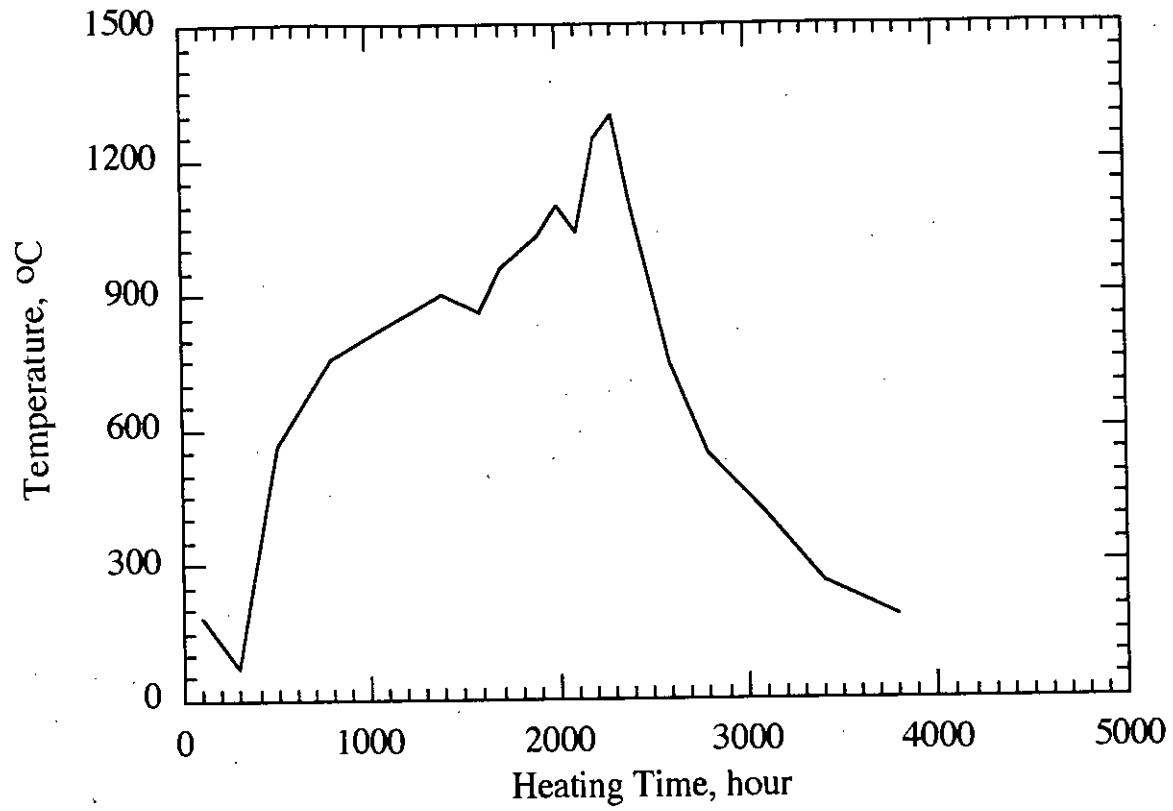


Fig. 2.25 Length changes of quartz, tridymite and cristobalite on firing. After Travers, M. and De Goloubinoff, *Rev. Metall.* 23 (1926) 27, 100 and Zwetsch, A. and Stumpfen, H., *Ber. dtsh. keram. Ges.* 10 (1930) 561



**Figure 3.1** Flow chart of the insulator body processing used at the BISF.



**Figure 3.2(a) Heating Cycle of the BISF Tunnel Kiln used for Firing the Ceramic Insulator Materials**

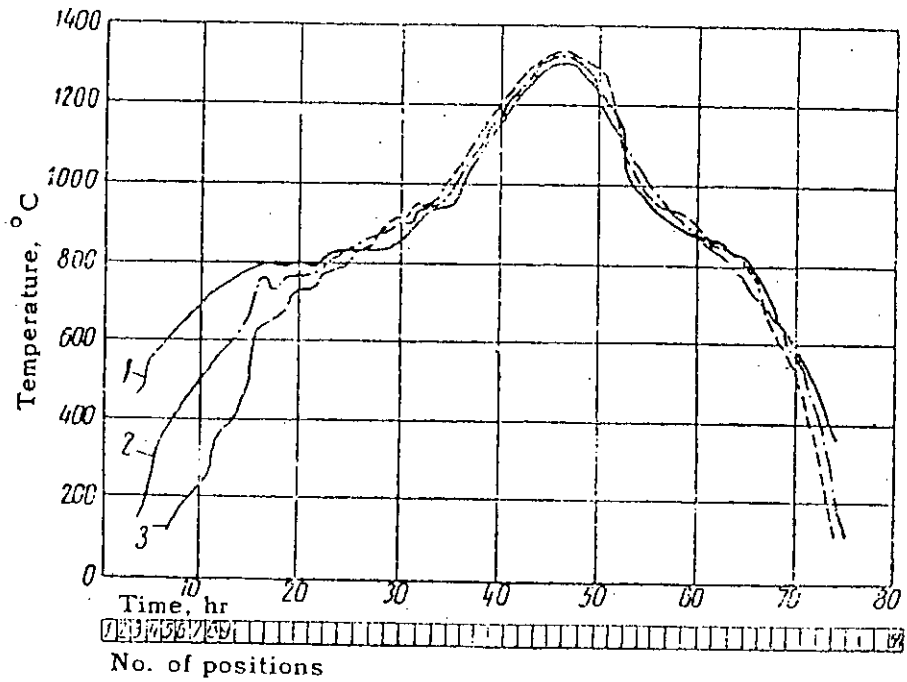


Figure 3.2(b) Standard firing curves for high-voltage insulators in a tunnel kiln (thermocouples are located inside the sagger)

1-upper sagger; 2-middle sagger; 3-lower sagger

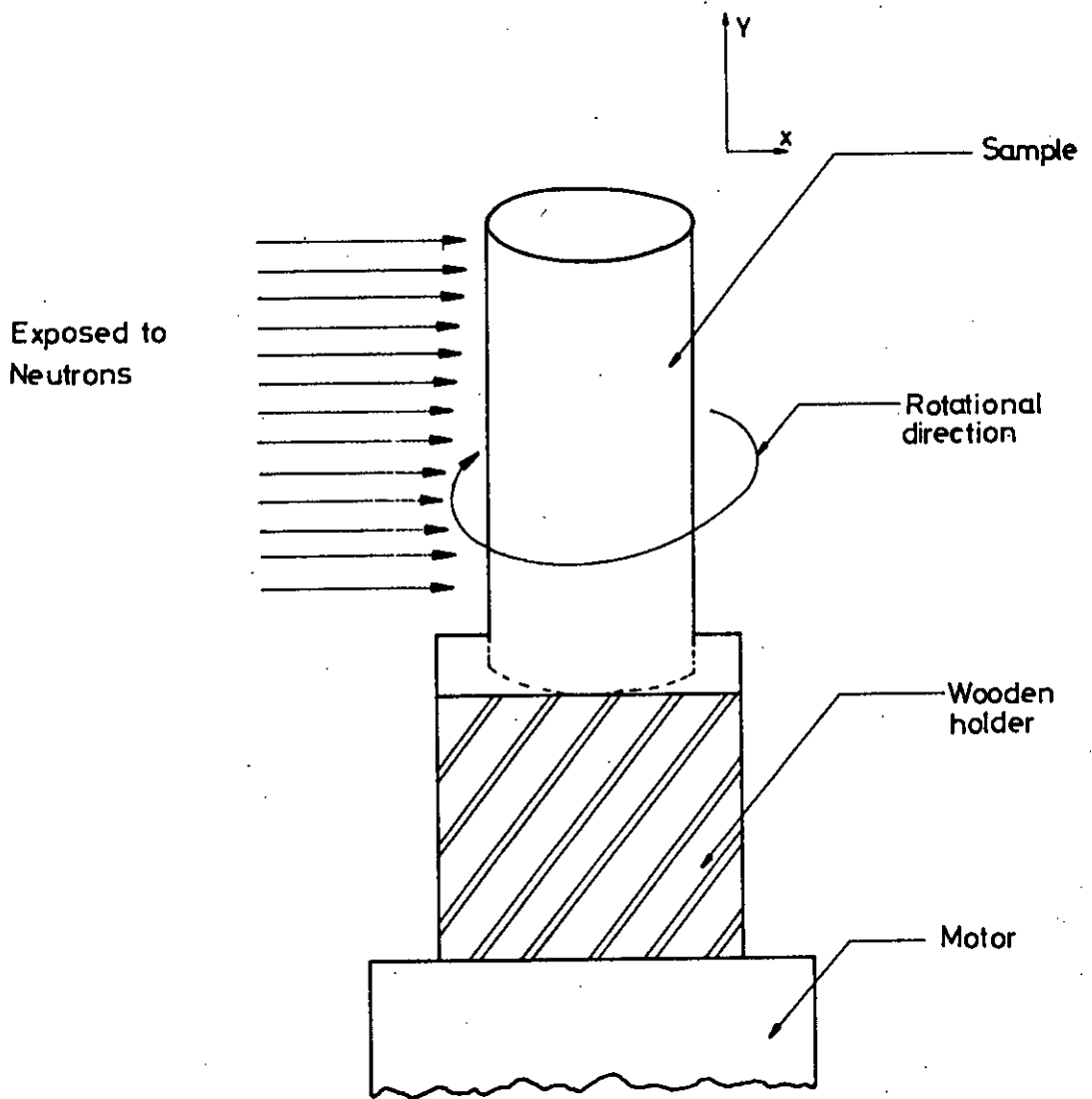
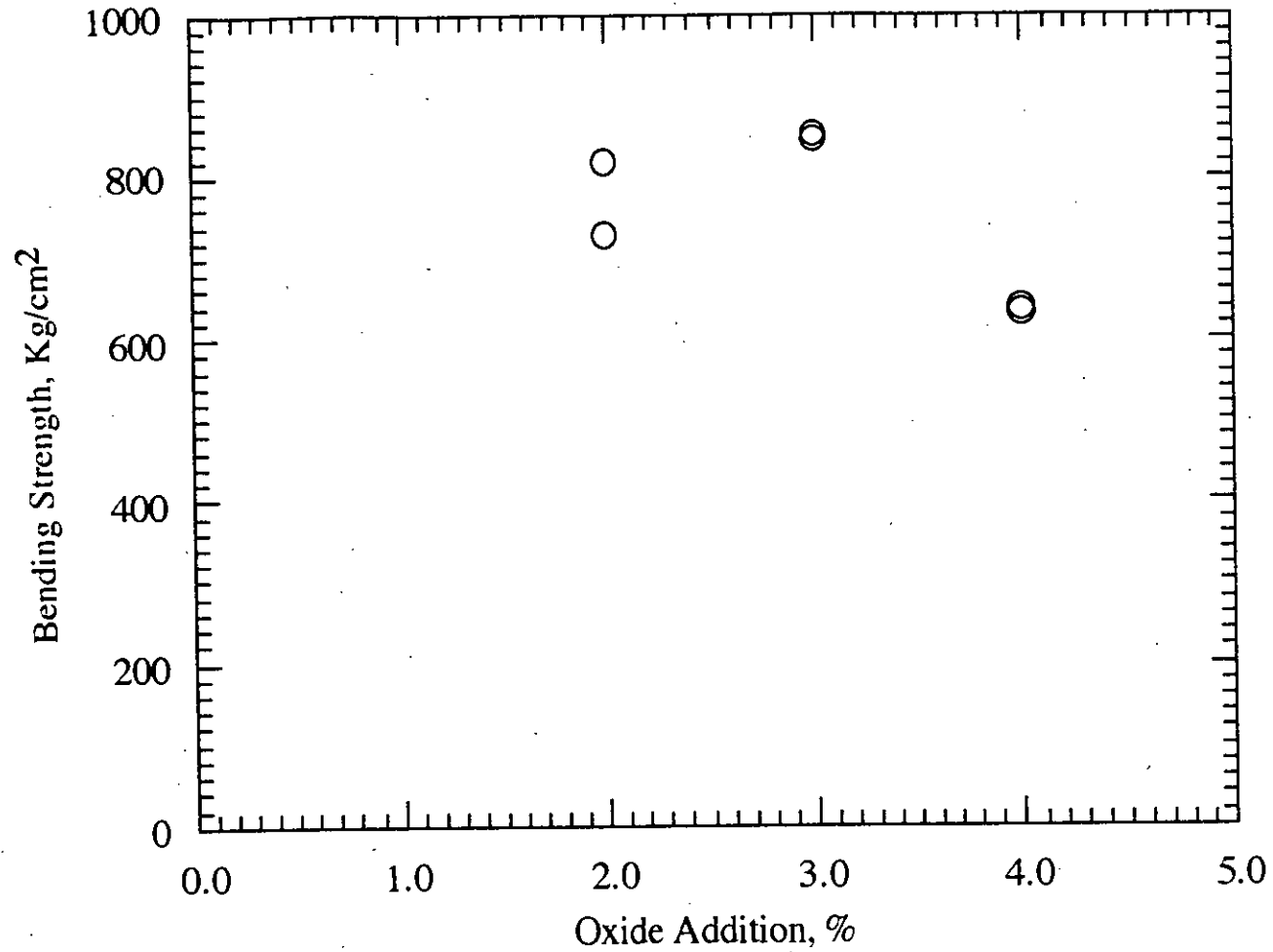
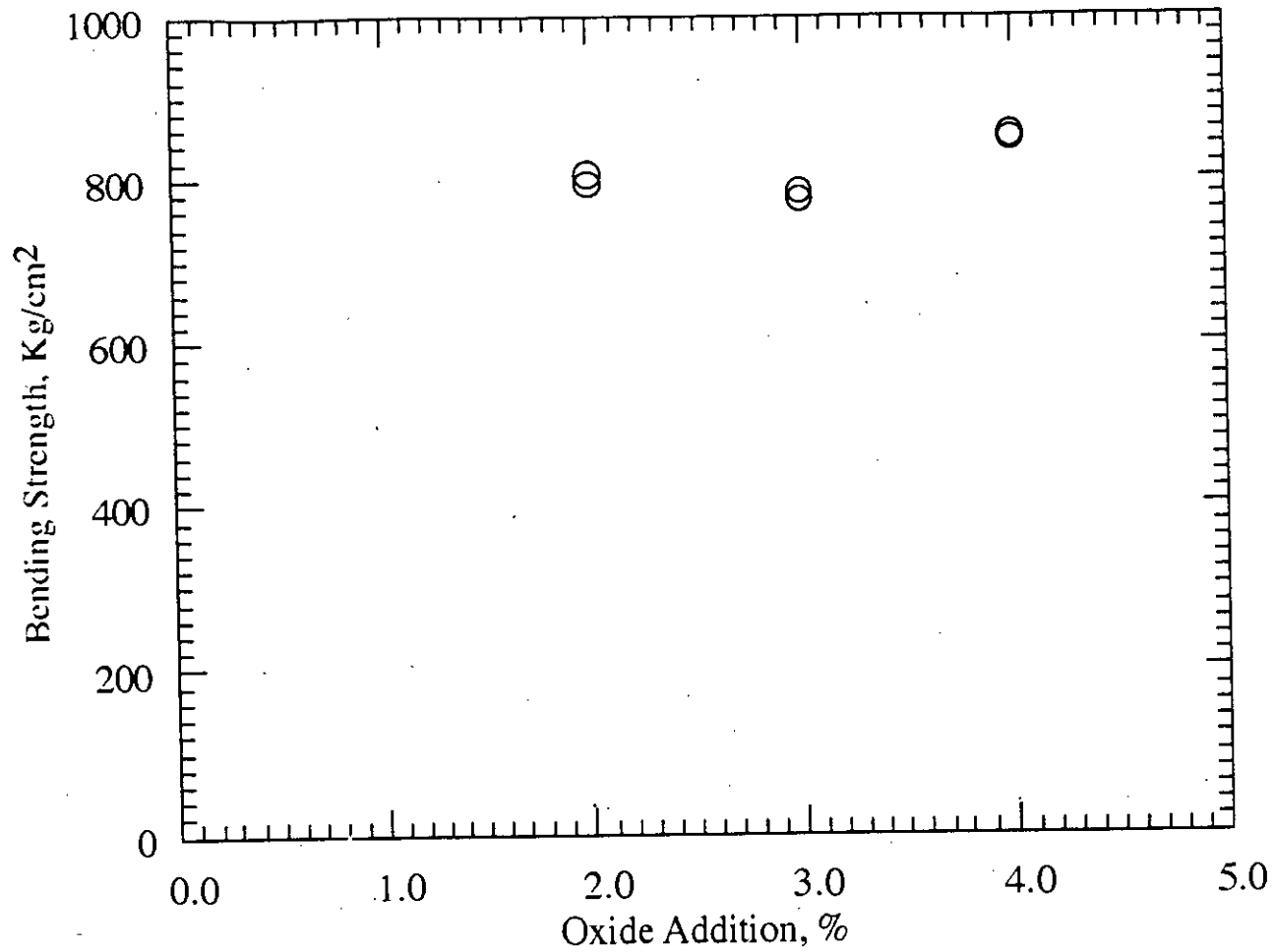


Fig. 3.3 Schematic view of texture analysis



**Figure 4.1 Effect of  $ZrSiO_4$  Addition on Bending Strength of Ceramic Insulator Materials**





**Figure 4.2** Effect of ZnO Addition on Bending Strength of Ceramic Insulator Materials

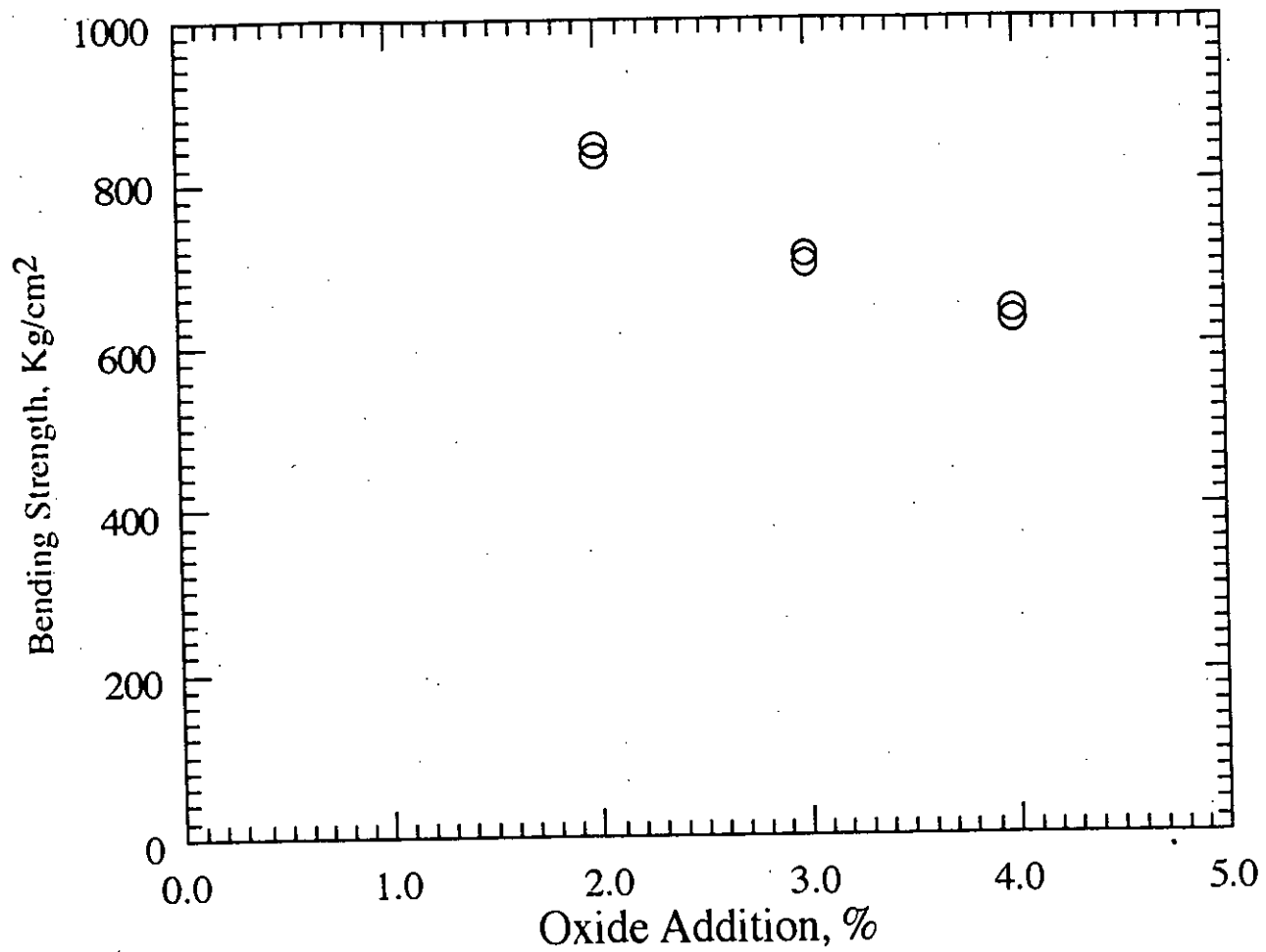


**Figure 4.3 Effect of (MnO<sub>2</sub>+TiO<sub>2</sub>) Addition on Bending Strength of Ceramic Insulator Materials**

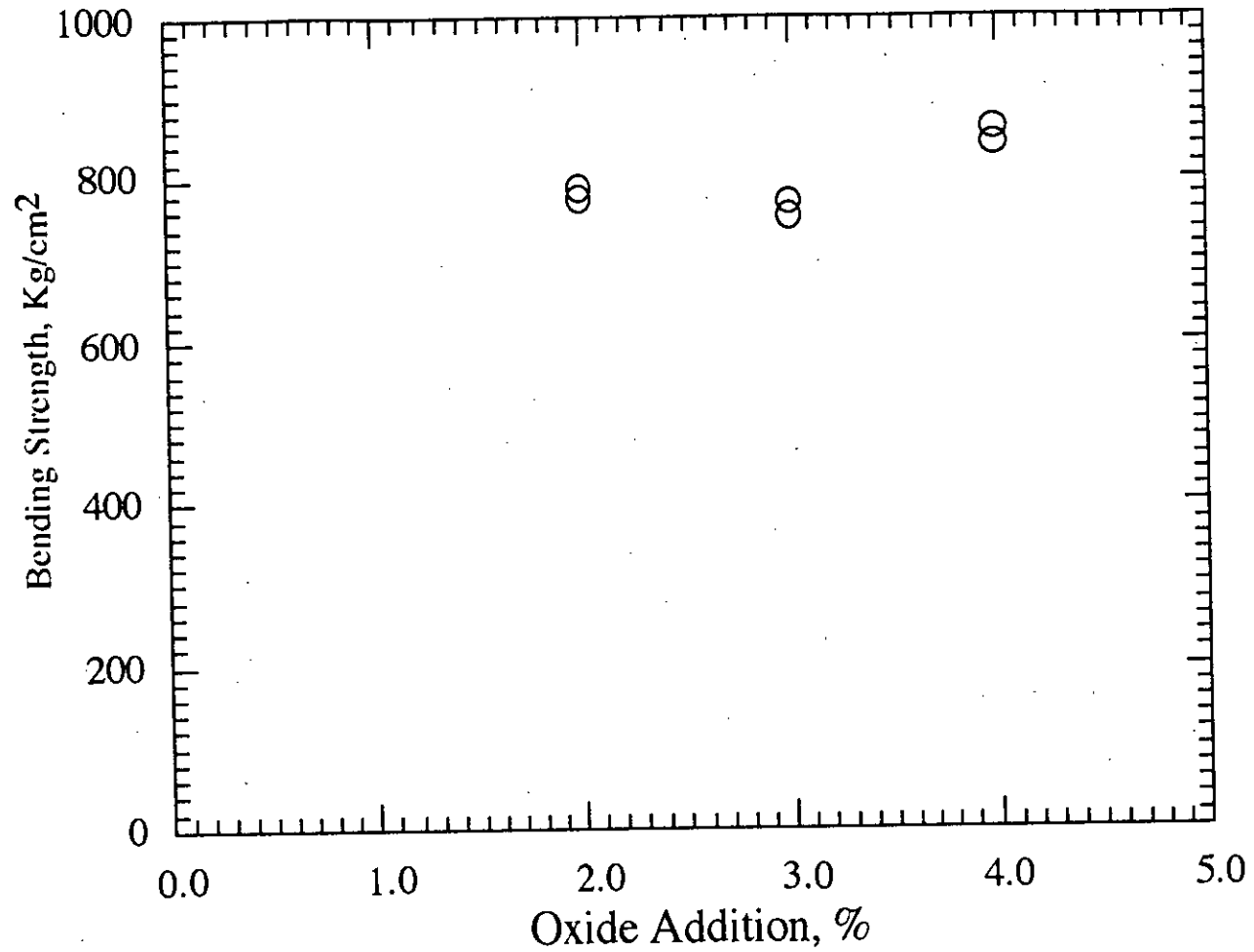


**Figure 4.4** Effect of  $(\text{ZrSiO}_4 + \text{TiO}_2)$  Addition on Bending Strength of Ceramic Insulator Materials

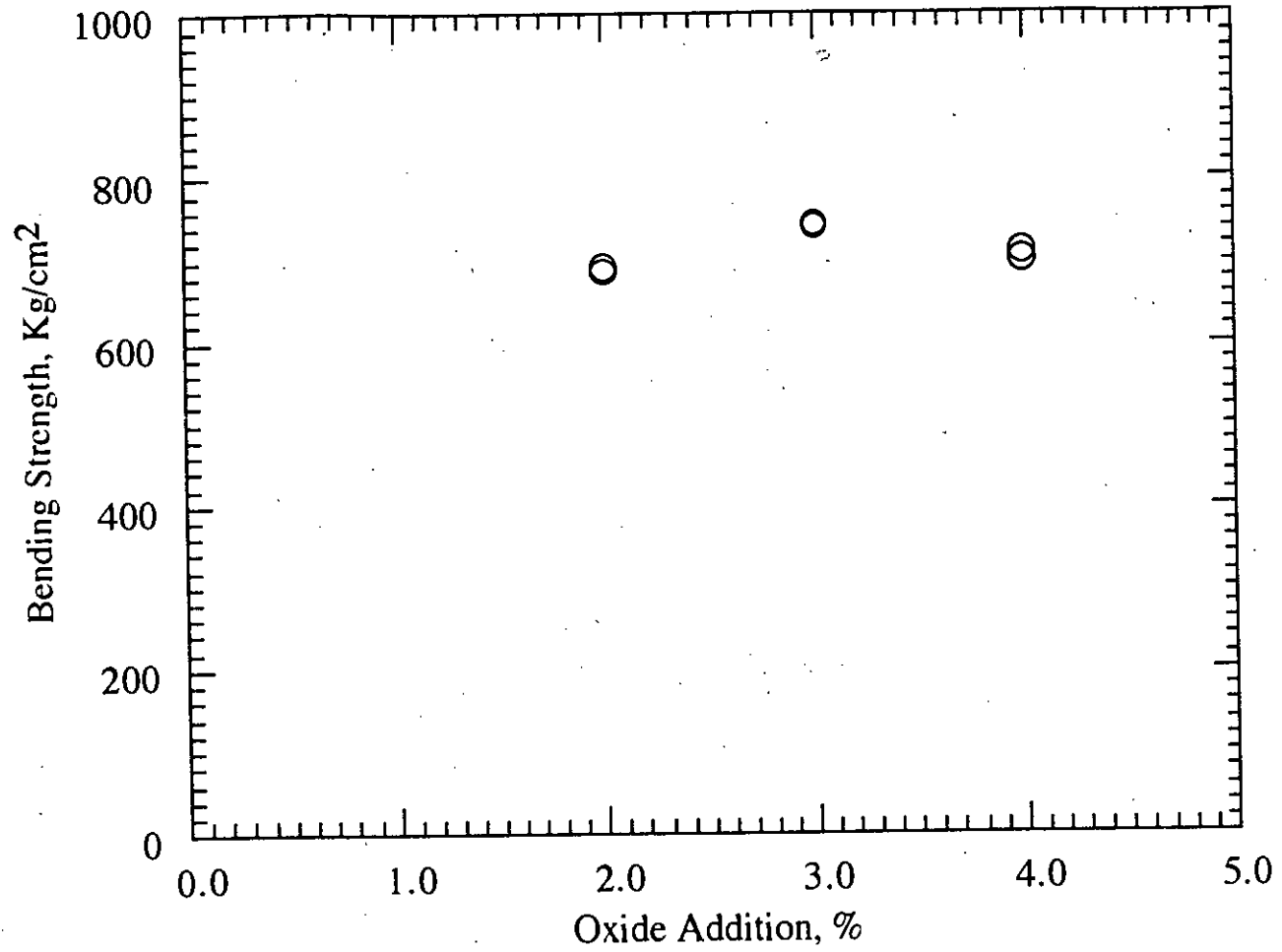


**Figure 4.5** Effect of (ZnO+TiO<sub>2</sub>) Addition on Bending Strength of Ceramic Insulator Materials

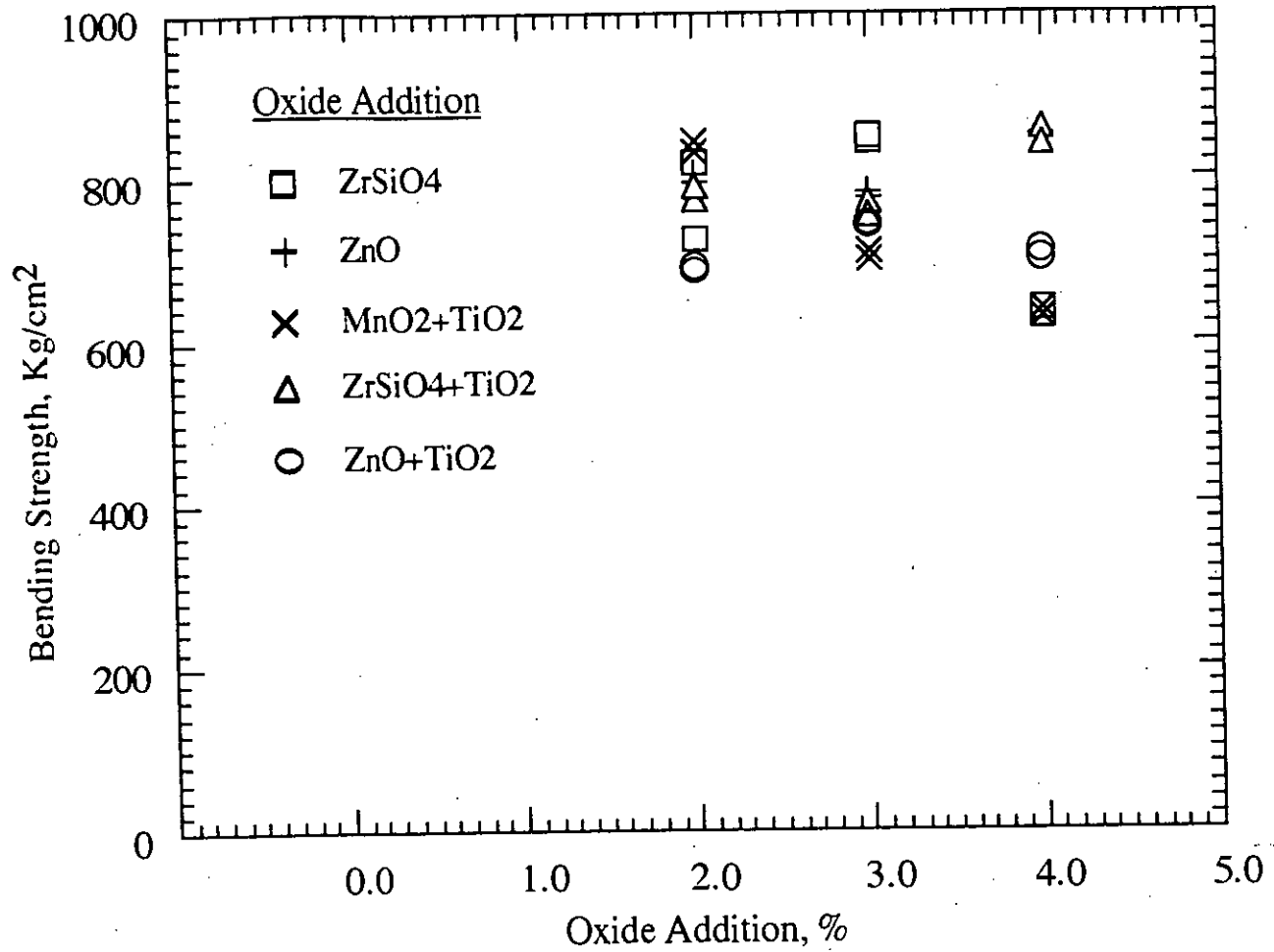


**Figure 4.6 Effect of Different Alkaline Earth Oxides Addition on Bending Strength of Ceramic Insulator Materials**

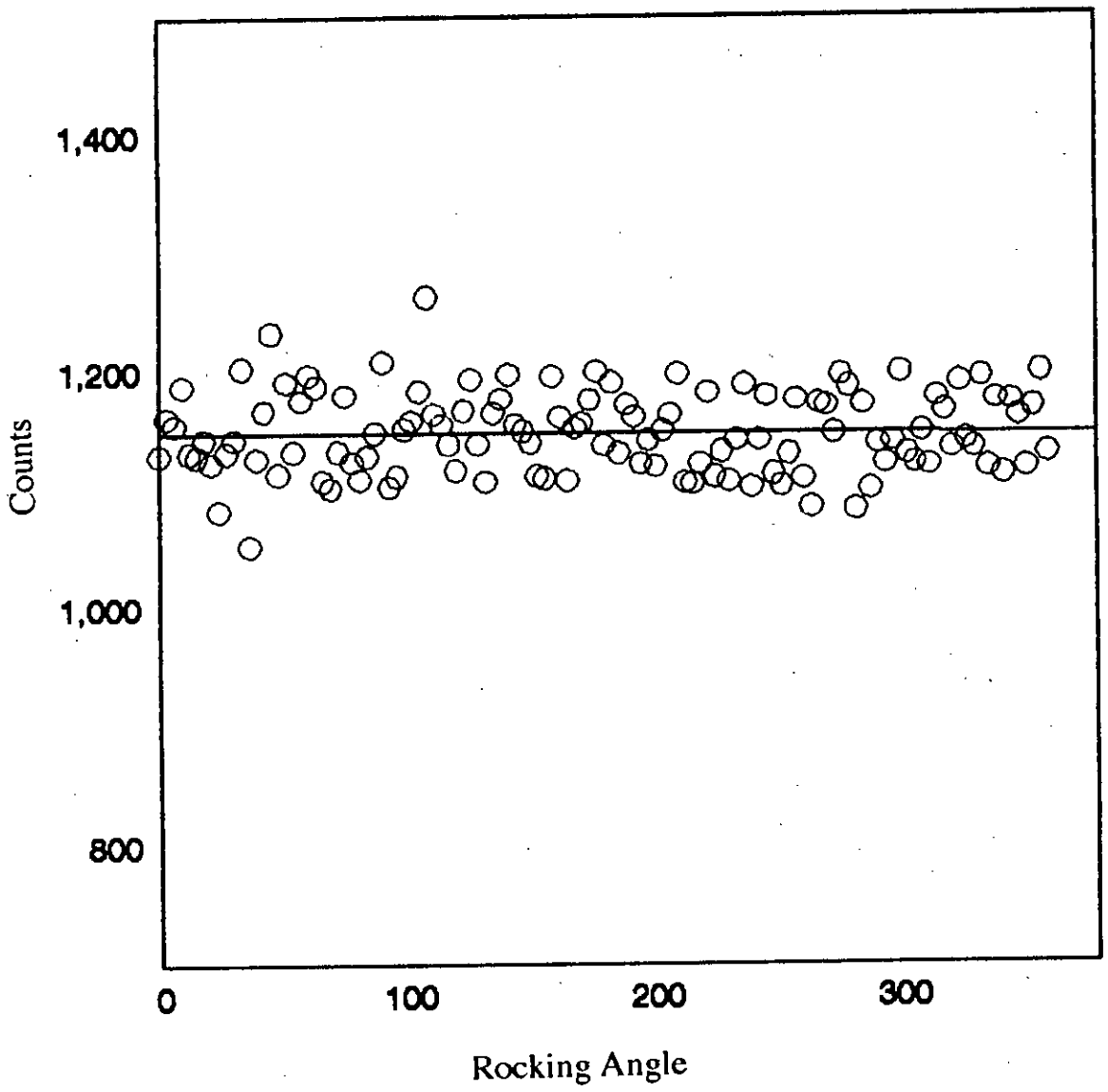


**Figure 4.7** Counts versus Rocking Angle for non fired BISF body

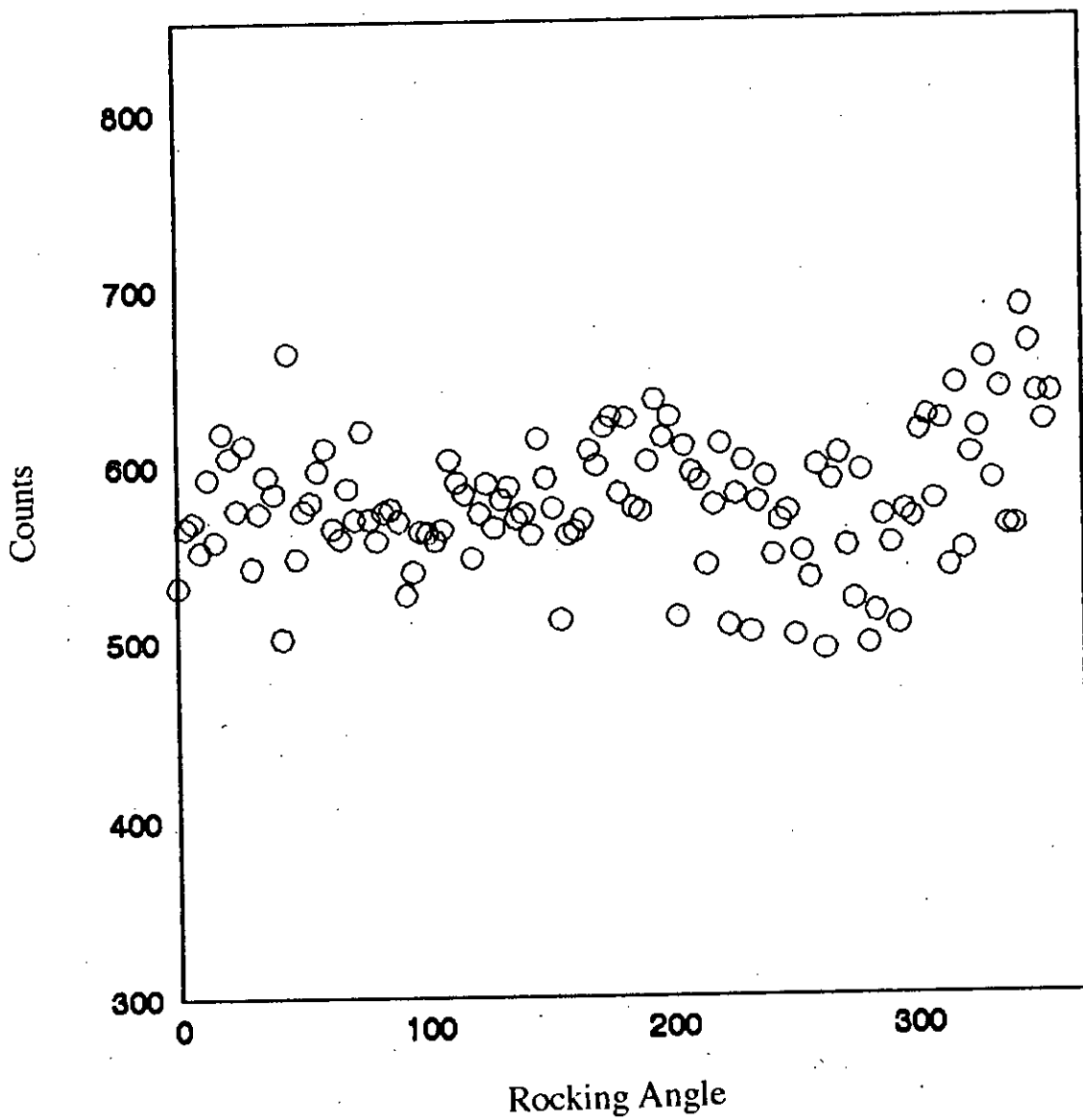


**Figure 4.8 Counts versus Rocking Angle for fired BISF body**

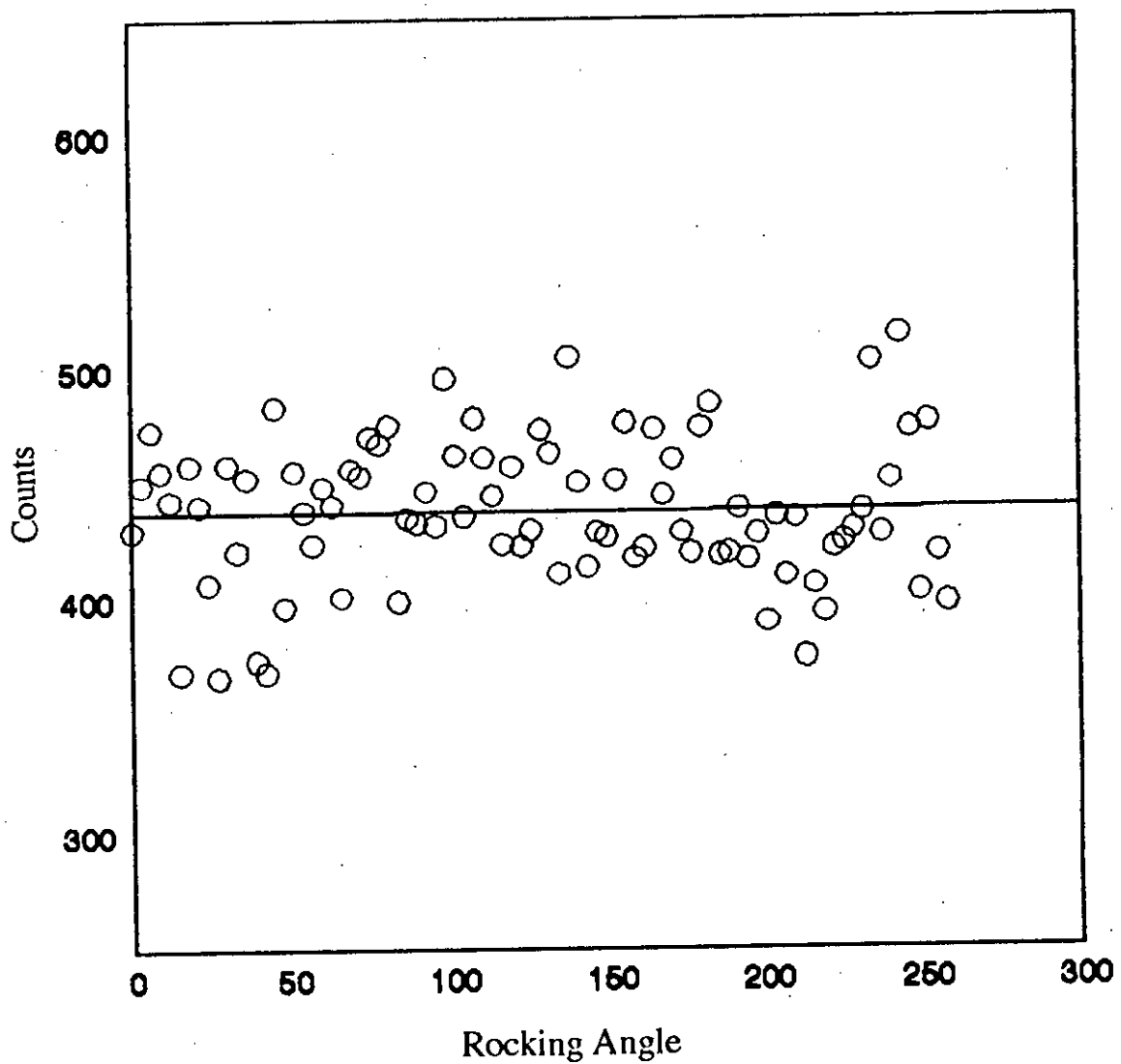


**Figure 4.9** Counts versus Rocking Angle for fired modified sample with 4 per cent ZnO<sub>2</sub>



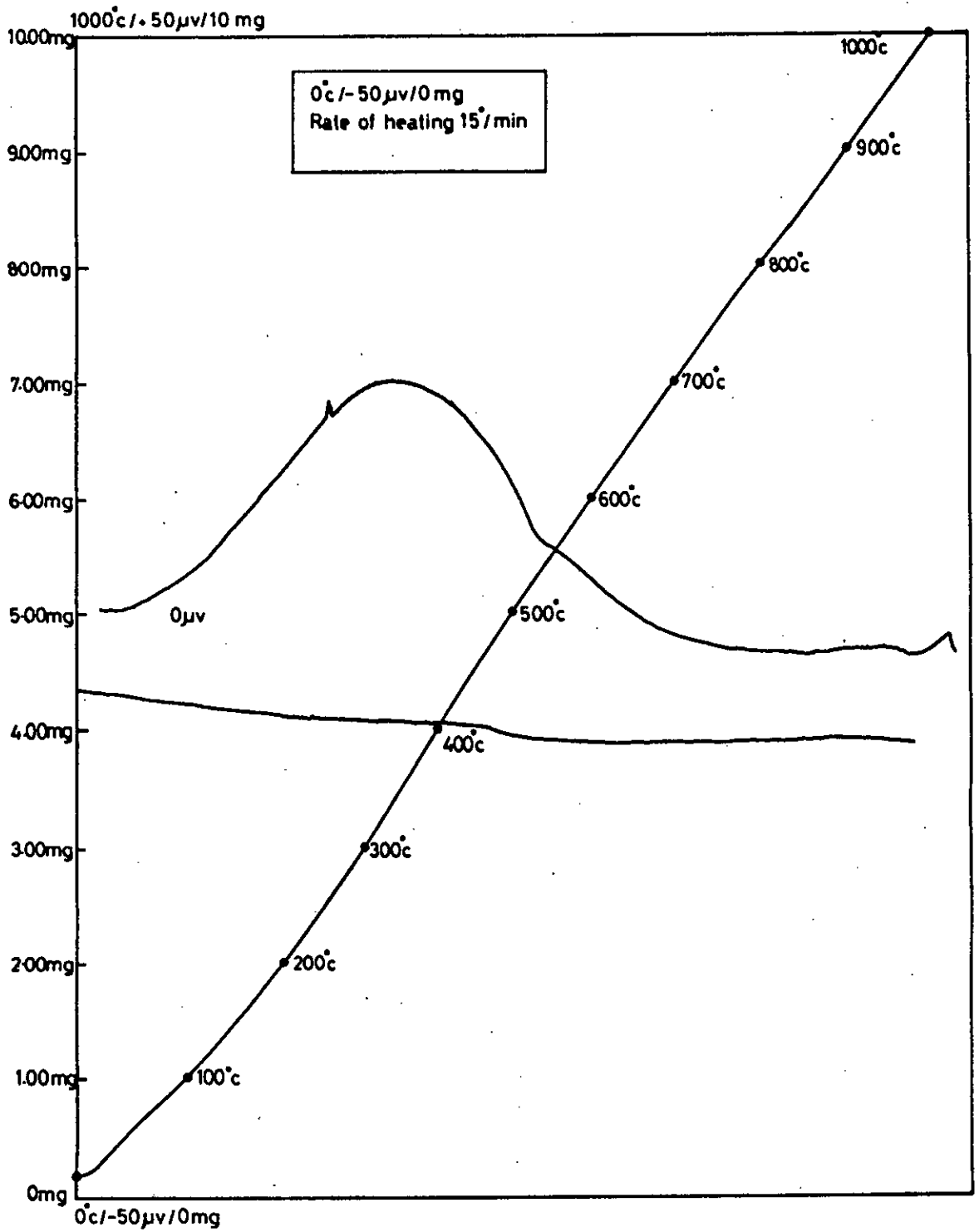


**Figure 4.10 Differential Thermal Analysis and Thermo Gravimetric Pattern of BISF Original Body**

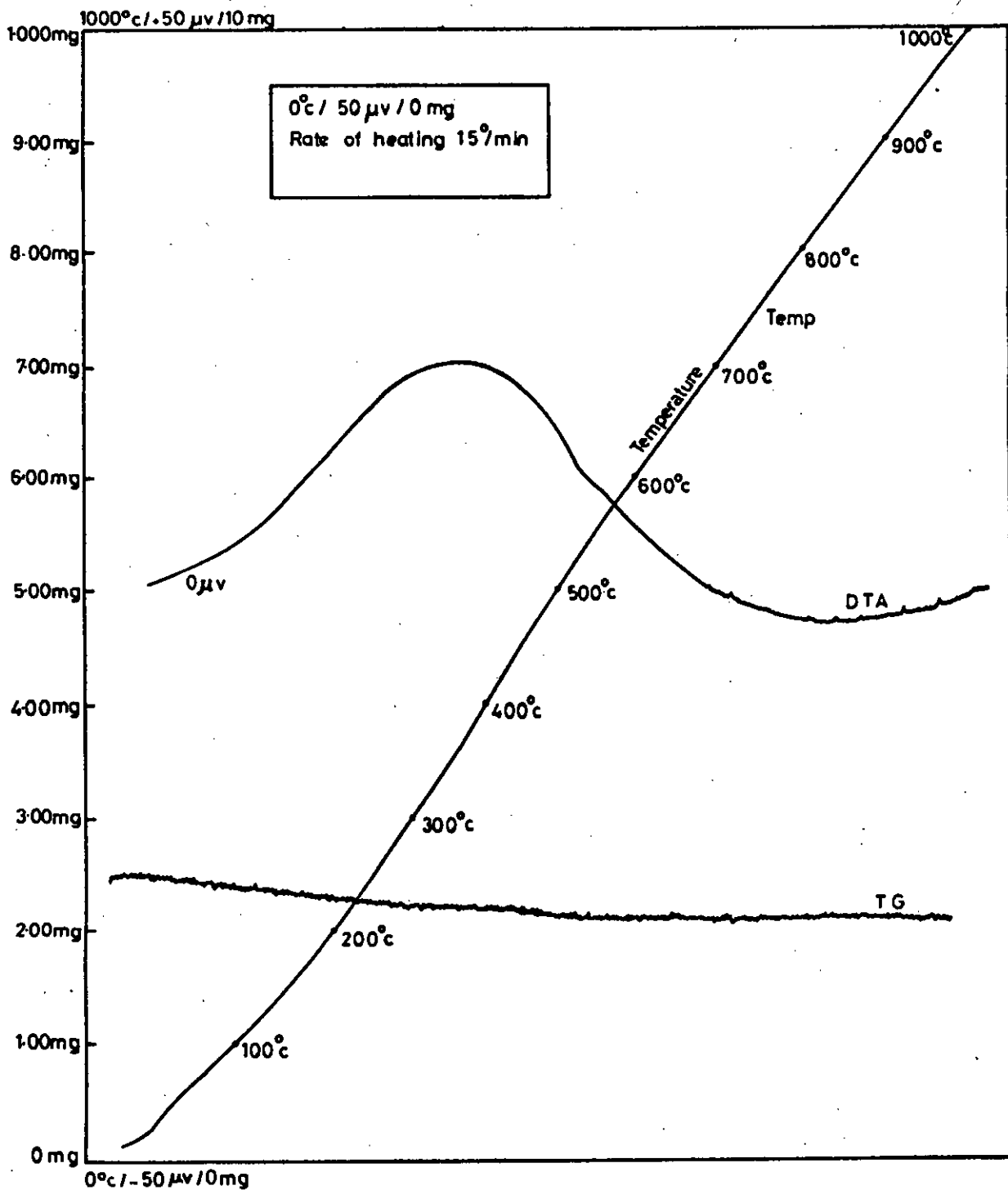


**Figure 4.11 Differential Thermal Analysis and Thermo Gravimetric Pattern of the modified sample with 3 per cent zirconium silicate**

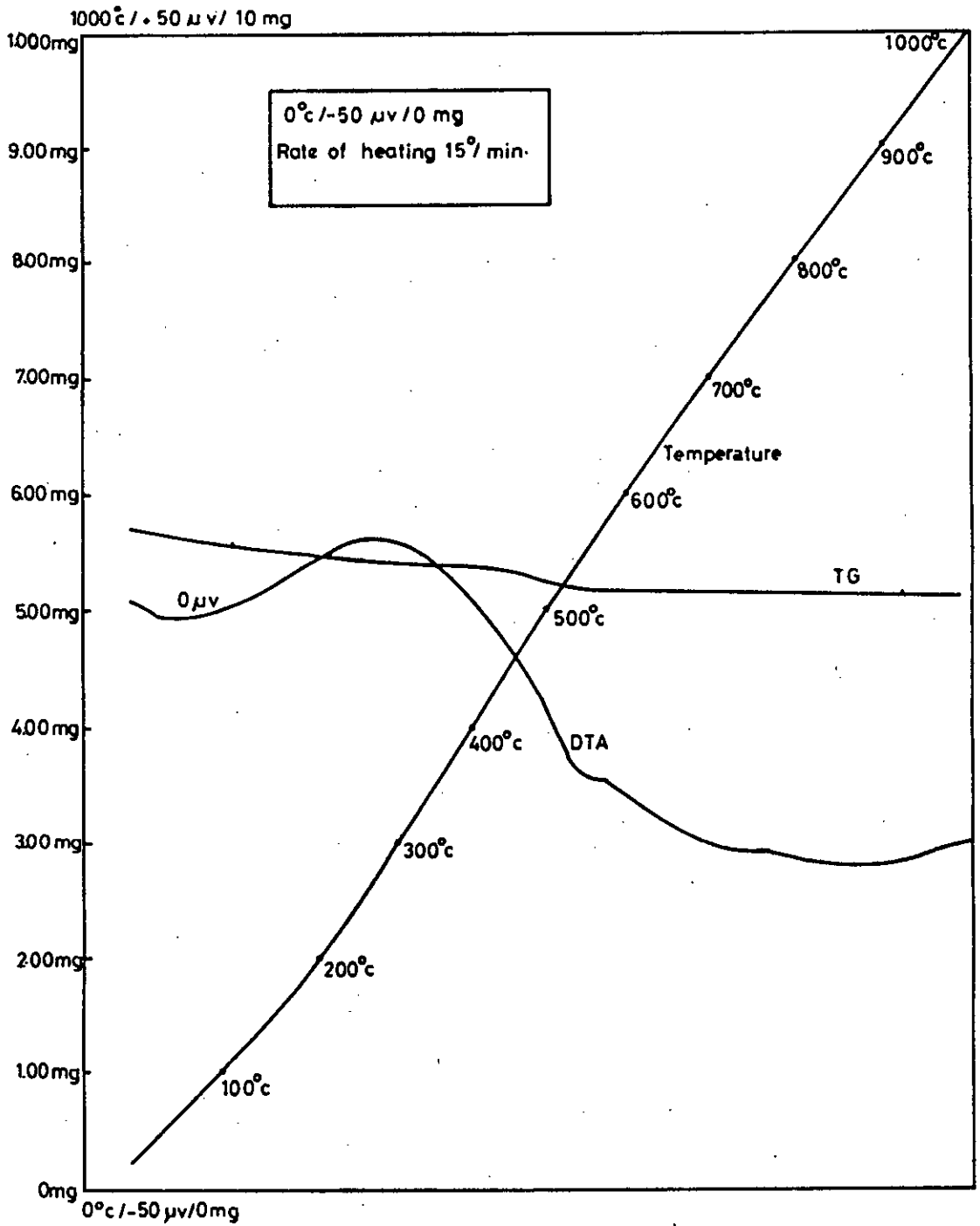


**Figure 4.12 Differential Thermal Analysis and Thermo Gravimetric Pattern of of the modified sample with 4 per cent zinc oxide**

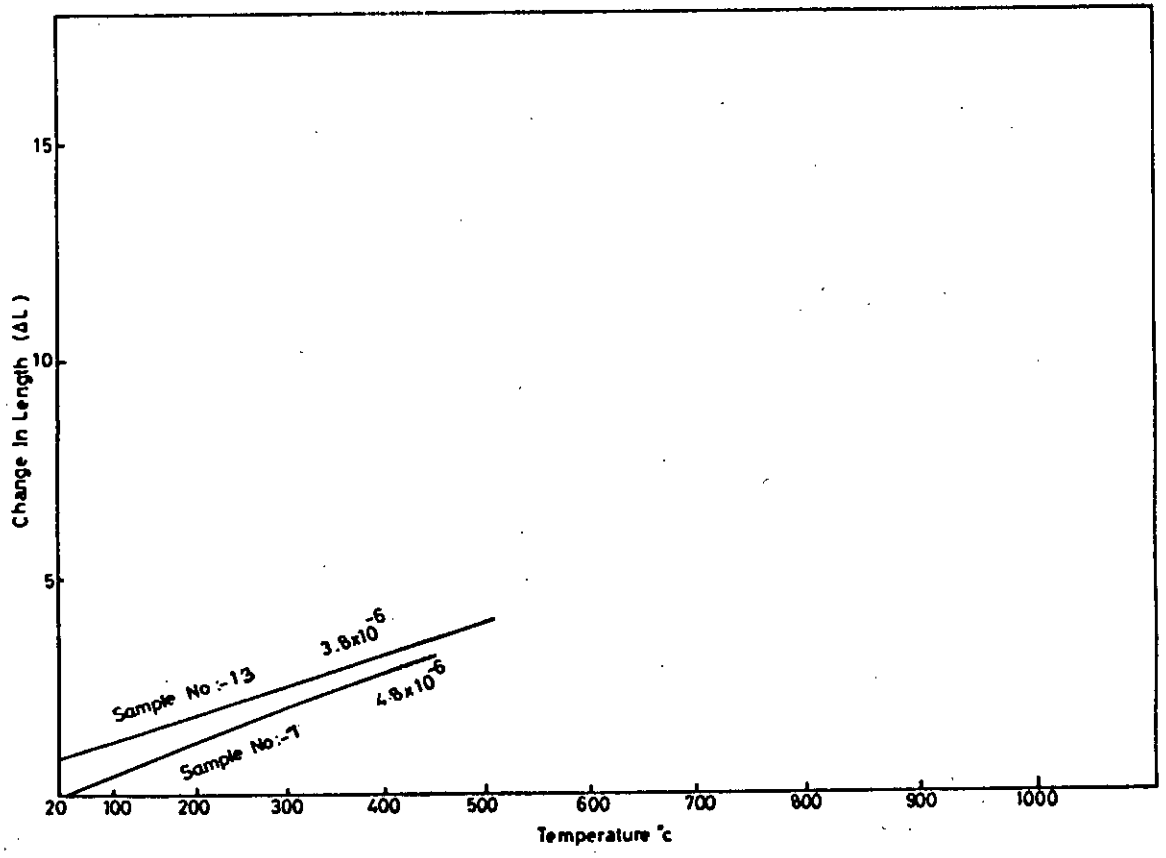


**Figure 4.13 Thermal Expansion versus Temperature diagram of sample no.7 (4% ZnO addition) and 13 (4% ZrSiO<sub>4</sub> and TiO<sub>2</sub>) by dilatometer**

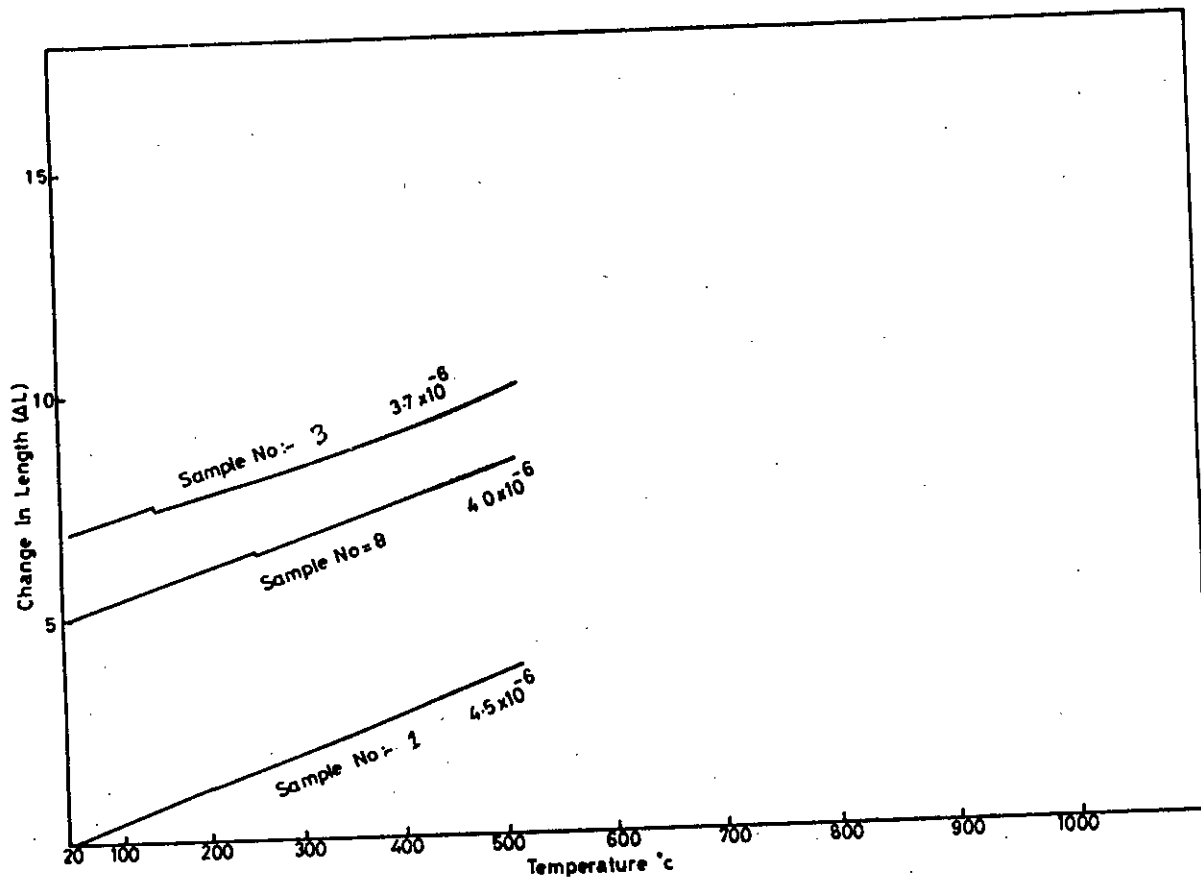


**Figure 4.14 Thermal Expansion versus Temperature diagram of sample no.1 (BISF body) 8 (3% ZnO), and 3 (3% ZrSiO<sub>4</sub>) by dilatometer**

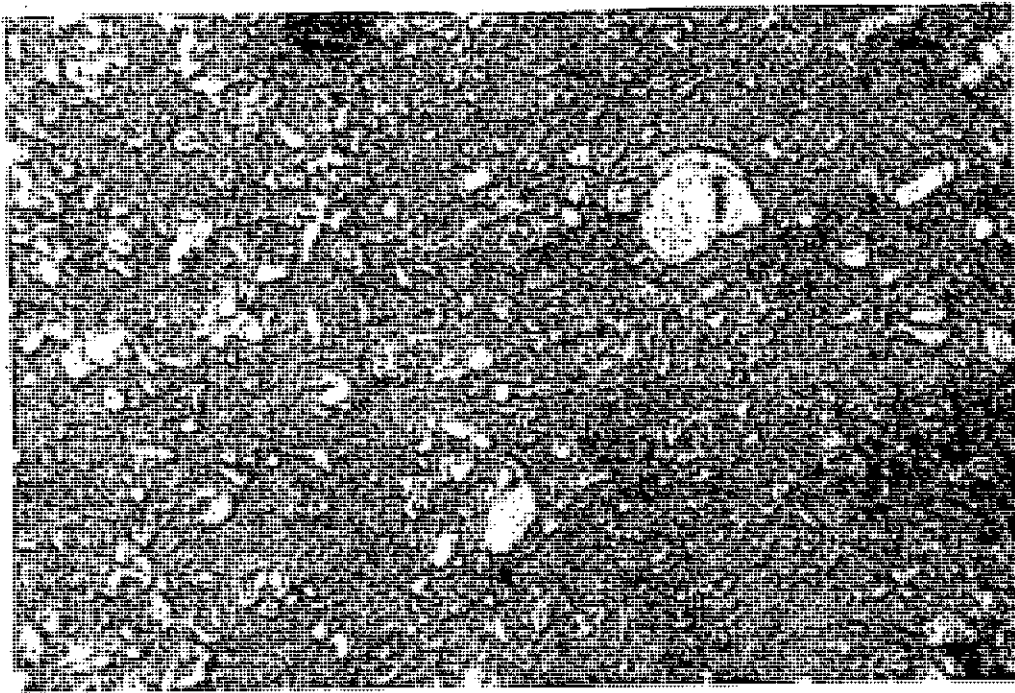


**Figure 4.15** Microstructure of sample no. 1 (original BISF body) showing quartz phases (white areas), Magnification: 500X

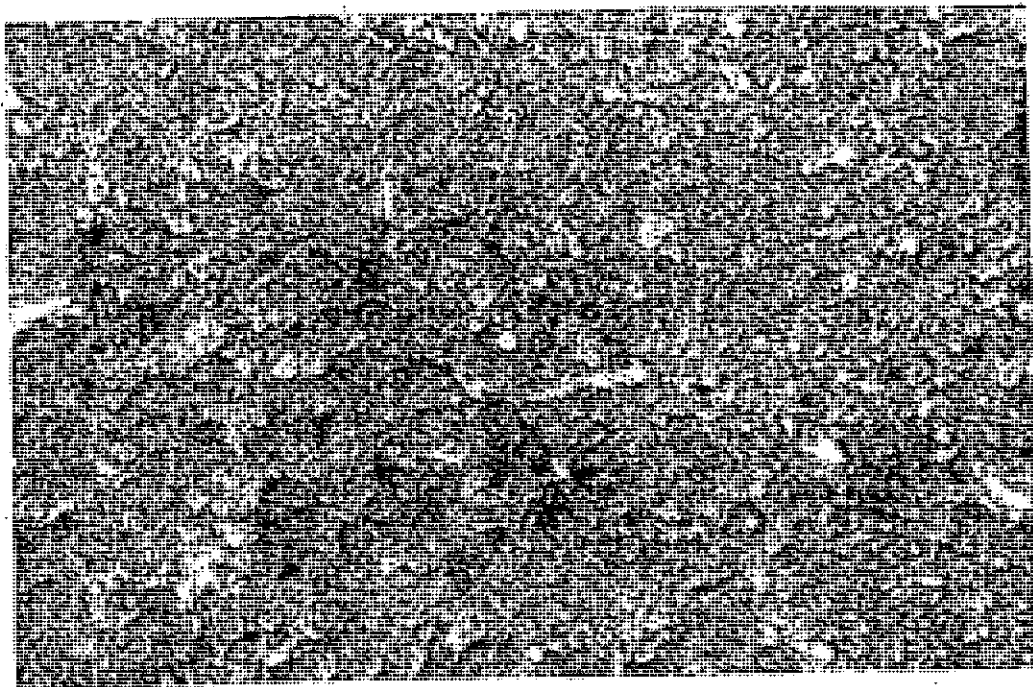


**Figure 4.16** Microstructure of sample no. 2 (2%  $ZrSiO_4$  addition) showing quartz phases (white areas), Magnification: 500X

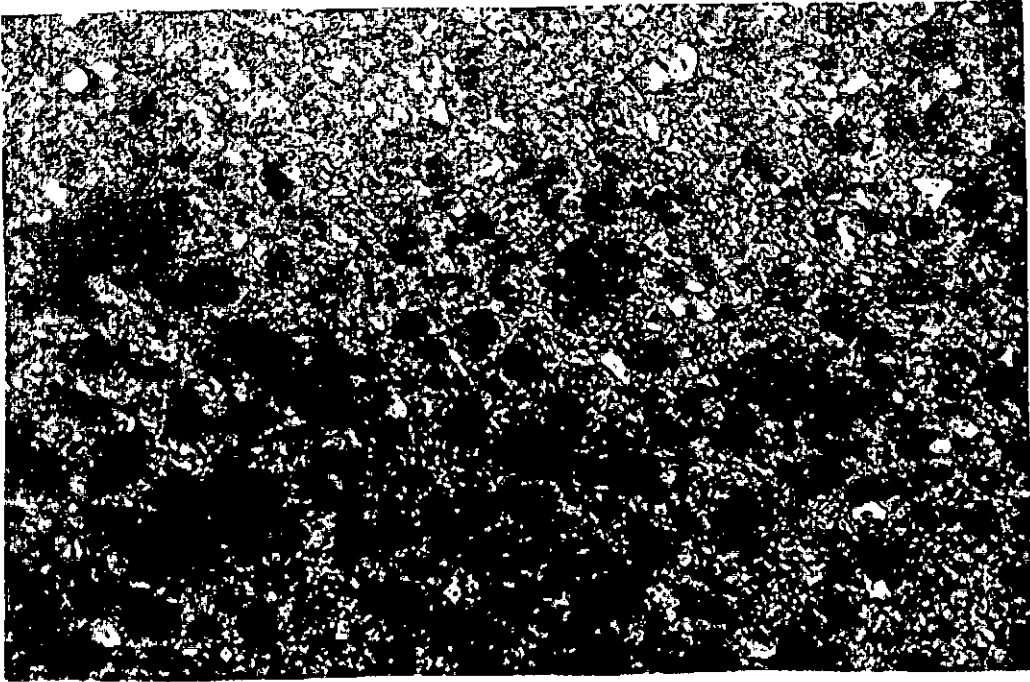


**Figure 4.17** Microstructure of sample no. 3 (3%  $ZrSiO_4$  addition) showing quartz phases (white areas), Magnification: 500X

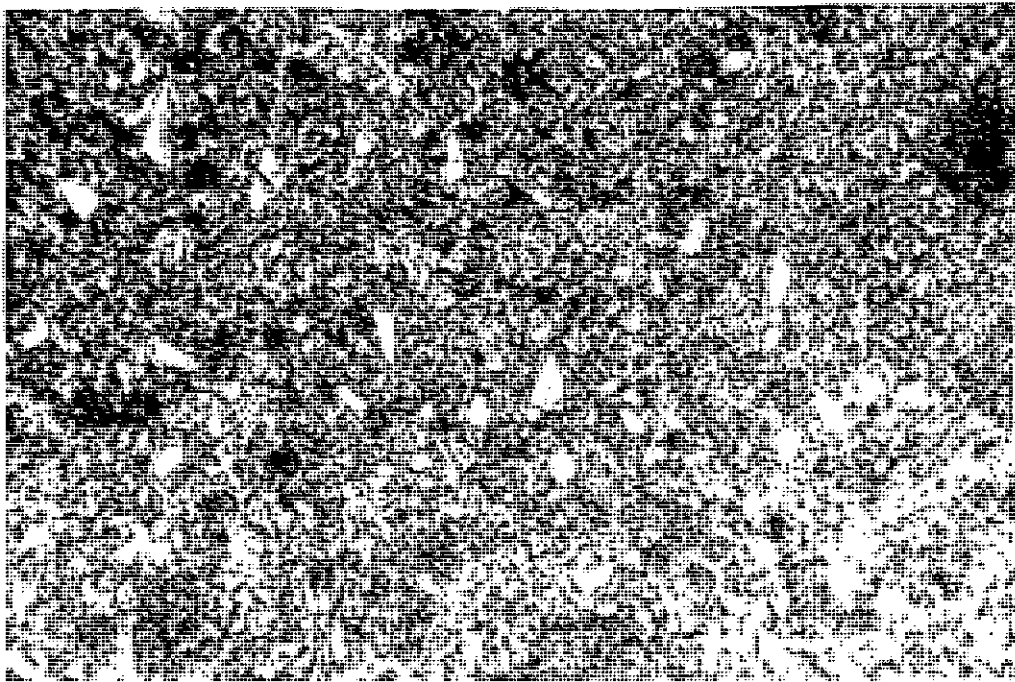


**Figure 4.18** Microstructure of sample no. 4 (4%  $ZrSiO_4$  addition) showing quartz phases (white areas), Magnification: 500X

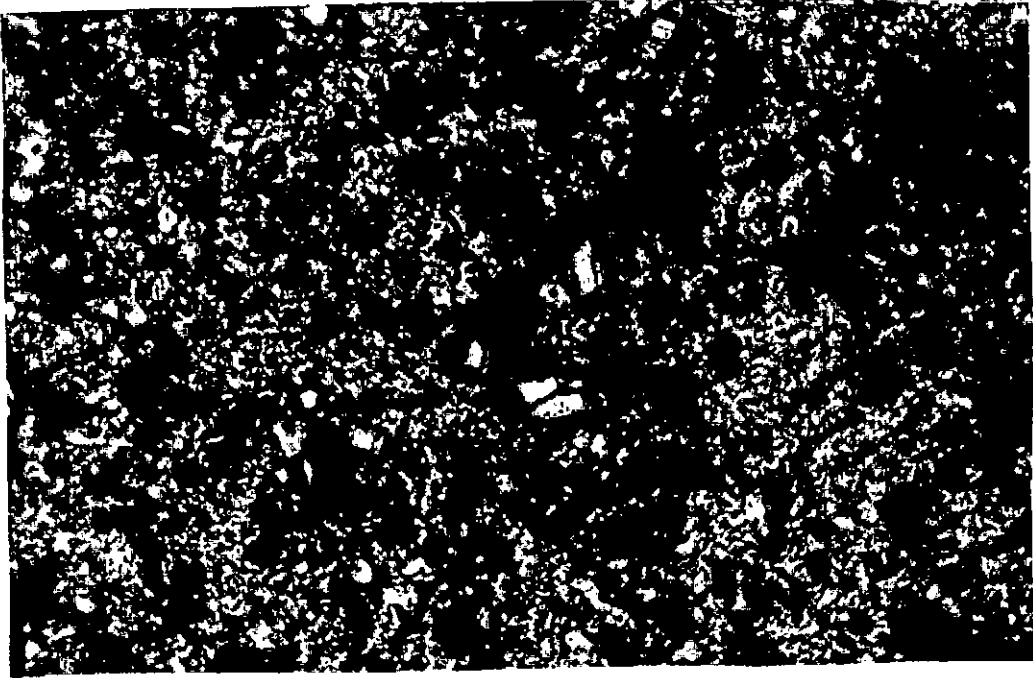


**Figure 4.19** Microstructure of sample no. 5 (2% ZnO addition) showing quartz phases (white areas), Magnification: 500X

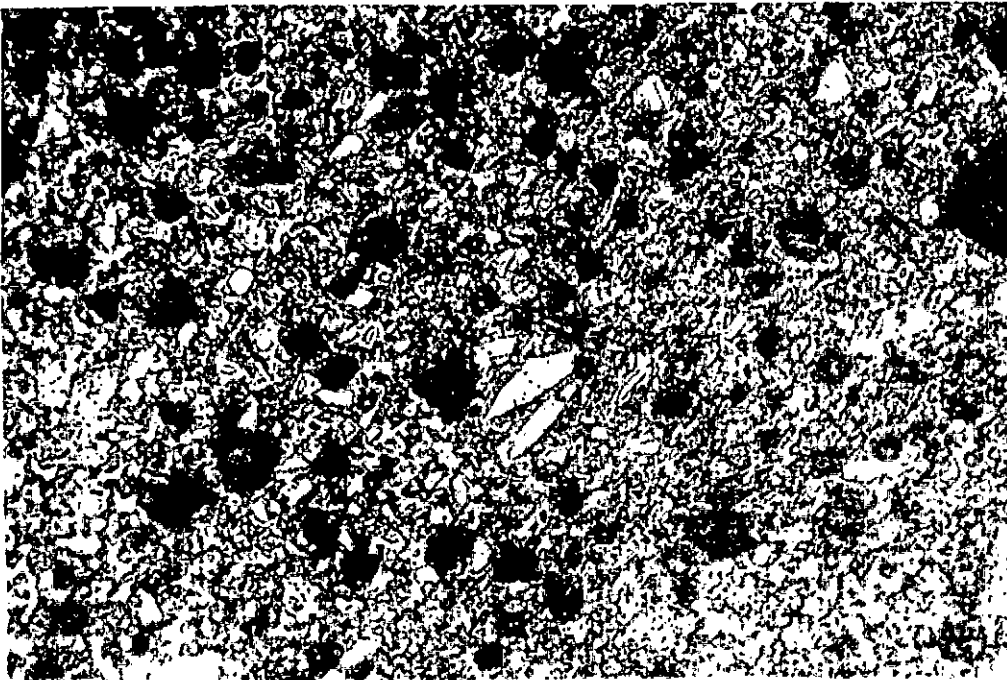


**Figure 4.20** Microstructure of sample no. 6 (3% ZnO addition) showing quartz phases (white areas), Magnification: 500X



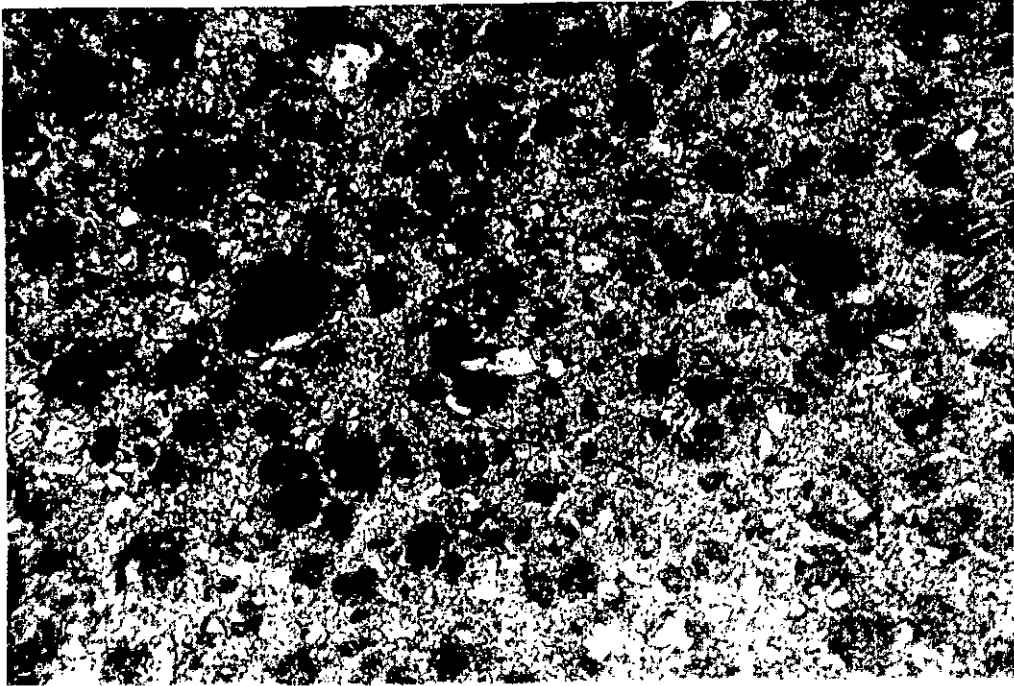


**Figure 4.21** Microstructure of sample no. 7 (4% ZnO addition) showing quartz phases (white areas), Magnification: 500X

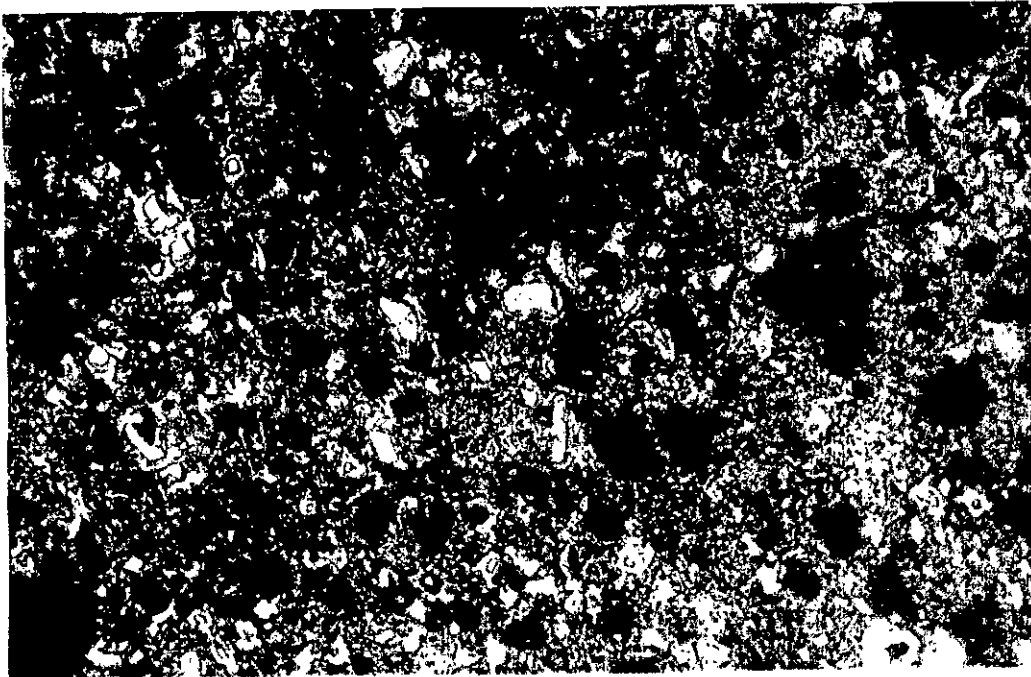


**Figure 4.22** Microstructure of sample no. 8 (2% MnO<sub>2</sub> and TiO<sub>2</sub>) showing quartz phases (white areas), Magnification: 500X

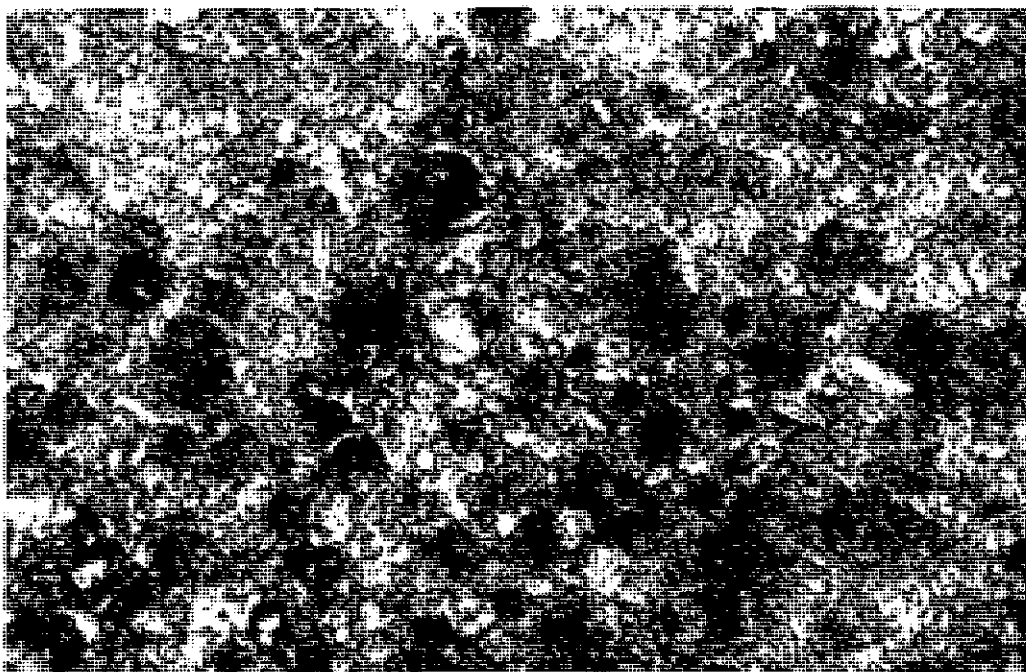


**Figure 4.23** Microstructure of sample no. 9 (3% MnO<sub>2</sub> and TiO<sub>2</sub>) showing quartz phases (white areas), Magnification: 500X.

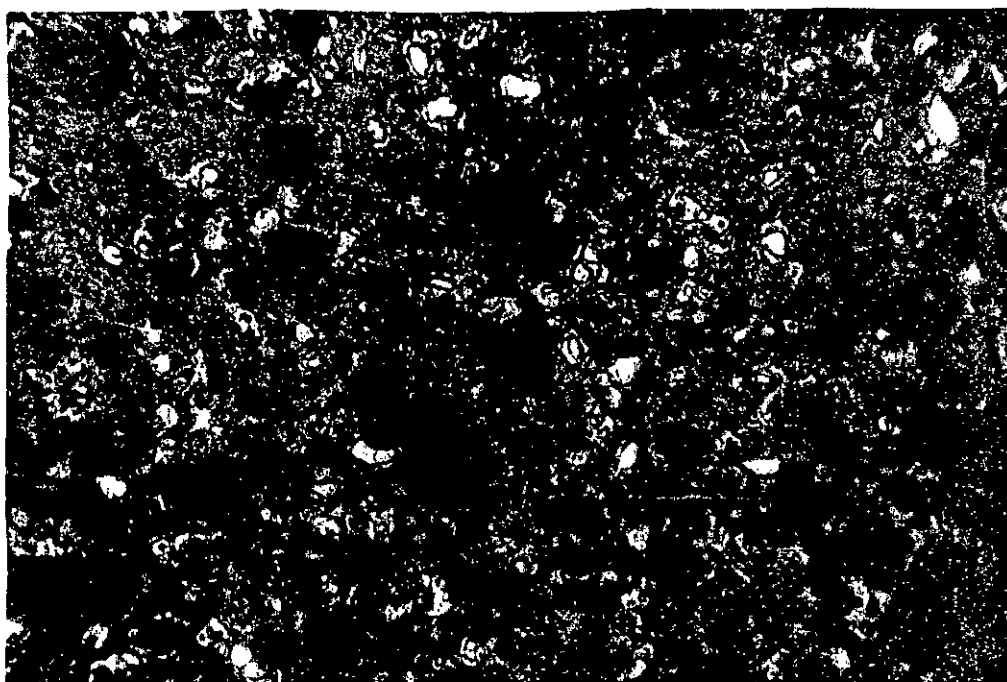


**Figure 4.24** Microstructure of sample no. 10 (4% MnO<sub>2</sub> and TiO<sub>2</sub>) showing quartz phases (white areas), Magnification: 500X

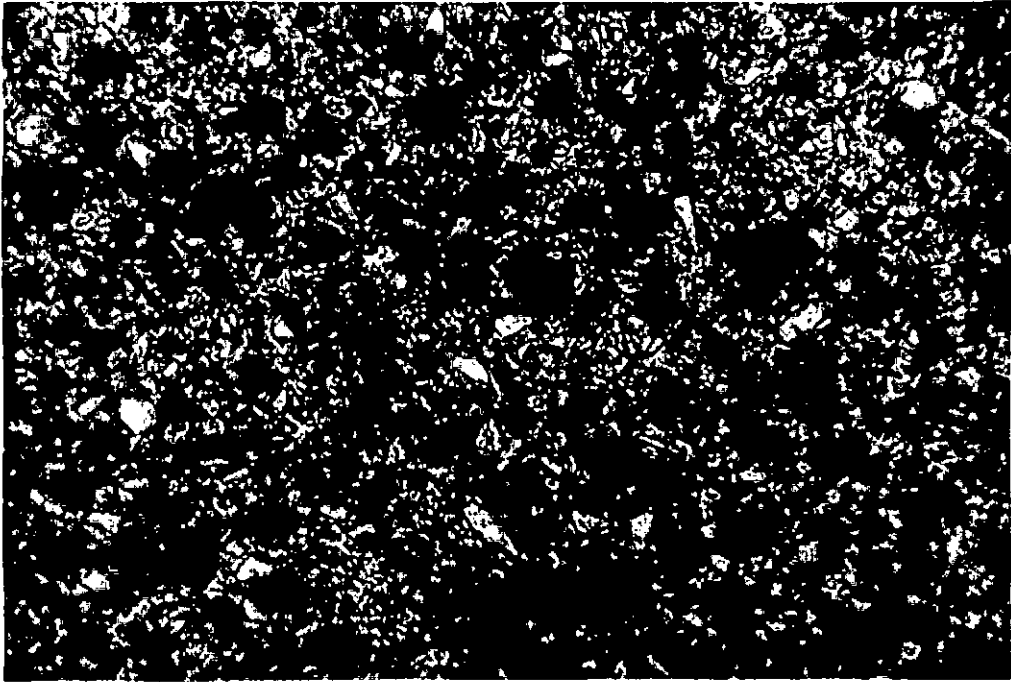


**Figure 4.25** Microstructure of sample no. 11 (2%  $ZrSiO_4$  and  $TiO_2$ ) showing quartz phases (white areas), Magnification: 500X

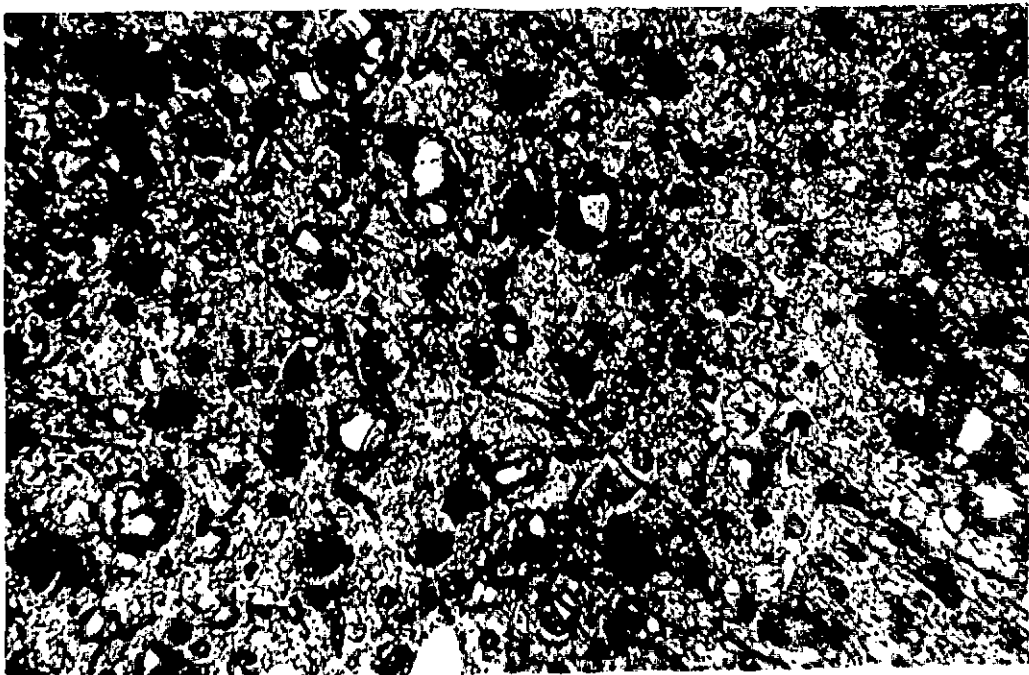


**Figure 4.26** Microstructure of sample no. 12 (3%  $ZrSiO_4$  and  $TiO_2$ ) showing quartz phases (white areas), Magnification: 500X

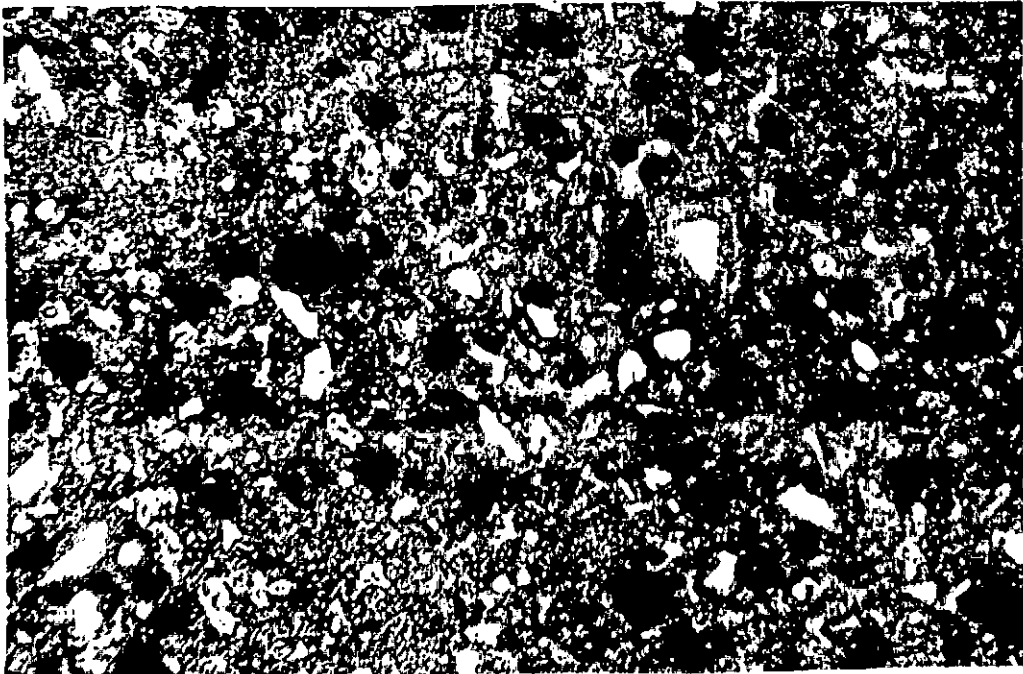


**Figure 4.27** Microstructure of sample no. 13 (4%  $\text{ZrSiO}_4$  and  $\text{TiO}_2$ ) showing quartz phases (white areas), Magnification: 500X

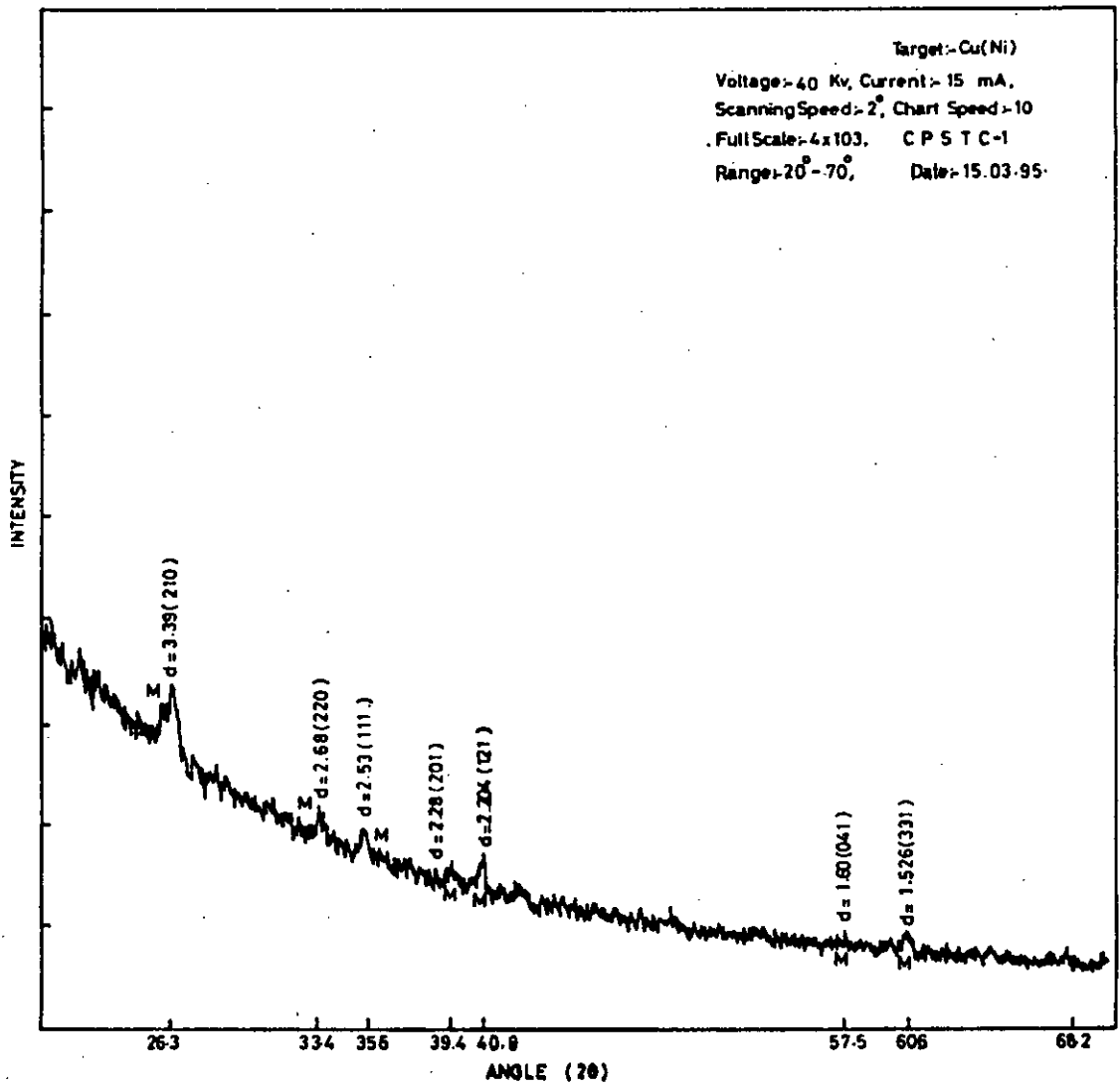


Figure 4.28 X-ray diffraction pattern of sample no.1 (BISF Original body); M - Mullite

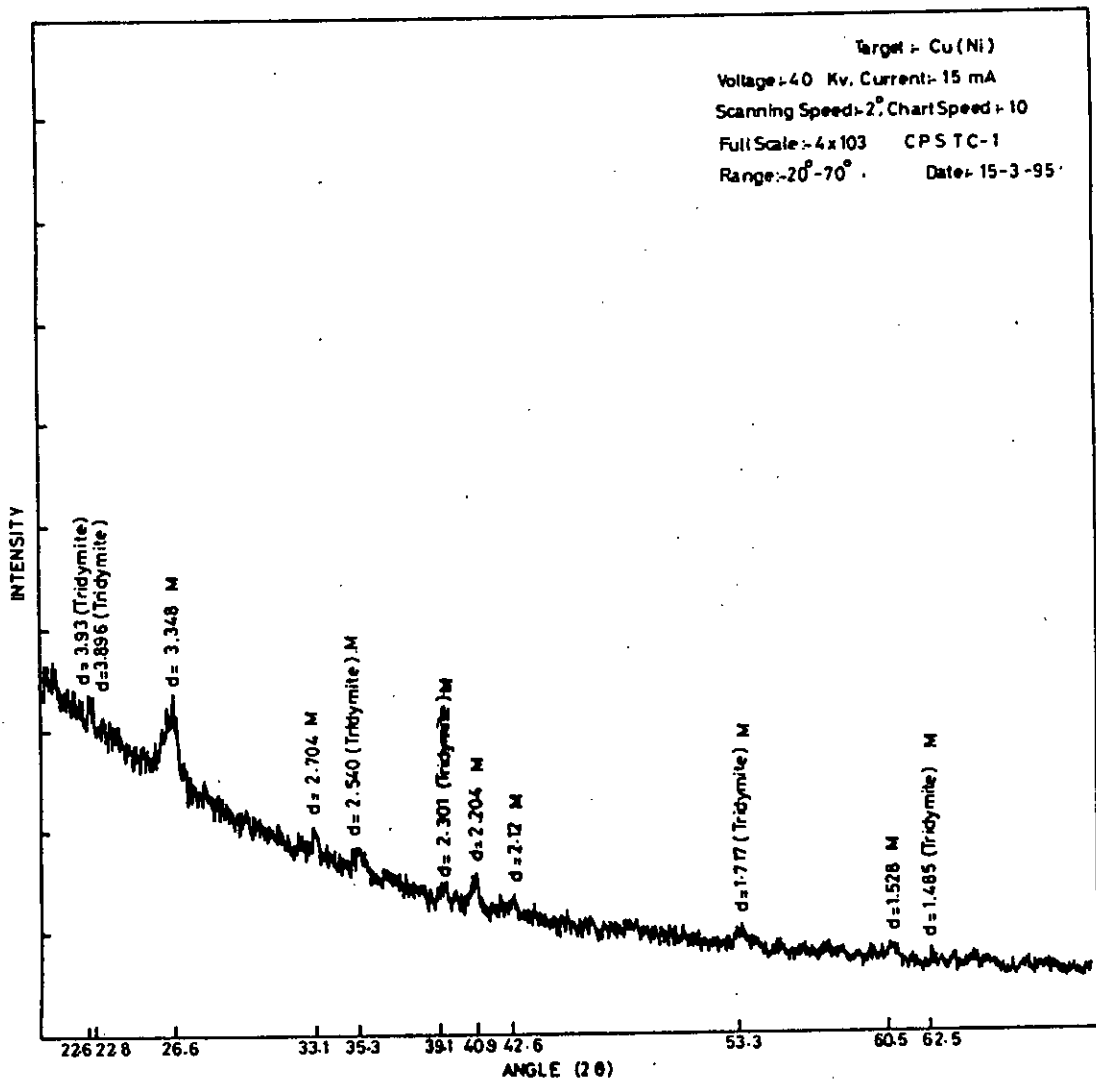
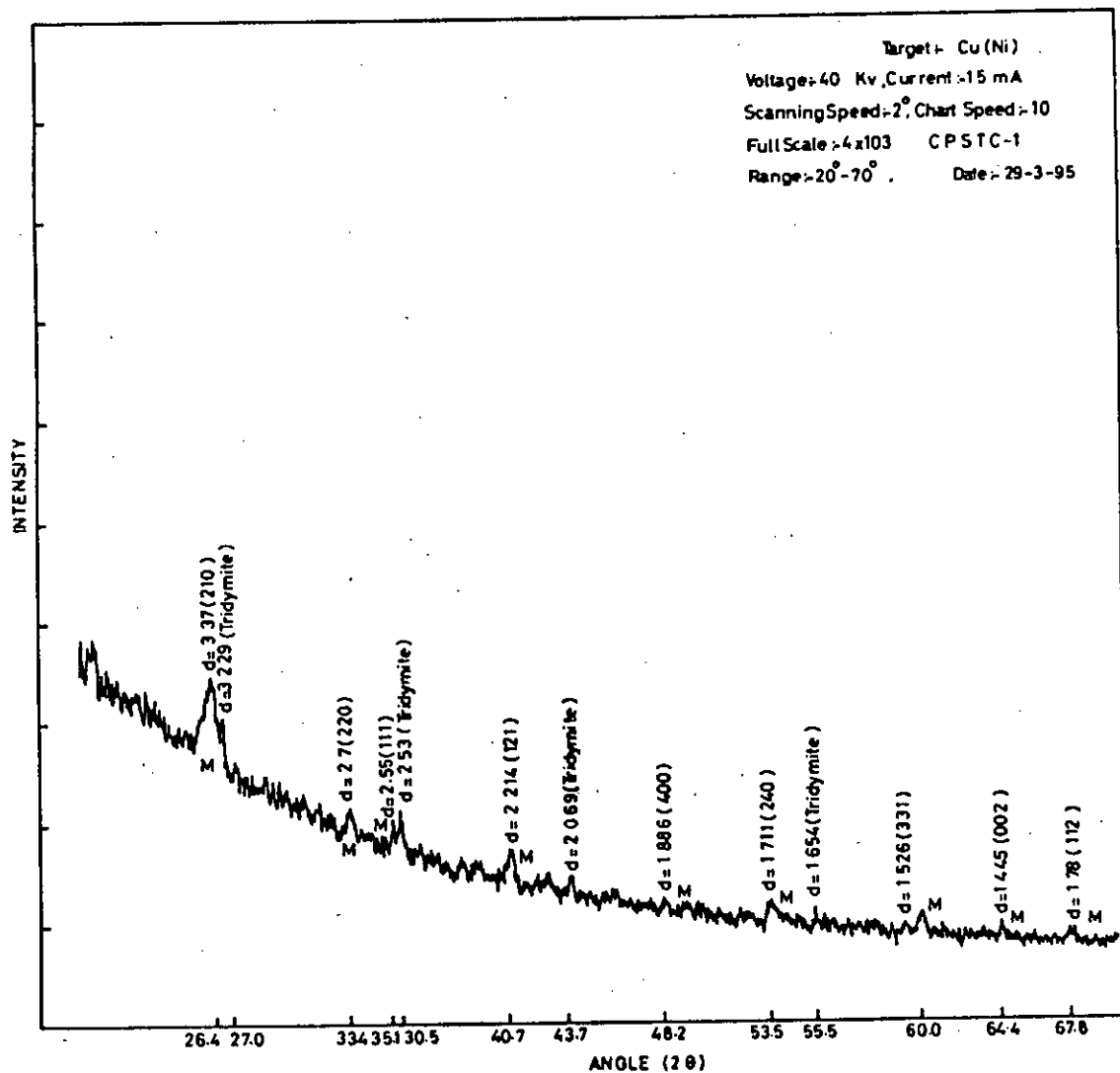


Figure 4.29 X-ray diffraction pattern of sample no. 2 (2% ZrSiO<sub>4</sub> addition); M - Mullite; T - Tridymite



**Figure 4.30 X-ray diffraction pattern of sample no. 3 (3% ZrSiO<sub>4</sub> addition); M - Mullite; T - Tridymite**

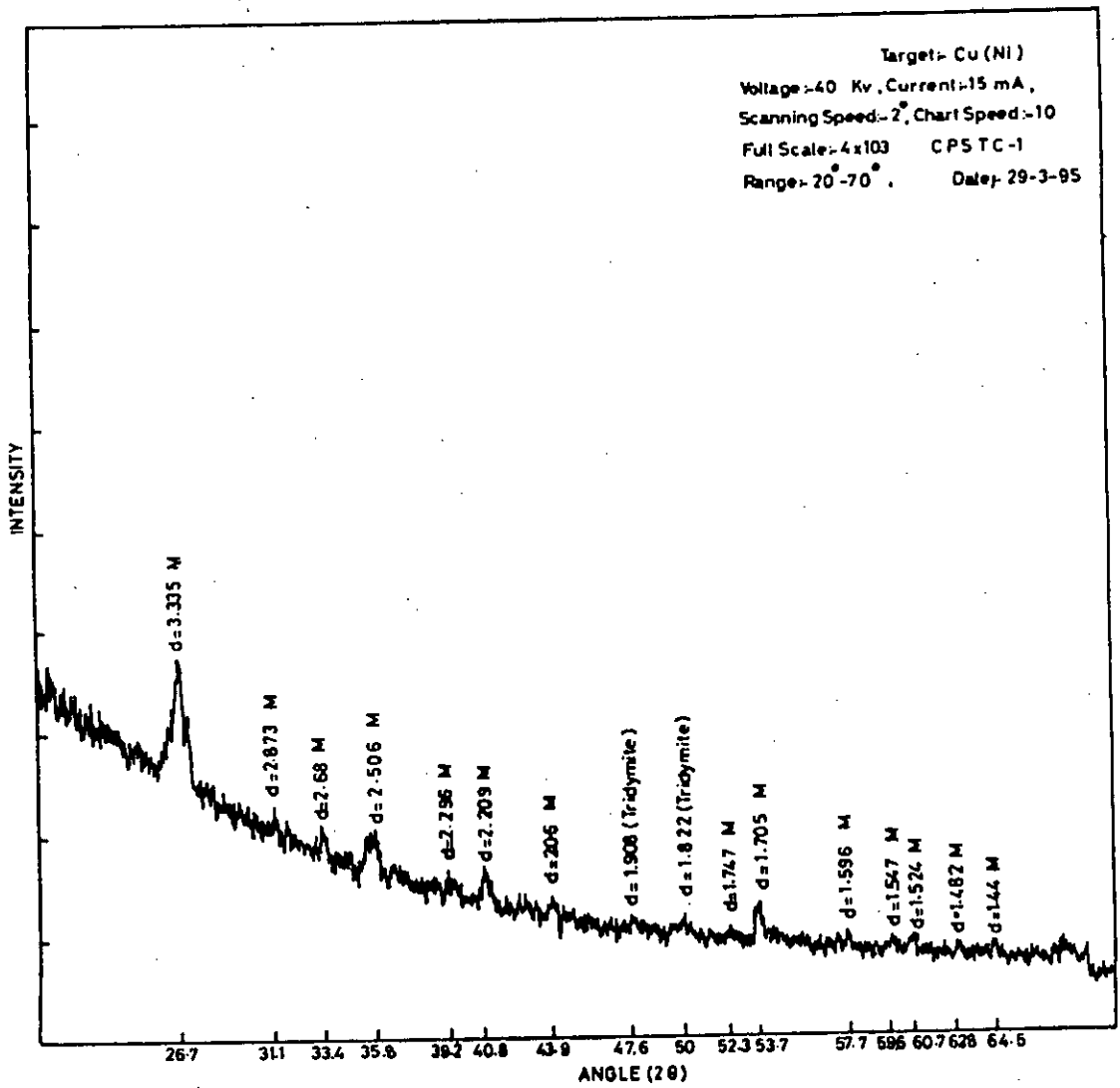


Figure 4.31 X-ray diffraction pattern of sample no. 4 (4% ZrSiO<sub>4</sub> addition); M - Mullite; T - Tridymite



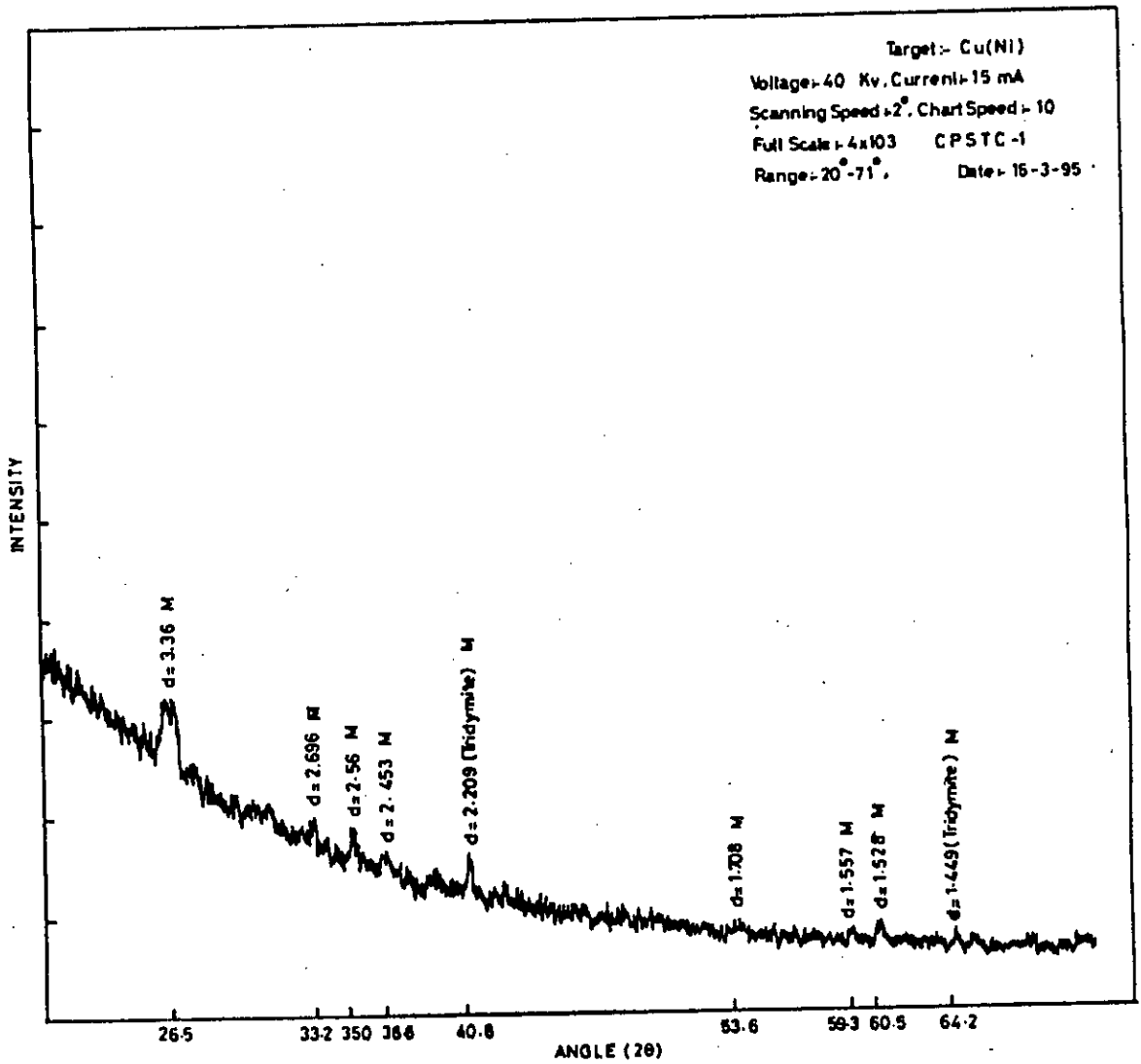


Figure 4.32 X-ray diffraction pattern of sample no. 5 (2% ZnO addition); M - Mullite; T - Tridymite

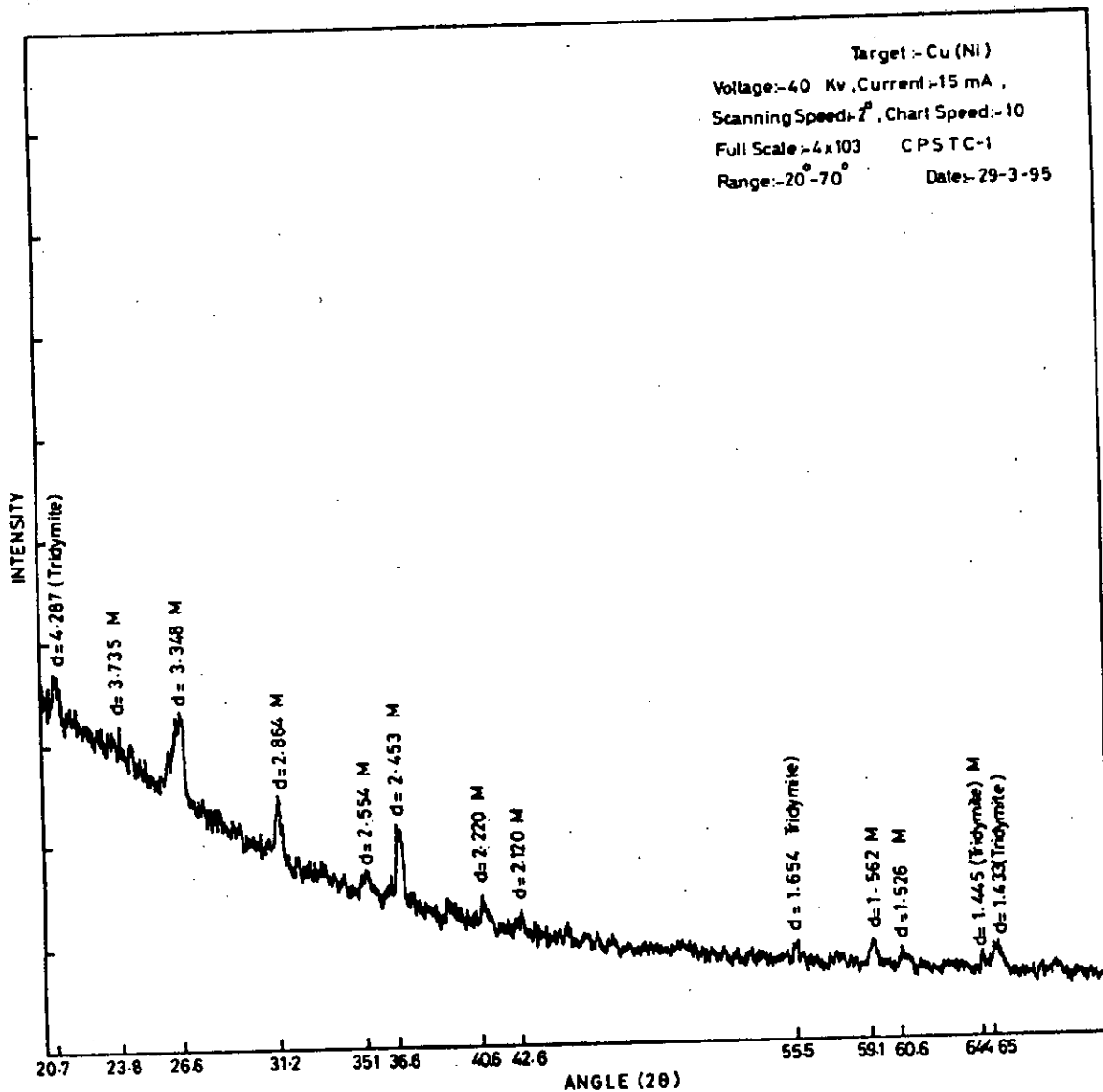


Figure 4.33 X-ray diffraction pattern of sample no. 6 (3% ZnO addition); M - Mullite; T - Tridymite

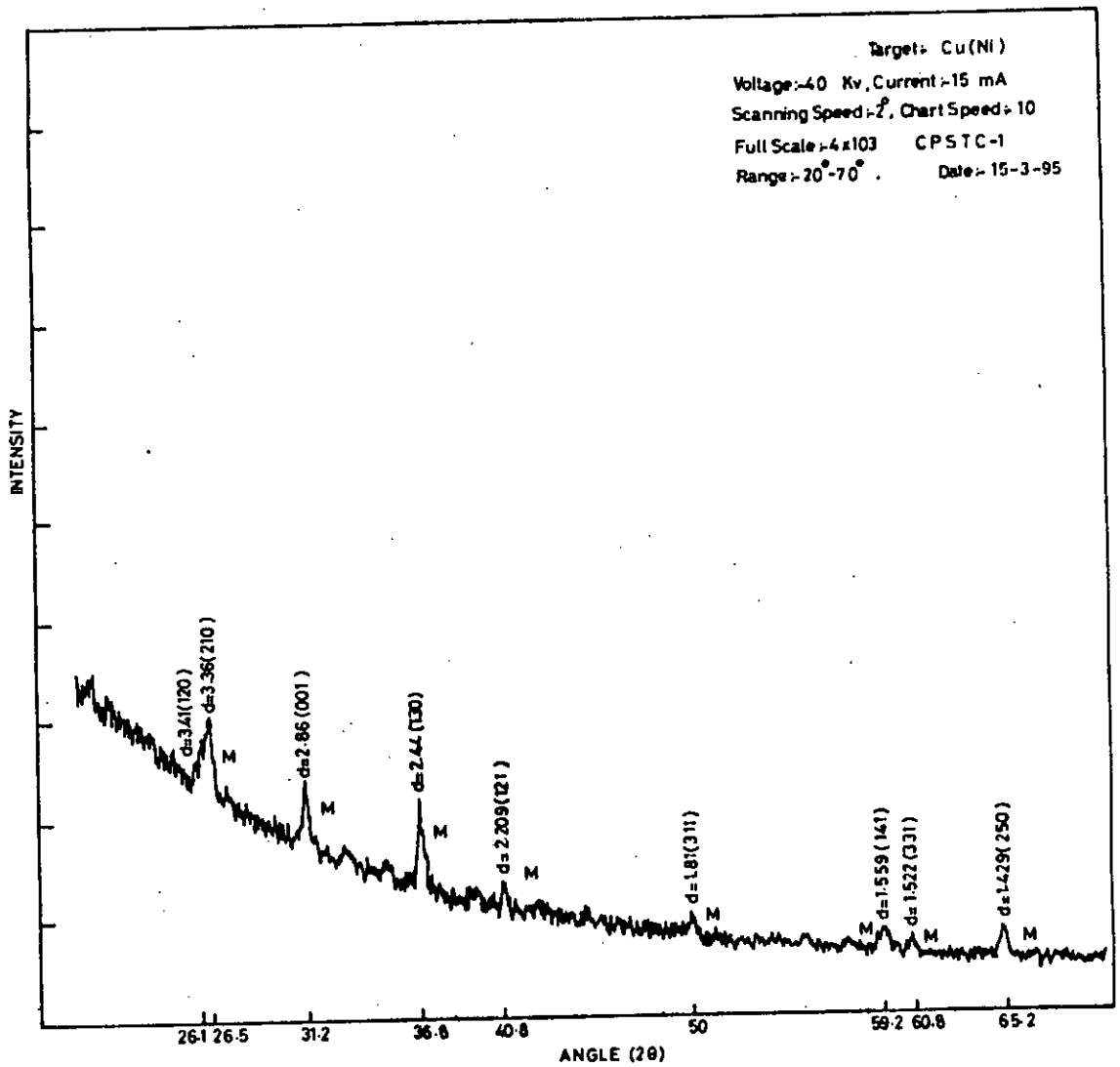


Figure 4.34 X-ray diffraction pattern of sample no. 7 (4% ZnO addition); M - Mullite;

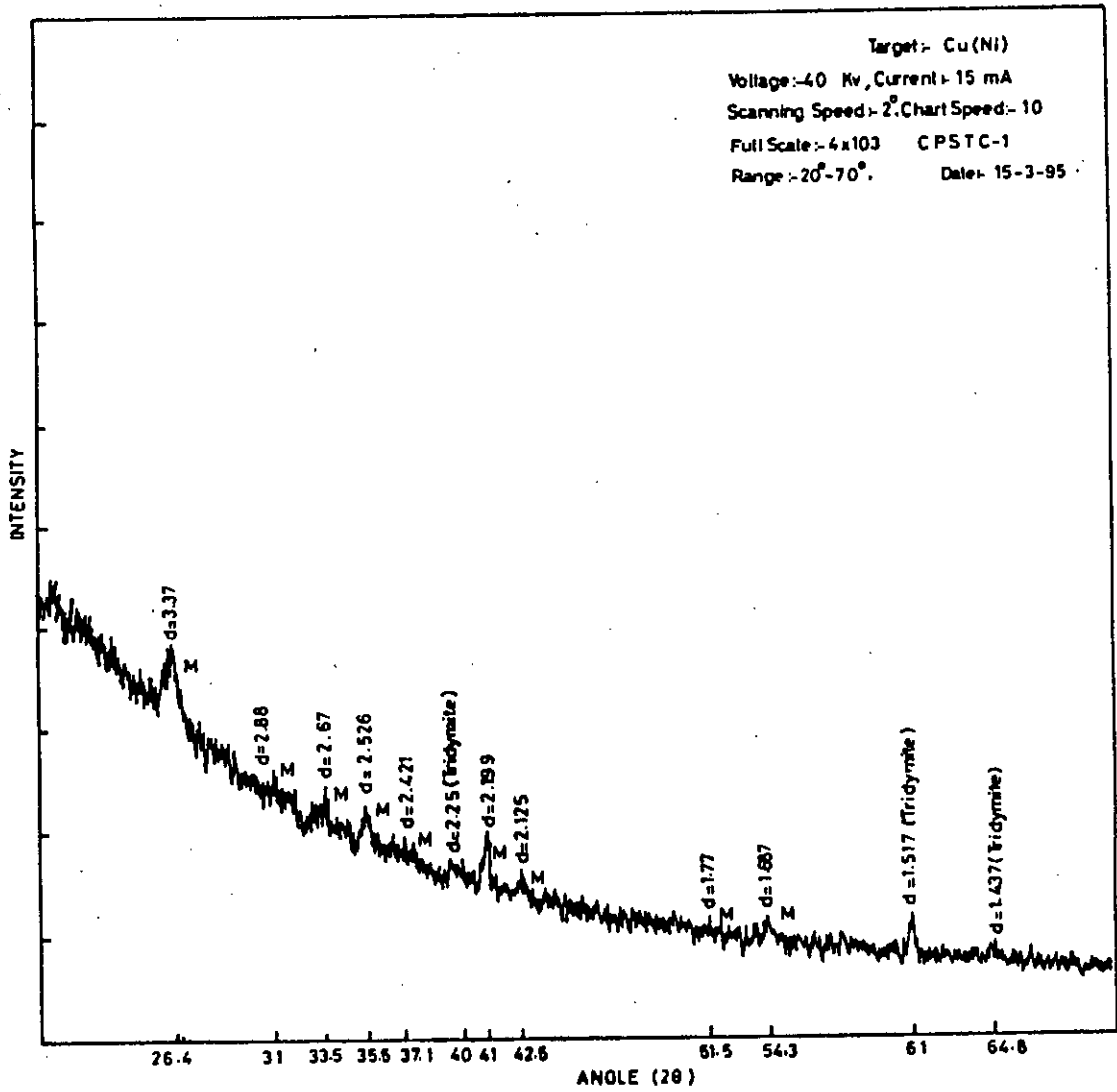
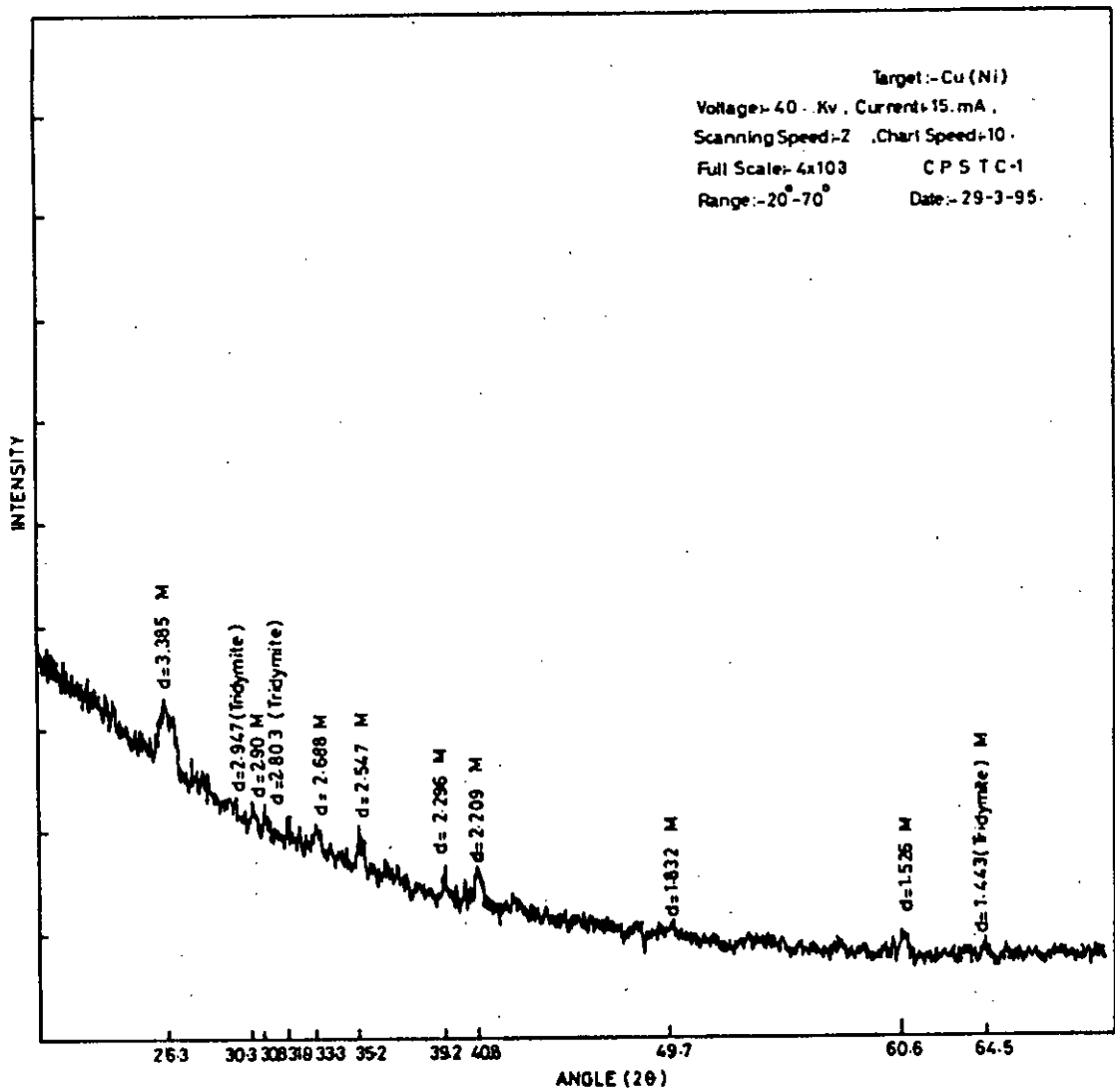


Figure 4.35 X-ray diffraction pattern of sample no. 8 (2% MnO<sub>2</sub> and TiO<sub>2</sub>); M - Mullite; T - Tridymite



**Figure 4.36 X-ray diffraction pattern of sample no. 9 (3% MnO<sub>2</sub> and TiO<sub>2</sub>); M - Mullite; T - Tridymite**

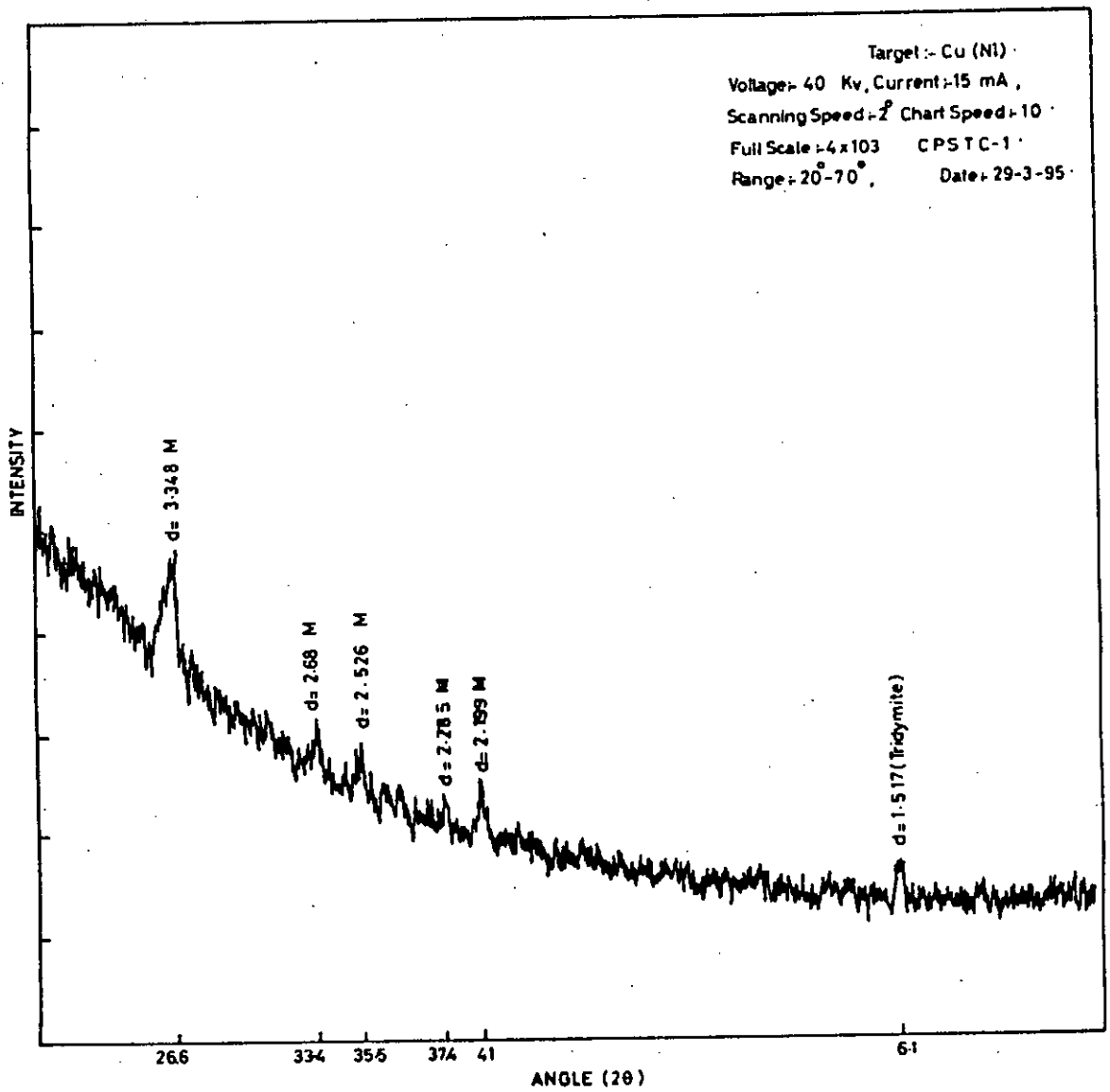


Figure 4.37 X-ray diffraction pattern of sample no. 10 (4% MnO<sub>2</sub> and TiO<sub>2</sub>); M - Mullite; T - Tridymite

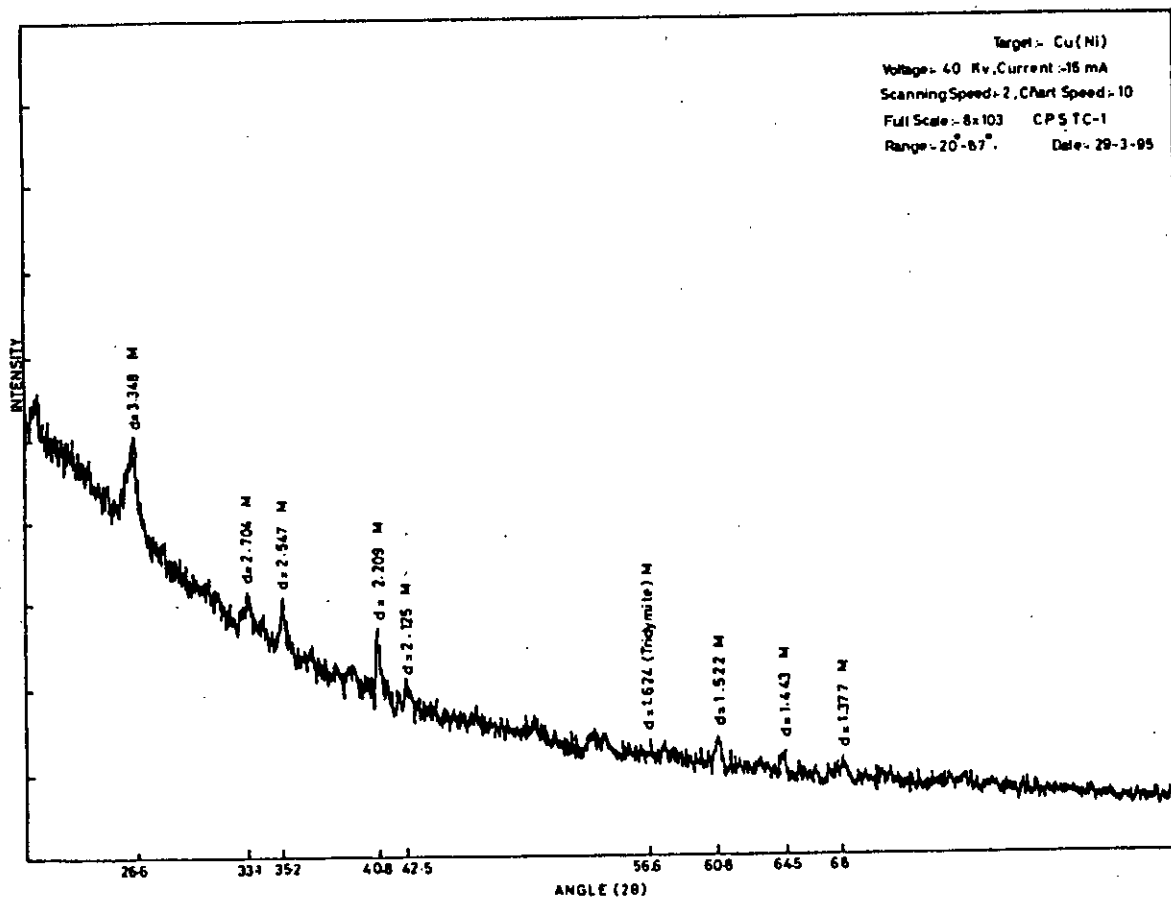


Figure 4.38 X-ray diffraction pattern of sample no. 11 (2% ZrSiO<sub>4</sub> and TiO<sub>2</sub>); M - Mullite;

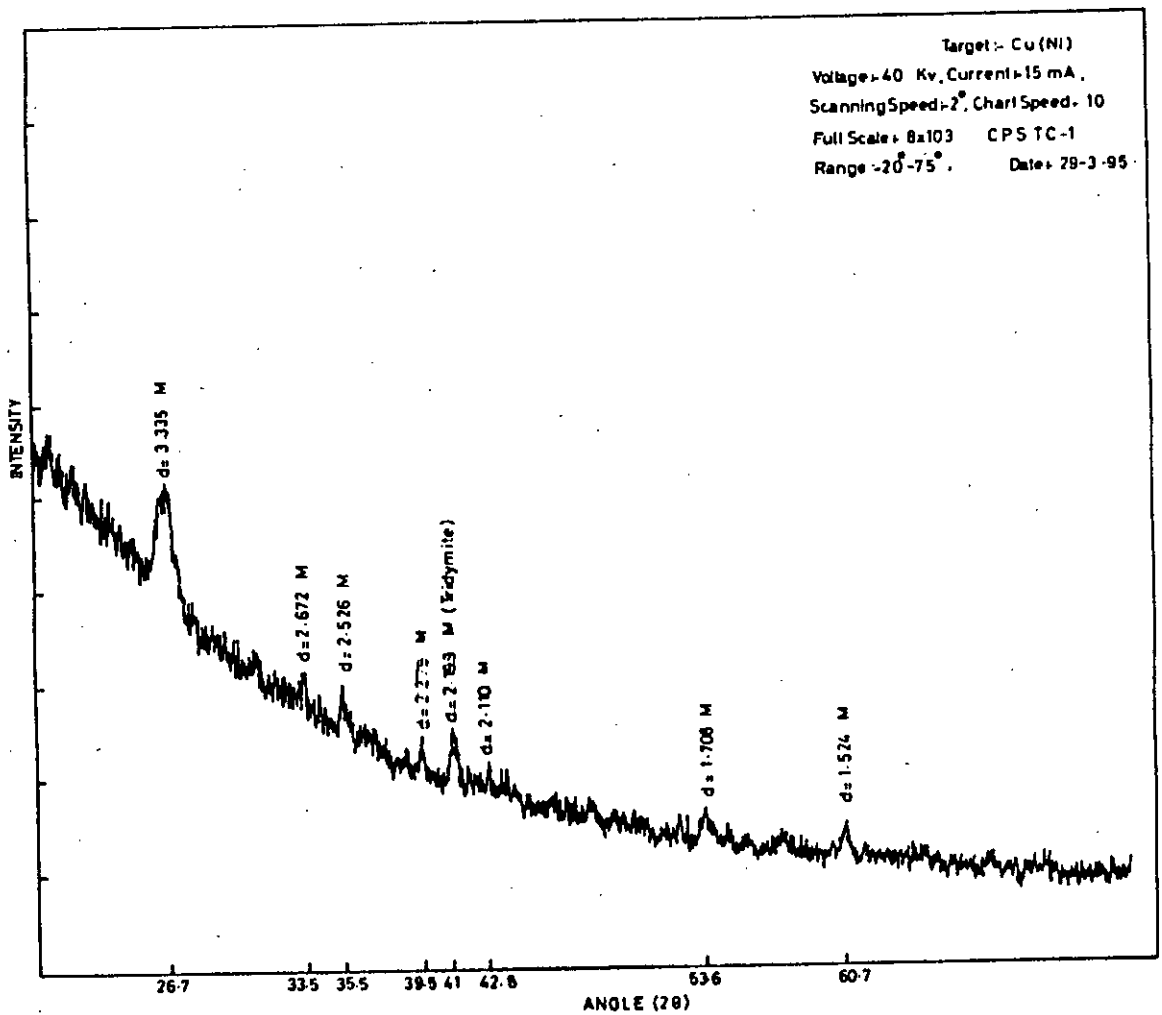


Figure 4.39 X-ray diffraction pattern of sample no. 12 (3% ZrSiO<sub>4</sub> and TiO<sub>2</sub>); M - Mullite; T - Tridymite



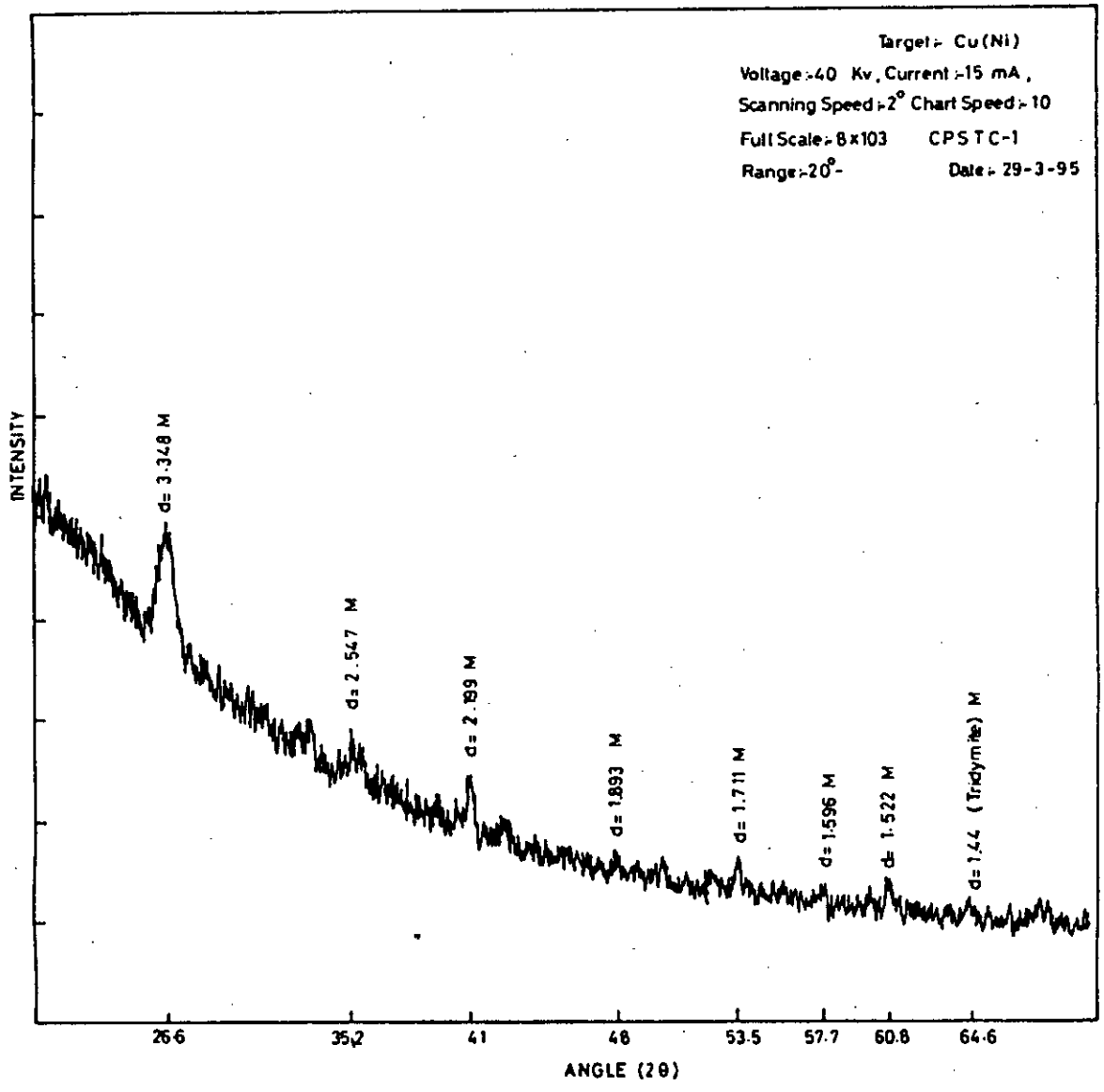


Figure 4.40 X-ray diffraction pattern of sample no. 13 (4% ZrSiO<sub>4</sub> and TiO<sub>2</sub>); M - Mullite; T - Tridymite

89225  
24-9-95\*  
कारखाना, जका